

Realistic bending stiffness of diaphragm walls for structural analysis

*A comparison with the uncracked and totally cracked stiffness for the case of
The Waalbrug Nijmegen*

APPENDICES



Ranjana Soekhoe
Delft, December 2015



Gemeente Rotterdam

TABLE OF CONTENTS

| | |
|--------------|---|
| Appendix A: | Literature survey |
| Appendix B: | Geotechnical Soil Profiles |
| Appendix C1: | Iteration process right wall – ‘Walls only; hinged’, Case a: EI (κ) |
| Appendix C2: | Iteration process right wall – ‘Walls only; hinged’, Case b: EI (κ , N) |
| Appendix C3: | Iteration process right wall – ‘Walls only; clamped’, Case a: EI (κ) |
| Appendix C4: | Iteration process right wall – ‘Walls only; clamped’, Case b: EI (κ , N) |
| Appendix D: | Properties Stiff Structure |
| Appendix E1: | Variation hinged connection 1 – $\rho_{1,tot} = 1\%$, Case a: EI (κ) |
| Appendix E2: | Variation hinged connection 1 – $\rho_{1,tot} = 1\%$, Case b: EI (κ , N) |
| Appendix F1: | Variation hinged connection 2 – Soil Type 2, Case a: EI (κ) |
| Appendix F2: | Variation hinged connection 2 – Soil Type 2, Case b: EI (κ , N) |

APPENDIX A

LITERATURE SURVEY

Table of Contents

| | |
|--|-----------|
| List of Symbols | 4 |
| 1. DIAPHRAGM WALLS | 6 |
| 1.1. In general..... | 6 |
| 1.1.1. Available standards..... | 7 |
| 1.1.2. Loads, Load Distribution and Failure Mechanisms..... | 8 |
| 1.1.3. Safety Approach regarding Design and Verification: SLS & ULS | 9 |
| 1.1.4. Reliability class & design approach diaphragm wall..... | 9 |
| 1.1.5. The design | 10 |
| 1.2. Deformations and settlements | 11 |
| 1.2.1. Factors influencing the deformations..... | 12 |
| 1.2.2. Relationship deformations and settlements..... | 12 |
| 1.2.3. Reducing deformations and settlements..... | 16 |
| 1.2.4. Calculation software | 16 |
| 1.3. Soil-structure interaction | 16 |
| 1.4. Deformation requirements (ProRail) | 17 |
| 2. SOIL MODELS..... | 18 |
| 2.1. Calculation methods..... | 18 |
| 2.2. Material models | 21 |
| 2.3. Soil parameters | 22 |
| 2.3.1. Horizontal soil pressure coefficients..... | 22 |
| 2.3.2. Cohesion (c) and Internal friction (ϕ)..... | 23 |
| 2.3.3. Wall friction (δ) | 25 |
| 2.3.4. Dilatancy (ψ) | 25 |
| 2.3.5. Permeabilities (k_x and k_y)..... | 25 |
| 2.3.6. Drained/ undrained loading | 26 |
| 2.3.7. Saturated and unsaturated weight (γ_{sat} and γ_{unsat})..... | 26 |
| 2.3.8. Modulus of subgrade reaction (k_s) - Secant | 26 |
| 2.3.9. Stiffness moduli (E) | 27 |
| 2.3.10. OCR and POP | 28 |
| 2.4. Calculation software | 28 |
| 2.4.1. PCSheetPileWall..... | 29 |
| 2.4.2. Plaxis 2D | 30 |
| 3. THE M-(N)-κ DIAGRAM..... | 35 |

| | | |
|-----------|--|-----------|
| 3.1. | Introduction | 35 |
| 3.2. | Relation Moment – Curvature | 36 |
| 3.3. | The loading phases..... | 37 |
| 3.4. | M-(N)- κ diagram ULS: principle..... | 39 |
| 3.5. | M-(N)- κ diagram SLS: principle | 43 |
| 3.6. | Characteristics in M-(N)- κ diagram..... | 46 |
| 3.7. | EC2: Minimum and maximum reinforcement ratio diaphragm walls | 48 |
| 3.8. | Software programs using M-N- κ diagram: PCSheetPileWall..... | 48 |
| 4. | DESIGN STANDARDS: CRACKED VS. UNCRACKED BENDING STIFFNESS.... | 50 |
| 4.1. | EC2: Behaviour of not fully cracked member..... | 50 |
| 4.2. | EC2 & ACI 318-05: Fully cracked bending stiffness | 51 |
| 4.3. | Bending stiffnesses: EI_0 , EI_{var} and EI_∞ | 55 |
| 4.4. | Additional information..... | 55 |
| | References..... | 56 |

List of Symbols

Upper case letters

| | |
|-----------------------|---|
| A_c | Cross sectional area of concrete |
| A_{sv} | Area of the vertical reinforcement |
| A_s | Cross sectional area of tension reinforcement |
| A'_s | Cross sectional area of compression reinforcement |
| $E_{c,eff}$ | Effective modulus of elasticity of concrete (for long-term loading) |
| E_{cd} | Design value of modulus of elasticity of concrete |
| E_{cm} | Secant modulus of elasticity of concrete (for short-term loading) |
| E_f | Fictitious modulus of elasticity |
| E_s | Design value of modulus of elasticity of reinforcing steel |
| E_{50}^{ref} | Secant stiffness in standard drained triaxial test |
| E_{oed}^{ref} | Tangent stiffness for primary oedometer loading |
| E_{ur}^{ref} | Unloading and reloading stiffness |
| EA | Normal stiffness |
| EI | Bending stiffness |
| EI_0/EI_{uncr} | Uncracked bending stiffness |
| EI_{∞}/EI_{cr} | Fully or totally cracked bending stiffness |
| EI_{var} | Realistic (variable) bending stiffness |
| I_g | Moment of inertia of the gross concrete section, neglecting reinforcement |
| I_{cr} | Moment of inertia of the fully cracked section |
| $I_{c,eff}$ | Effective moment of inertia |
| K | Horizontal soil pressure coefficient |
| K_0 | Neutral horizontal soil coefficient |
| K_a | Active horizontal soil pressure coefficient |
| K_p | Passive horizontal soil pressure coefficient |
| M | Bending moment |
| M_a | Maximum bending moment in member |
| M_e | Yield moment |
| M_{Ed} | Occurring bending moment |
| M_{pl} | Crushing moment |
| M_f | Cracking moment |
| M_u | Ultimate moment |
| M_x | Arbitrary bending moment |
| N'_c | Axial compressive force |
| R_{inter} | Strength reduction factor |
| W | Section modulus |

Lower case letters

| | |
|--------------|---|
| b | Width |
| c | Cohesion |
| $c_{concr.}$ | Concrete cover |
| d | Diaphragm wall thickness |
| d_{eq} | Equivalent plate thickness |
| f_c | Compressive strength of concrete |
| f_{cd} | Design value of concrete compressive strength |
| f_{ck} | Characteristic compressive cylinder strength of concrete at 28 days |
| f_{ctm} | Mean value of axial tensile strength of concrete |
| f_{yd} | Design yield strength of reinforcement |
| f_{yk} | Characteristic yield strength of reinforcement |

| | |
|------------|--|
| $k_{x,y}$ | Soil permeability in x,y-direction |
| k_s | Modulus of subgrade reaction or soil spring stiffness |
| m | Power for stress-level dependency of stiffness |
| n | Modular ratio of steel and concrete (E_s/E_c) |
| p | Porewater pressure |
| q | Partially distributed surface loading |
| w | Displacement |
| w_{line} | Line load due to self-weight diaphragm wall |
| x | Height of concrete compression zone |
| x_e | Height of concrete compression zone when reinforcement starts yielding |
| x_{pl} | Height of concrete compression zone when concrete starts to crush |
| x_u | Maximum height of the concrete compression zone |
| x_{uncr} | Height of concrete compression zone in the uncracked phase |

Greek lower case letters

| | |
|------------------------------------|--|
| $\gamma_{concrete}$ | Specific weight concrete |
| γ_{dry} | Soil unit weight above phreatic level |
| γ_{sat} | Soil unit weight below phreatic level |
| δ | Wall friction angle |
| ϵ'_c | Compressive strain in concrete |
| ϵ_c | Tensile strain in concrete |
| ϵ'_s | Compressive strain in steel |
| ϵ_s | Tensile strain in steel |
| $\epsilon_{c3} = \epsilon'_{c,pl}$ | Crushing strain of concrete (compressive strain in concrete at peak stress f_c) |
| $\epsilon_{cu3} = \epsilon'_{cu}$ | Ultimate compressive strain in the concrete |
| $\epsilon_{s,pl}$ | Yielding strain of reinforcement |
| ϵ_{su} | Ultimate strain of reinforcement |
| θ | Inclination of failure plane |
| κ | Curvature |
| κ_e | Curvature corresponding to the yield moment |
| κ_{pl} | Curvature corresponding to the crushing moment |
| κ_r | Curvature corresponding to the cracking moment |
| κ_u | Curvature corresponding to the ultimate moment |
| ρ | Radius of curvature |
| $\rho_{l,min}$ | Minimum reinforcement ratio |
| $\rho_{l,max}$ | Maximum reinforcement ratio |
| σ'_c | Compressive stress in concrete |
| σ_c | Tensile stress in concrete |
| σ'_s | Compressive stress in steel |
| σ_s | Tensile stress in steel |
| σ'_H | Horizontal effective soil stress |
| σ'_V | Vertical effective soil stress |
| σ_p | The greatest effective vertical soil stress previously reached |
| σ^{0}_{yy} | The in-situ effective vertical soil stress |
| τ_f | Shear strength |
| ν | Poisson's ratio |
| $\varphi(\infty, t_0)$ | Final value of creep coefficient |
| Ψ | Dilatancy angle |
| ϕ | Internal friction angle |

1. DIAPHRAGM WALLS

1.1. In general

Diaphragm walls are reinforced in-situ concrete elements formed in the ground, which by placing multiple elements in line with each other form a continuous unanchored wall. They have an earth-retaining, water-retaining and/ or load-bearing function. The excavation work is carried out under the supporting pressure of a bentonite slurry, after which the reinforcement is placed. The excavated trench is then filled with concrete, while displacing the bentonite slurry. Figure 1 gives a schematic overview of the construction of a diaphragm wall.

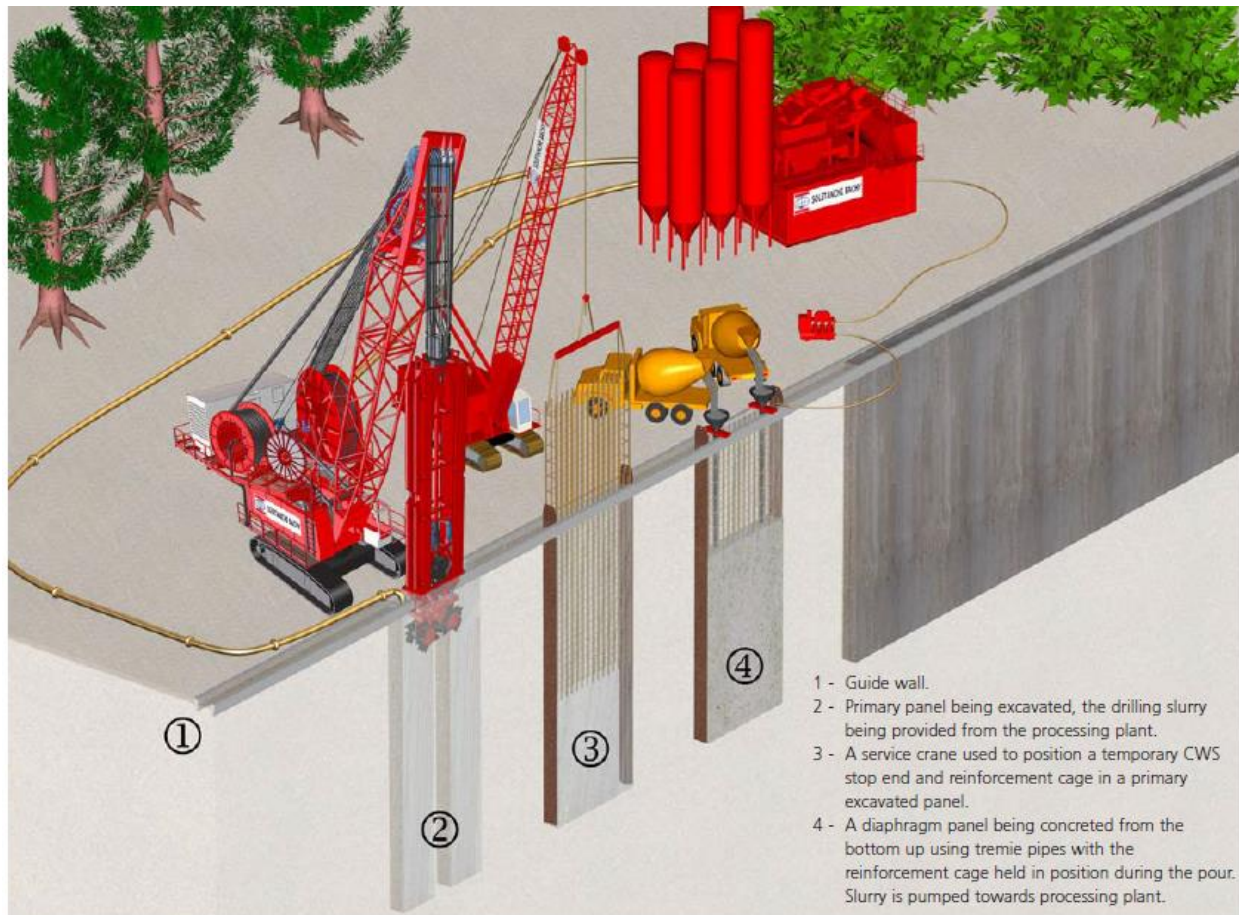


Figure 1: Construction of a diaphragm wall [1]

The process for the construction of the diaphragm wall is as follows:

- *Guide-wall construction:*

Before starting with the excavation for the panels, guiding beams are placed at surface level. The function of the guiding beams is to fix the dimensions of the diaphragm wall, to guide the service crane during excavation and to prevent caving in of the surface level.

- *Panel excavation:*

During the excavation, the trench is filled with a bentonite slurry in order to ensure the stability of the trench.

- *De-sanding bentonite:*

After the panel has been dug till the required depth, the bentonite slurry is returned to the surface for sedimentation and de-sanding. Cleaned bentonite slurry may be re-used.

▪ *Placing joint profiles and reinforcement cage:*

Joint profiles are then placed on the head-ends of the panel. These provisions are necessary to achieve tight-fitting joints between the panels, which are casted against each other. Subsequently, the reinforcement cage is positioned in the excavated trench.

▪ *Casting the diaphragm wall panels:*

The trench can now be filled with concrete using tremie pipes. The concrete has a specific composition in order to be able to displace the contaminated bentonite solution towards the top, and to maintain the density and quality of the concrete.

Instead of reinforced concrete, the diaphragm walls can also be executed, totally or partially, in prestressed concrete. The application of prestressing would particularly be useful in the SLS (Serviceability Limit State), since a more rigid wall can be accounted for (no cracking), which is favourable in the case of adjacent buildings.

The wall acts as a cantilever beam which is ‘elastically’ clamped into the soil or as a beam supported at both ends (at the bottom the soil and at the top an anchor). At the bottom the support pressure to provide equilibrium is mobilized by the passive earth resistance.

An important advantage of the installation of diaphragm walls is the vibration-free execution method. The main difference with a single steel sheet pile wall is the difference in the stiffness behaviour and the influence of friction on the force distribution. When compared to other wall types, diaphragm walls are considered to be very stiff with respect to ground movement control.

The following properties/ advantages can be attributed to the diaphragm wall:

- The execution is free from vibration and produces less noise;
- The wall is applicable in almost any soil;
- The wall can be used as a permanent wall;
- The wall can also be used as a foundation element;
- Large depths are possible, up to 100 meters;
- Large earth-and water-retaining heights are possible;
- High vertical and horizontal loads can be carried;
- High bending moment capacity and high bending stiffness;
- Low soil deformations just behind the wall as a result of the high bending stiffness of the wall;
- The wall provides structural stiffness which reduces ground movements and settlements during excavation;
- Execution is also possible in case of hard layers and small obstacles in the subsoil;
- A higher durability compared to steel sheet piling.

1.1.1. Available standards

So far, only a few standards are available in The Netherlands for the construction of diaphragm walls. The following standards can be listed:

- CUR Recommendation 76 (“Rekenregels voor diepwanden”) - Additional provisions on NEN-EN 1992-1-1;
- German standard DIN4126
- NEN-EN-1538: 2000 (“Voorschriften voor de uitvoering van diepwanden”)
- CUR Publication 189 (“Cement-bentonieschermen”). This publication can also be consulted since diaphragm walls have many similarities with cement bentonite screens.
- CUR166 (“Damwandconstructies”): For loading and stability calculations.

1.1.2. Loads, Load Distribution and Failure Mechanisms

- Loads:

From the point of view of stability, the diaphragm wall is carried out until the load-bearing (sand) layer. The horizontal load can be transferred via the diaphragm wall to the subsoil. In addition to this, the diaphragm wall sections are able to transmit large vertical loads to the subsoil (load-bearing layer).

- Load distribution:

The strength and stability of a diaphragm wall structure are determined by the material (reinforced concrete) and the surrounding soil. On the one hand, the soil gives a load on the wall (on the active side) and on the other hand it contributes to the support reaction and equilibrium (on the passive side). Because the diaphragm wall generally reaches until the load-bearing (Pleistocene) sand layer, the wall can be considered as a cantilever beam clamped into the load-bearing layer, subjected to bending. Depending on the cone resistance in the top of the load-bearing layer, hardly any or no settlement of the diaphragm wall will occur.

- Failure mechanisms:

For a diaphragm wall the following failure mechanisms can be distinguished:

- Failure due to insufficient external stability (instability of the slope by a deep (straight or circular) slip plane);

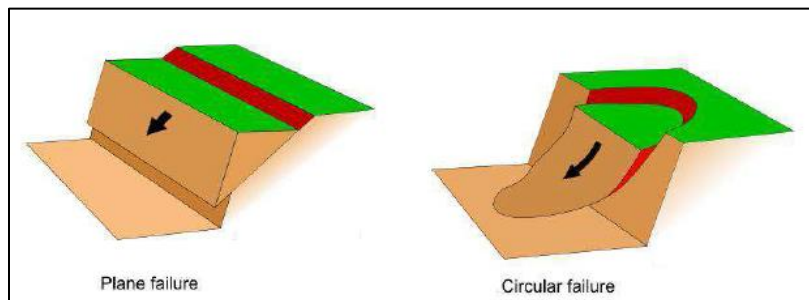


Figure 2: Simplified illustrations of most common slope failure modes [14]

- Failure due to insufficient passive earth resistance;

The active earth pressure is the force that causes the collapse of a retaining wall, while the passive earth pressure is the resisting force of the soil.

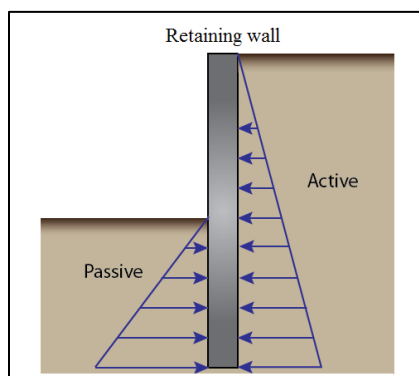


Figure 3: Active and passive earth pressure on retaining wall

- Failure of the diaphragm wall;

- When a reinforced concrete wall is subjected to bending, crack formation will occur in the concrete at the tension side for a certain curvature. As a result, the rigidity of the wall will decrease. When the load is increased further, the reinforcement may start to yield and the concrete will eventually fail at the compression side. The stiffness, which changes as a result of loading and unloading, follows a certain pattern which can be displayed by means of the M - (N) - κ diagram representing the bending moment-curvature-relationship. From this diagram the uncracked and cracked stiffnesses EI_{uncr} and EI_{cr} , as shown in Figure 4 can be derived, respectively. More detailed information on the M - (N) - κ diagram will be given in chapter 3.

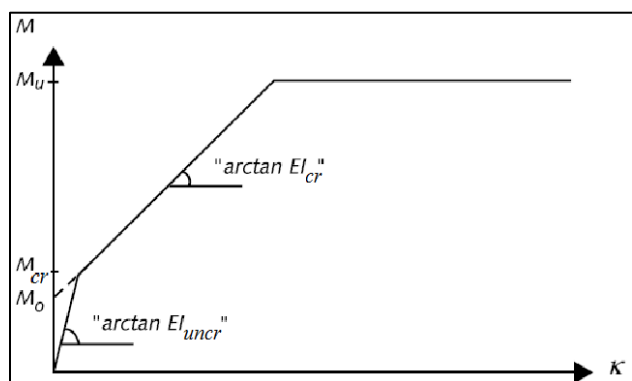


Figure 4: M - κ -diagram

1.1.3. Safety Approach regarding Design and Verification: SLS & ULS

Diaphragm walls must be designed and checked, such that the required safety is achieved. In the Eurocodes distinction is made between the Serviceability Limit State (SLS) and the Ultimate Limit State (ULS).

In practice it is important that, in addition to the ULS (namely, failure of the diaphragm wall), also the SLS is checked. This implies that it should be checked whether the structure meets the requirements of serviceability during its service life. Loss of serviceability may occur when the structure deforms too much or loses its water tightness. As a rule, the serviceability limit state is checked by calculating the deformation using the so-called "characteristic" values (conservative values for all parameters). In this deformation calculation no (partial) safety factors are included.

Practical experience has taught that the SLS is often decisive for the design. In that case, the optimization of the design based on strength, is not that relevant. For the stability of the structure the deformation/displacement behaviour is important.

1.1.4. Reliability class & design approach diaphragm wall

Considering the consequences of failure or malfunction of a structure, consequence classes (CC) have been defined for the purpose of reliability differentiation. According to NEN-EN 1990 retaining structures can be distinguished into three reliability classes (RC), of which a description is given in Figure 5. The reliability classes may be associated with the consequence classes. For most diaphragm wall structures RC2 is applicable. In case the diaphragm wall is part of a primary retaining structure, RC3 must be applied. RC1 is almost never applied for diaphragm wall structures.

Three different design approaches are given in NEN-EN 1997-1 (Eurocode 7). These approaches differ in the way allowance is made for uncertainties in modelling the effects of actions and resistances in the ULS by means of partial factors. These partial factors are applied to actions or the effects of actions from the structure, resistances or ground parameters. For the design of retaining structures in The Netherlands 'Design Approach 3' is applicable for the ULS.

| Consequences Class | Description |
|--------------------|---|
| RC3/CC3 | High consequence for loss of human life, <i>or</i> economic, social or environmental consequences very great |
| RC2/CC2 | Medium consequence for loss of human life, economic, social or environmental consequences considerable |
| RC1/CC1 | Low consequence for loss of human life, <i>and</i> economic, social or environmental consequences small or negligible |

Figure 5: Reliability classes of a structure

1.1.5. The design

- Thickness of the diaphragm wall:

The thickness of the diaphragm wall affects the required clamped length; a thicker wall will deform less, implying that the clamped length will be less compared to a thinner diaphragm wall. The thickness of the diaphragm wall depends on the equipment and can vary from 0.4 to 2.0 m.

- Embedment depth:

From the point of view of stability the diaphragm wall is generally embedded into the load-bearing layer (cantilever beam) and is therefore free of settlement.

- Reinforcement and concrete cover:

Due to the strongly varying bending moment over the height of the diaphragm wall, it is usually not efficient to apply the same reinforcement over the entire height of the diaphragm wall. As a result, the bending stiffness over the height is not constant. Depending on the applied reinforcement over the height, the diaphragm wall is divided into a number of sections. With the M- κ -diagram the relationship between the bending moment and bending stiffness can be determined for each wall section at a certain load case or load combination.

The reinforcement cage must have a high dimensional stability with regard to the placement of the reinforcement cage over the often large depth of the diaphragm wall. Furthermore, it is important to streamline the reinforcement cage as much as possible, such that the upward flowing concrete is obstructed by it as little as possible. Since the loading is mainly concentrated perpendicular to the diaphragm wall, these cages usually do not have to be linked to each other. The reinforcement ratio should, with regard to the execution (in particular, the casting of concrete), be limited to approximately 0.75%.

The service life of the diaphragm wall is substantially determined by the concrete quality of the cover. The cover needs to protect the reinforcement against corrosion. If sufficient care is taken into account during the execution, the diaphragm wall will certainly be able to achieve a lifetime of 100 years at a concrete cover of 100 to 150 mm.

- Concrete quality:

For the structural assessment of diaphragm walls no higher strength than is C45/55 must be applied.

- Diaphragm wall panels:

A diaphragm wall consists of successive wall panels, where a distinction can be made between starter-, intermediate- and closure-panels. The panel width depends on the wall layout, the possible rate of production, the stability analysis and settlement calculations. From an economic point of view it is chosen to make the panels as large as possible (6 to 8 m) and to apply the so-called 3-way corridor panels, see

Figure 6. If a large excavation depth is not possible, it can be chosen to apply 2-way panels (3 to 5 m). In case this still results in a too large excavation depth, 1-way panels are opted for in particular situations. 1-way panels are also used to limit the settlements of adjacent buildings which are very close to the diaphragm wall construction. Research has shown that a reduction of the panel width results in a reduction of the horizontal displacements.

The use of smaller and therefore more panels leads to a longer construction time and moreover, a large number of joints, which in many cases are the critical spots. The joints are in fact unreinforced zones. A relatively high number of unreinforced zones leads to a higher reinforcement ratio in the intermediate zones, which is disadvantageous for the flow during concreting. The choice for 1-way panels may also be based on logistical reasons, concerning mainly the continuous supply of concrete.

Kinks in a diaphragm wall trace are realized by means of corner panels. These should always be executed as 2- or 3-way panels.

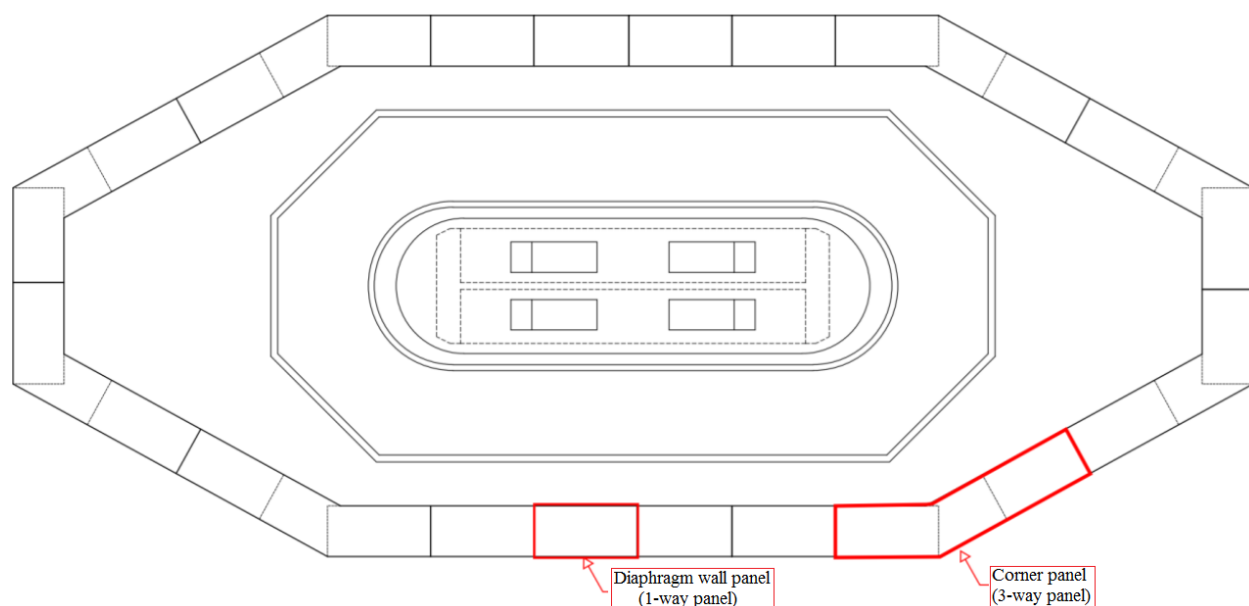


Figure 6: Panel layout consisting of 1-way and 3-way panels. The corner panels are executed as 3-way panels in order to reduce the risk of leakage at the joints.

1.2. Deformations and settlements

For the deformation state of the diaphragm wall, distinction is made between:

- The settlements;
- The horizontal deformations of the wall (or: 'lateral wall deflection')

Deformations and settlements are not only important from the perspective of meeting the functional requirements of the project, but they can also lead to collapse of the structure. Large deformations of the diaphragm wall result in large settlements of the surface level and also of the foundations of adjacent buildings. The settlement of the soil in response to the deformation of the diaphragm wall is also highly dependent on the soil properties and geological profile. The deformations depend on:

- The loading;
- The excavation depth and the draining level;
- The use of temporary struts and anchors;
- The bending stiffness of the wall. The stiffness of the diaphragm wall depends on the thickness of the diaphragm wall, the applied concrete class and the reinforcement.

In the soil, next to the diaphragm wall, deformations can be caused by:

- Relaxation of the soil;
- Deflection of the wall as a result of the excavation;
- Decrease of the water table (groundwater level) which leads to settlement.

In order to determine the lateral wall displacement, one needs to take into account:

- The deflection of the wall itself;
- The deformation of the soil;
- The deformation of anchors or struts, if applicable.

In the service state, the deformations can increase due to:

- Time effects in the soil (creep and consolidation);
- Changes in the bending stiffness of the concrete wall due to creep and crack formation.

1.2.1. Factors influencing the deformations

Several factors affect the deformation of the diaphragm wall. The most important factors will be mentioned and explained briefly to clarify their impact.

- **Soil properties:** The occurring deformations and settlements are highly dependent on the available soil properties. Stiff soil is relatively less sensitive to deformations and settlements compared to soft soil.
- **Water pressure:** The difference in water pressure against the diaphragm wall has large effects on the deformation of the wall. Higher pressure differences will lead to greater deformations.
- **Surface load:** Just like deformations of the wall affect the settlements of the surface level, so does the loading on the surface level affect the deformations of the wall. The higher the surface load, the greater the deformations.

The above-mentioned factors are imposed factors, which can be influenced very limitedly. The following factors can be influenced during the design and realization of the project:

- **Wall stiffness:** The stiffness of the diaphragm wall has a large impact on the deformations of the wall. Here it holds that: the stiffer the wall, the smaller the deformation. The deformations can be controlled by means of the thickness of the diaphragm wall, use of temporary struts and prestressing.
- **Construction method and construction phases:** The construction method and construction phases have an effect on the occurring deformations of the wall. Careful construction procedures may result in limited deformations.
- **Excavation depth:** The excavation depth is highly dependent on the design, the construction method and the construction phases. The greater the excavation depth, the greater the deformations will be due to the greater soil and water pressures.

1.2.2. Relationship deformations and settlements

In the study conducted by T. Masuda [2] an empirical approach concerning the lateral wall displacements and surface settlements in excavations is given. Figure 7 states the terms related to excavation as used in [2]. Figure 8 and Figure 9 show the maximum lateral wall deflection and the maximum surface settlements both as a function of the excavation depth (H), respectively for excavations in sands, stiff clays and residual soils. The wall types producing the data plotted in these figures are: soldier piles,

sheetpiles, diaphragm walls, soil nail walls, drilled pier walls and soil cement walls. Figure 8 and Figure 9 illustrate that:

- The maximum lateral wall deflections and maximum surface settlements were usually less than 0.5% H ;
- The maximum lateral wall deflections tended to average about 0.2% H ;
- The maximum surface settlements tended to average about 0.15% H .

Figure 10 presents typical modes of lateral wall displacements and surface settlements. In Figure 10(a) the wall deflects as a cantilever and the adjacent ground surface settles such that the settlements increase with a decreasing distance from the edge of the excavation. The settlements behind the wall form a triangular shape. The maximum displacement of the wall is located at the top of the wall, while the maximum settlement at surface level is found at the wall. When the excavation advances to deeper elevations, the upper lateral wall deflection is restrained by an excavation support and the maximum wall displacement is located at the excavation level as shown in Figure 10(b). The maximum settlement at surface level is then at a certain distance from the wall. The combination of deflections in Figure 10(a) and Figure 10(b) results in the cumulative lateral wall deflection and ground surface settlement as depicted in Figure 10(c).

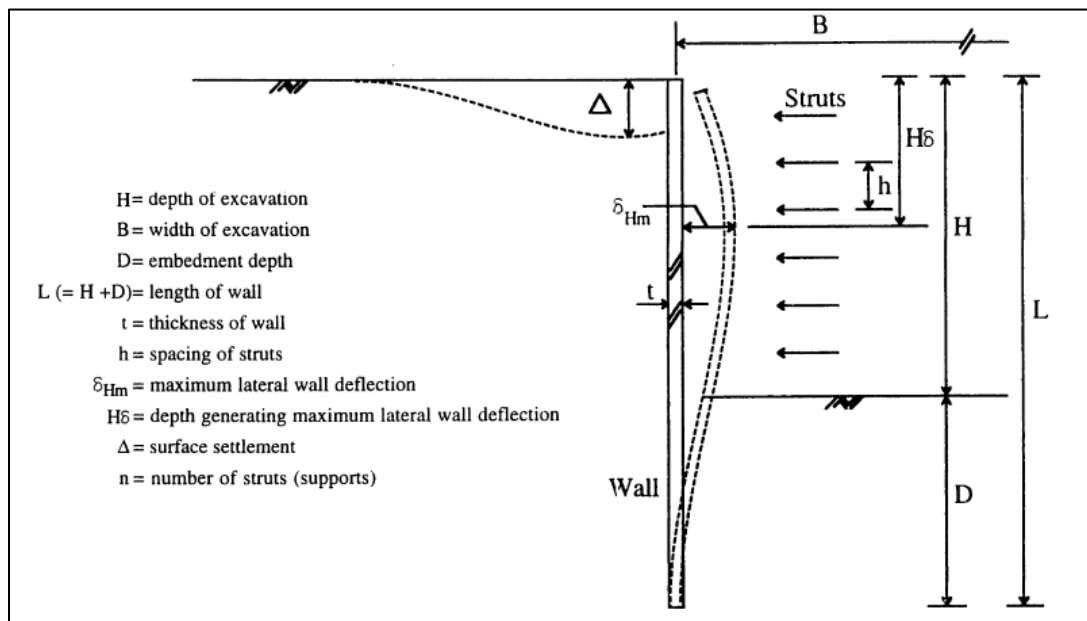


Figure 7: Terms related to excavation, according to [2]

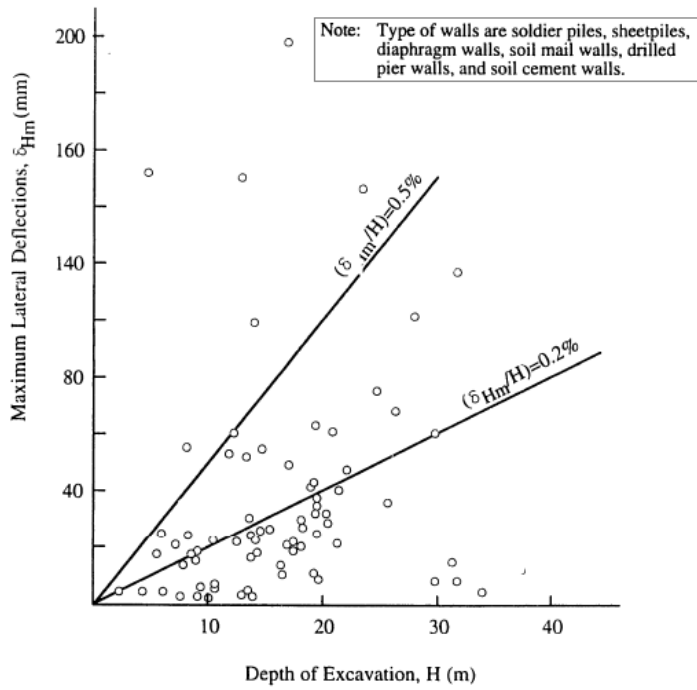


Figure 8: Maximum lateral wall deflections in Sands, Stiff Clays and Residual Soils [2]

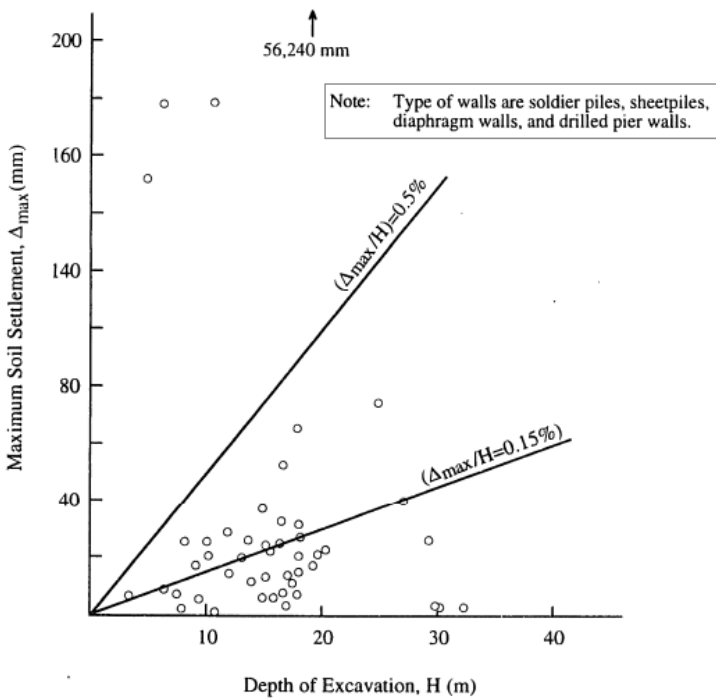


Figure 9: Maximum surface settlements in Sands, Stiff Clays and Residual Soils [2]

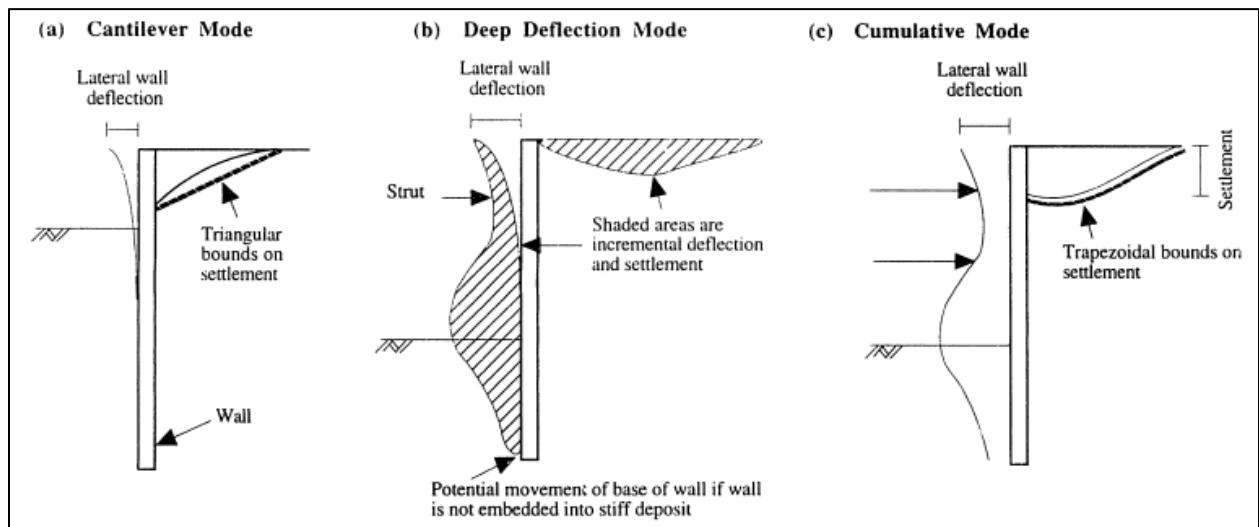


Figure 10: Typical mode of lateral wall displacement and surface settlements: (a) Initial stage of excavation, no support, (b) Upper lateral wall displacement restrained by a strut, (c) Combination of deflections of (a) and (b) [2]

1.2.3. Reducing deformations and settlements

The occurring settlements can be reduced by limiting the deformation of the structure. In order to reduce the deformations of the diaphragm wall, the following measures can be taken:

- Apply temporary struts;
- Increase the bending stiffness of the diaphragm wall by means of:
 - Increasing the wall thickness;
 - Applying more reinforcement;
 - Applying prestressing;
 - Applying steel profiles (e.g. HEM-profiles) in the diaphragm wall.

It is common practice to apply temporary struts and more reinforcement, instead of prestressing in the diaphragm walls.

1.2.4. Calculation software

In order to determine the interaction between loading, bending stiffness diaphragm wall and occurring deformations, the following calculation programs are available:

- PCSheetPileWall: Determination of force distribution, bending stiffness and deformation diaphragm wall;
- Plaxis 2D: Determination of force distribution, relationship between the deformation of the diaphragm wall and the occurring settlement.

In a discrete (spring) model, such as PCSheetPileWall, the soil stiffness has a great influence on the deformations, while its impact on the force distribution is much smaller. A better calculation model is the finite element model, such as Plaxis 2D. It gives a qualitative good insight into the deformations of the wall and the soil. In general, the calculated deformation mainly depends on the chosen soil model and the associated soil parameters.

1.3. Soil-structure interaction

Soil is a complicated material that behaves non-linearly and often shows anisotropic and time-dependent behaviour when subjected to stresses. The non-linear behaviour implies that the soil deformations do not increase linearly with the increasing soil stresses. In compression soil becomes stiffer. Sand, which at the surface shows no cohesion, exhibits an increasing stiffness and strength when subjected to all-sided compression. The explanation can be found in the fact that the space between the particles decreases as the soil is compressed. This leads to an increase of the forces between the particles, an increase of the number of contacts between the particles and an increase of the contact surface between the particles, resulting in a higher soil stiffness. Since in general the stresses increase with the depth, it can be expected that the soil stiffness increases with the depth. A pile foundation embedded in deep sand for instance, extracts a large part of its bearing capacity from the high stiffness of the soil (deep sand) lying under high pressure. The upper lying layers cause a high pressure in the deep sand, which now acts as a very stiff layer, making it possible to allow very large forces on the pile. It can be concluded that the soil stiffness depends significantly on the stress-level; the soil stiffness increases with compression and generally increases with the depth (higher stresses).

Diaphragm walls are in direct contact with the soil. When external forces act on the structure, neither the structural displacements nor the soil displacements, are independent of each other. The soil-structure interaction is a process in which the response of the soil influences the motion of the structure and the motion of the structure influences the response of the soil.

For the modelling of soil behaviour, several models are available which are based on the material behaviour in terms of stiffness and strength. Stiffnesses of soil and structural elements obviously play a role in the distribution of forces. On one hand, an accurate determination of the soil stiffnesses is important to obtain a proper load distribution in the structure; the stiffness behaviour of the soil mainly depends on the stress state present therein. On the other hand, the bending stiffness of the diaphragm wall plays an important role in the equilibrium of forces between the soil and the diaphragm wall, because the deformation of the diaphragm wall depends on the horizontal soil pressures.

Movements of the wall may lead to relatively large deformations in the soil, which may cause serious structural damage in parts of the construction, adjacent structures or facilities. Deformations will be judged by the impact they have on surface or underground objects. The deformation criteria for selected representative buildings or structures in the vicinity of the underground structure are determined on the basis of the deformation capacity. However, the stiffness of the structure will determine the deformation behaviour. A rigid structure will tilt; a weak structure can sag. In literature relative rotations of 1: 500 to 1: 2000 are regarded as permissible.

1.4. Deformation requirements (ProRail)

For deformations of retaining walls a distinction is made into the limit states:

- ULS, type B. This is achieved if the deformation of the retaining wall leads to failure of an adjacent structure;
- SLS. This is achieved if the deformation of the retaining wall results in exceeding the maximum allowable displacement for the wall and/or for the adjacent structure.

The ULS, type B does not always apply for retaining structures. For this research the SLS is representative, using calculations based on characteristic values of the parameters.

Railways – ProRail requirements

The CUR166 provides requirements concerning allowable horizontal deformations for retaining structures which are loaded by railways. These requirements are based on the design regulations and guidelines of ProRail. To reduce the rail maintenance, the deformation of retaining structures along and in the rails must be limited. The following requirements hold for the SLS:

- The horizontal displacement of a retaining structure at the level of the top of the rails may not be greater than 10 mm;
- The total deflection of the retaining wall should not be greater than 1/100 of the depth of excavation with a maximum of 40 mm (aesthetic requirement).

2. SOIL MODELS

2.1. Calculation methods

In general three calculation methods, incorporating the interaction of the soil and the structure, are available for retaining walls. The calculation-based approaches can be used to predict stresses, loads, and system movements. In the following, these methods will be addressed briefly:

- Blum's Equivalent Beam Method
- Beam on Elastic Foundation Method
- Finite Element Method

2.1.1. Blum method

The Blum method assumes a failure situation in the soil in which the deformations are so large that maximum shear stresses can develop. This method uses calculations with minimum active and maximum passive earth pressures. The magnitudes of the earth pressures are determined and the wall calculation can be carried out as a supported beam calculation (the wall can be unanchored, single or multiple anchored, freely supported or with fixed ends). The Blum method cannot be used for walls with a very high bending stiffness, such as diaphragm walls. The deformations that occur usually remain so limited that no minimum active and maximum passive earth pressures can develop [3].

2.1.2. Beam on Elastic Foundation Method (BEF)

The soil pressures are modelled with a series of independent spring supports similar to the Winkler elastic foundation model. The spring constant is the ratio of stress (p) to displacement (w), which can be expressed as follows:

$$k_s = \frac{p}{w} \quad (\text{Eq. 2.1})$$

where the constant k_s is called the modulus of subgrade reaction or soil spring constant. The modulus of subgrade reaction is not a true soil property, but rather depends on both the soil conditions and the geometry of the excavation being modelled.

The Winkler elastic foundation model approximates the wall-soil interaction with a one-dimensional model instead of a two-dimensional model that includes the soil mass, and hence does not include the effects of arching within the soil mass. The strength of this model is that it greatly simplifies the analysis, for it assumes the elements are individually acting without interaction.

Winkler's idealization represents the soil medium as a system of identical but mutually independent, closely spaced, discrete, linearly elastic springs (Figure 11a). In general, the soil behaviour is linear and the model lacks continuity among the springs. According to this idealization, deformation of the structure due to the applied load is confined to loaded regions only. If the structure is subjected to a partially distributed surface loading (q), the springs will not be affected beyond the loaded region. For such a situation, an actual foundation is observed to have the surface deformation as shown in Figure 11b. Hence, by comparing the behaviour of a theoretical model and an actual structure (Figure 11c), it can be seen that this model essentially suffers from a complete lack of continuity in the supporting medium. The fundamental problem with the use of this model is to determine the stiffness of the elastic springs used to replace the soil. The predicted wall displacements are very sensitive to the values of subgrade modulus used in the analysis. The BEF-method does not directly estimate vertical ground movements behind the wall. Ground movements behind the wall are evaluated using the calculated wall displacement from the model. An empirical relationship between wall movement and ground movements must then be used [4,5,6].

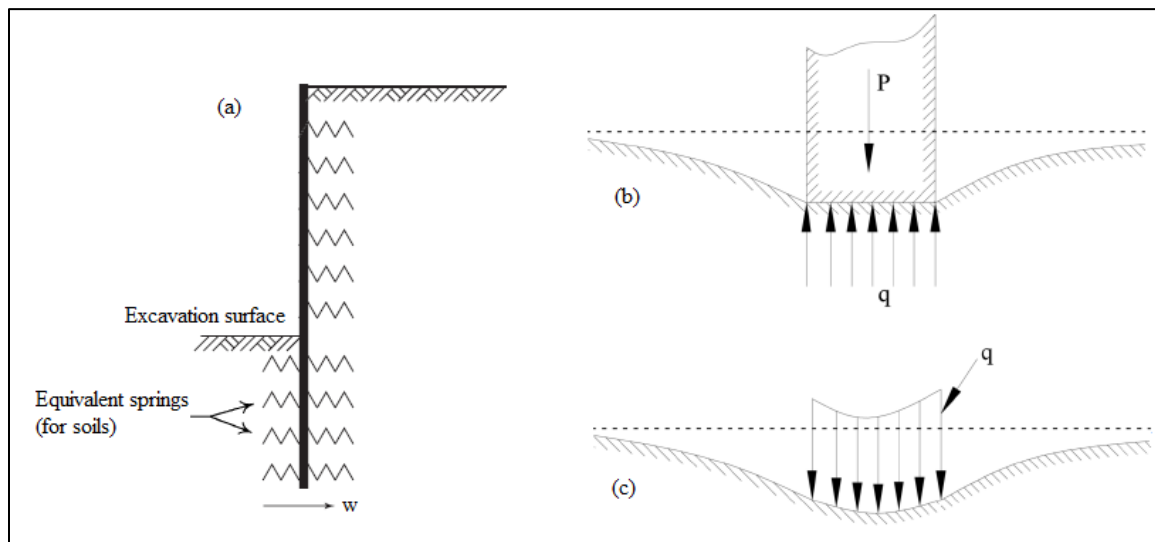


Figure 11: Interaction model: (a) Distribution of soil reactions on the wall; (b) Behaviour according to theoretical model; (c) Behaviour of real structure.

The soil-structure interaction is taken into account by modelling the wall as an elastic beam resting on uncoupled springs. Based on the displacement method, the following differential equation needs to be solved:

$$EI \frac{d^4 w}{dx^4} + kw = f \quad (\text{Eq. 2.2})$$

This formula consists of three terms, where:

- Term 1: Represents the bending stiffness of the wall
- Term 2: Represents the spring supports for soil and anchors.
- Term 3: Represents the external load, other than from the subsoil.

▪ Influence of EI and k_s on the wall behaviour

For the BEF-analysis it is found that the calculated load distribution over the wall is usually closer to reality than the calculated displacements. The k_s has a lower impact on the bending moments than on the displacements. The reason behind it is that the displacement is a direct function of k_s , whereas the bending moment is proportional to the 4th root of k_s . The occurring load distribution and the displacements are not only determined by the soil spring stiffness, but are rather a result of the mutual relationship between the wall stiffness (EI), the soil spring stiffness (k_s) and the spring stiffness of anchors.

Assuming a homogeneous soil profile at an unanchored wall, the magnitude of k_s has a negligible influence on the maximum moment and a great influence on the deformation. The effect of EI on both the moment and the deformation remains small in absolute terms, which is made clear in Figure 12. For an anchored wall this interaction between EI, k_s , the bending moments and the deformations is not so obvious. In Figure 13 the influence of variations of the above-mentioned factors is outlined schematically. For anchored walls with a relatively low bending stiffness the deformation pattern of the wall is strongly influenced by the anchor stiffness.

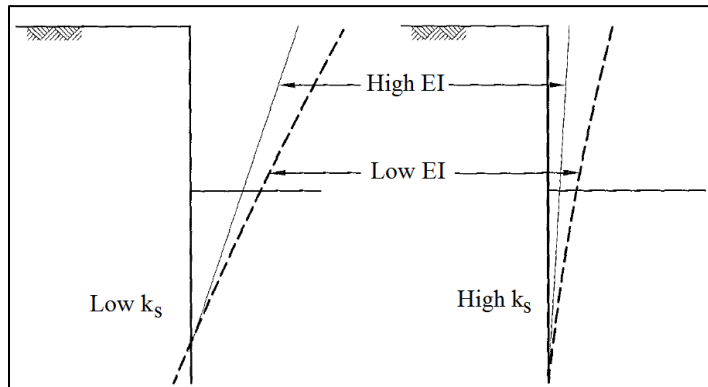


Figure 12: Influence of the wall stiffness (EI) for an unanchored wall. The occurring moment is equal for both cases

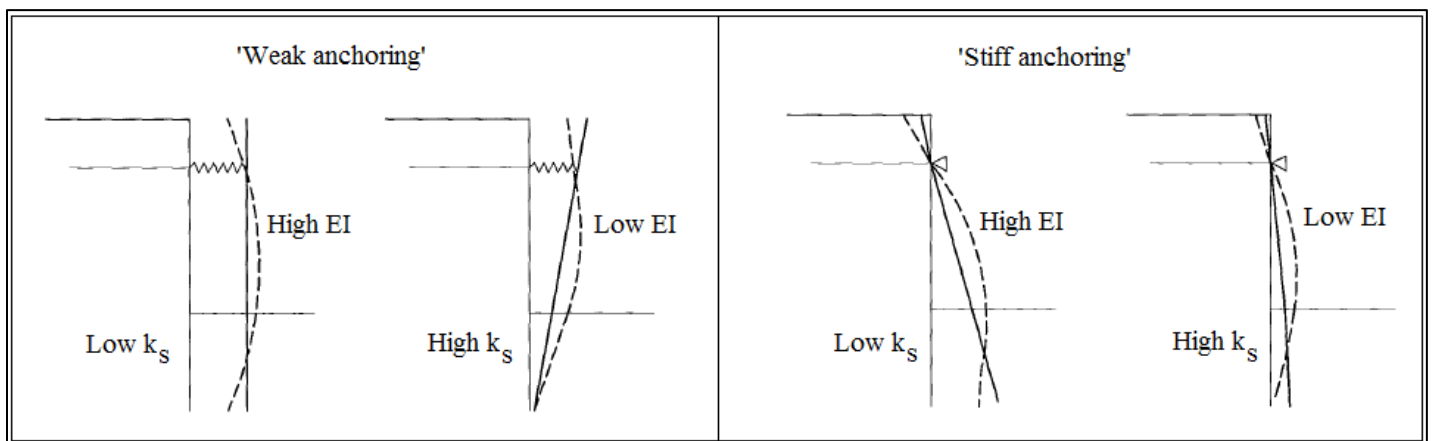


Figure 13: Influence of the wall stiffness (EI) and the soil stiffness (k_s) for an anchored wall

2.1.3. Finite Element Method (FEM)

The finite element method is based on a model in which the behaviour of soil and structure is integrated. The properties of soil are introduced by means of stress-deformation relations. With this method fundamental calculations of stresses and deformations of soil and structural members can be made. The method can be used to calculate sectional forces of the structural members, verify the global stability of the structure and to calculate and verify deformations [7].

In contrast to the BEF-analysis, the FEM-analysis can provide direct information on the ground movements outside of and inside the excavation. It can also be used to model the soil-structure interaction response of nearby structures to the excavation-induced ground movements. Another difference between the FEM- and BEF-methods is that variations in the soil stiffness (modulus) can have a greater effect on predicted loadings and movements due to the inclusion of soil arching in the FEM-model [4]. An example is shown in Figure 14.

Because the FEM-analysis gives, compared to the BEF-analysis, a more accurate prediction of the soil-structure interaction, this calculation method will mainly be used throughout this research for determining the load distribution and deformations. Herewith, the software package PLAXIS 2D will be used to analyse and calculate geotechnical structures. The software package PCSheetPileWall is based on the BEF-analysis, and is especially used in order to define the bending stiffness of the diaphragm wall over its height. A description of the above-mentioned calculation programs, together with their features, is given in section 2.4.

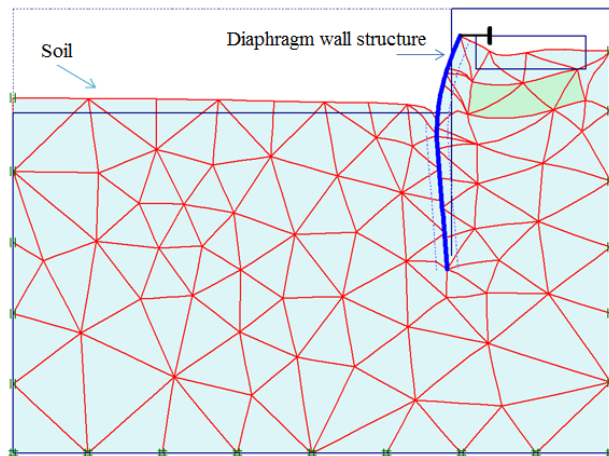


Figure 14: Deformed mesh in Plaxis 2D

2.2. Material models

This paragraph briefly describes the conventional constitutive soil models in FEM. The description of these models will be based on the material models in PLAXIS, as the latter can be considered to be the most commonly used FEM in the geotechnical field in the Netherlands. The different material models are [7]:

- **The Linear Elastic Model (LE)**

This model represents Hooke's law of isotropic linear elasticity, which is used to simulate the soil behaviour.

- **The Mohr-Coulomb Model (MC)**

The Mohr-Coulomb model is characterized by a transition from linear elastic to perfectly plastic, defined by the Mohr-Coulomb failure criterion.

- **The Hardening Soil Model (HS)**

The Hardening Soil Model also uses the Mohr-Coulomb failure criterion. However, the description of the soil stiffness is much more advanced. It includes shear hardening, compression hardening, stress-dependency of stiffness moduli, it allows for the introduction of pre-consolidation and it distinguishes between elastic behaviour during unloading and reloading.

- **The Hardening Soil Small Strain Model (HSS)**

This model can be considered to be a modification of the HS-model. It includes an increased stiffness at small strains, resulting in more reliable deformations.

- **The Soft Soil Creep Model (SSC)**

The Soft Soil Creep Model includes the description of viscous behaviour of soils (e.g. creep), which is especially of interest when encountering soft soils. The SSC-model also uses the Mohr-Coulomb failure criterion, it includes stress-dependency of stiffness moduli, it allows for the introduction of pre-consolidation stress and it distinguishes between unload/reload behaviour. For unloading problems the SSC-model provides comparable results as the MC-model.

Generally speaking the HS-model (with or without small strain stiffness) is considered to be the most suitable model for retaining structures. This model is suitable for all soils, but does not account for viscous effects. The LE-model is very limited for the simulation of soil behaviour and it is primarily used for stiff structures in the soil. The MC-model should only be used for a relatively quick and simple first analysis of the problem considered. When good soil data is lacking, there is no use in further more

advanced analyses. The SSC-model should be used whenever time-dependent behaviour becomes dominant due to the presence of pre-dominantly soft soils. The HSS-model must be considered especially when it is important that deformations are calculated with higher accuracy [7, 8].

In Plaxis 2D (version 8) we also distinguish the Soft Soil Model (SS) and the Jointed Rock Model (JR). Although the capabilities of the SS-model are superseded by the HS-model, this model is retained and can be used for normally consolidated clay-type soils. The JR-model can be used to simulate the behaviour of stratified or jointed rock.

2.3. Soil parameters

When designing geotechnical structures, it is necessary to know the pertinent parameters controlling the soil behaviour. Most of the characteristic soil parameters can be determined based on soil investigation. In case it is not feasible to measure the necessary soil parameters directly, these parameters can be derived from statistical analyses of test results. The soil parameters used in this research are described in the following.

2.3.1. Horizontal soil pressure coefficients

Effective stresses:

When a load is applied to soil, it is carried by the water in the pores as well as the solid grains. The increase in pressure within the porewater causes drainage (flow out of the soil), and the load is transferred to the solid grains. The rate of drainage depends on the permeability of the soil. The strength and compressibility of the soil depend on the stresses within the solid grains called effective stresses. The effective stresses are a measure for the forces in the contact points of the grains. Thus, the total stress is a summation of the effective stress and the porewater pressure:

$$\sigma = \sigma' + p \quad (\text{Eq. 2.3})$$

Where:

| | | |
|-----------|--------------------|----------------------|
| σ | Total stress | [kN/m ²] |
| σ' | Effective stress | [kN/m ²] |
| p | Porewater pressure | [kN/m ²] |

It needs to be noted that an important special feature of soil is that it can transfer compressive stresses, but no tensile stresses. Furthermore, shear stresses can only be transferred if they are relatively small, compared to the normal stresses.

Horizontal soil pressure coefficients:

The importance of the effective stresses lies in the fact that the soil behaviour is governed by it. The horizontal and vertical effective stresses are assumed to be proportional to each other, expressed in the horizontal soil pressure coefficient:

$$K = \frac{\sigma'_H}{\sigma'_V} \quad (\text{Eq. 2.4})$$

Where:

| | | |
|-------------|--------------------------------------|----------------------|
| K | Horizontal soil pressure coefficient | [-] |
| σ'_H | Horizontal effective stress | [kN/m ²] |
| σ'_V | Vertical effective stress | [kN/m ²] |

The horizontal soil pressure coefficient K depends on the physical soil properties ϕ , c , and δ and the sliding plane (straight or curved). In case of no horizontal underground deformation (wall does not move), the relationship between the horizontal and vertical effective stress is expressed in terms of the neutral horizontal soil coefficient K_0 . The dimensioning calculations for the wall are based on the active and the passive horizontal effective stress. For an active sliding plane the ground wedge moves downwards (wall moves away from the soil in horizontal direction). For a passive sliding plane the ground wedge moves upwards as a result of the counterpressure provided by the soil in order to resist the displacement of the wall. The active and passive horizontal soil pressure coefficients are expressed as K_a and K_p , respectively.

For the neutral horizontal soil coefficient K_0 the following correlation according to Jaky is applicable for cohesionless soils:

$$K_0 = 1 - \sin \phi \quad (\text{Eq. 2.5})$$

According to the theory of Müller-Breslaue, the active and passive horizontal soil pressure coefficients for straight sliding planes are expressed as follows [15, 16]:

$$K_a = \frac{\cos^2 \phi}{\left(1 + \sqrt{\frac{\sin \phi \sin(\phi + \delta)}{\cos \delta}}\right)^2} \quad (\text{Eq. 2.6})$$

$$K_p = \frac{\cos^2 \phi}{\left(1 - \sqrt{\frac{\sin \phi \sin(\phi + \delta)}{\cos \delta}}\right)^2} \quad (\text{Eq. 2.7})$$

Where:

| | | |
|----------|-------------------------|-----|
| ϕ | Internal friction angle | [°] |
| δ | Wall friction angle | [°] |

Determination of the horizontal stresses as a result of the effective stresses according to the earth pressure theory of Rankine results in the following formulas for the soil pressure coefficients K_a and K_p [17]:

$$K_a = \frac{1 - \sin \phi}{1 + \sin \phi} \quad (\text{Eq. 2.8})$$

$$K_p = \frac{1 + \sin \phi}{1 - \sin \phi} \quad (\text{Eq. 2.9})$$

2.3.2. Cohesion (c) and Internal friction (ϕ)

The shear strength of a soil mass is the internal resistance per unit area that the soil mass can offer to resist failure and sliding along any plane inside it. Understanding shear strength is the basis to analyze soil stability problems such as bearing capacity, slope stability, and lateral pressure on earth-retaining structures. Soil derives its shear strength from two sources:

- Cohesion between particles (stress independent component).
According to soil mechanics the cohesion (c) is defined as the shear strength when the compressive stresses are equal to zero.
- Frictional resistance between particles (stress dependent component).
The internal friction angle (ϕ) is the measure of the shear strength of soils due to friction [10,11, 13].

Mohr-Coulomb Failure Criterion

Mohr (1900) presented a theory for rupture in materials that contended that a material fails because of a critical combination of normal stress and shearing stress, and not from either maximum normal or shear stress alone. Mohr's failure envelope is a curved line. For most soil mechanics problems, it is sufficient to approximate the shear stress on the failure plane as a linear function of the normal stress (Coulomb, 1776). The functional relationship between normal stress and shear stress on a failure plane can be expressed by means of the Mohr-Coulomb failure criterion (see Figure 15) [9, 11]:

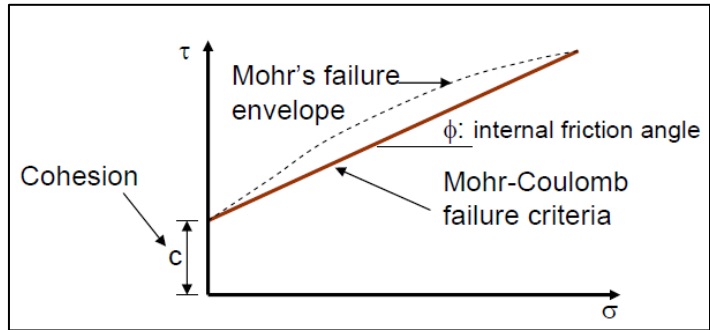


Figure 15: Failure envelope [9]

$$\tau_f = c + \sigma' \cdot \tan \phi \tag{Eq. 2.10}$$

Where:

| | | |
|----------------|--|----------------------|
| c | Cohesion | [kN/m ²] |
| φ | Internal friction angle | [°] |
| σ' | Normal effective stress on the failure plane | [kN/m ²] |
| τ _f | Shear strength | [kN/m ²] |

As stated by the Mohr-Coulomb failure criterion, failure from shear will occur when the shear stress on a plane reaches the shear strength (τ_f). The inclination of the failure plane (θ) is determined with the major and minor principal plane, see Figure 16, where σ₁ and σ₃ are the major and minor effective principal stresses. To determine the angle θ and the relationship between σ₁ and σ₃, reference is made to Figure 16 (b), which is a plot of the Mohr's circle for the stress-state shown in Figure 16 (a). The soil element does not fail if the Mohr circle is contained within the envelope. As the loading progresses, the Mohr circle becomes larger and finally failure occurs when Mohr circle touches the envelope [11,12].

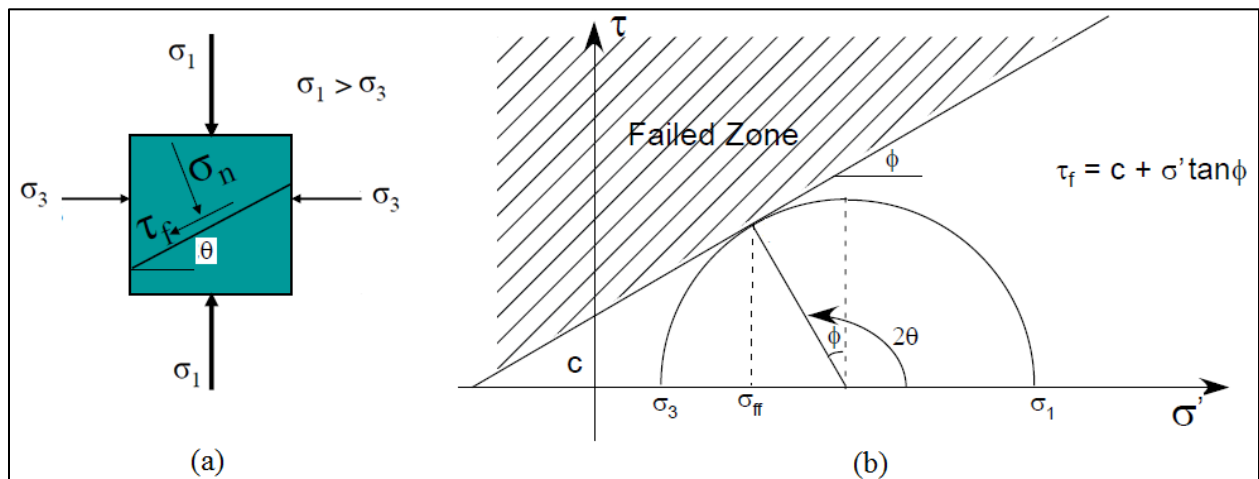


Figure 16: (a) Inclination of failure plane in soil with major principal plane; (b) Mohr's circle and failure envelope [10]

2.3.3. Wall friction (δ)

An important parameter in the calculation of the horizontal soil pressure against the wall is the wall friction angle δ . This is the angle between the force due to the soil pressure and the normal to the plane of the wall. The direction of the wall friction angle has a large influence on the value of the soil pressure at both the active and the passive side. The wall friction angle δ is positive when it is directed counterclockwise.

For an active sliding plane the ground wedge is moving downwards resulting in a positive δ , while for a passive sliding plane the ground wedge is moving upwards resulting in negative δ . This is represented in Figure 17. In this figure the straight sliding surfaces are used to schematize the situation. The dotted lines represent the actual sliding surfaces. A decrease of the wall friction angle results in an increase of the active and passive soil pressure.

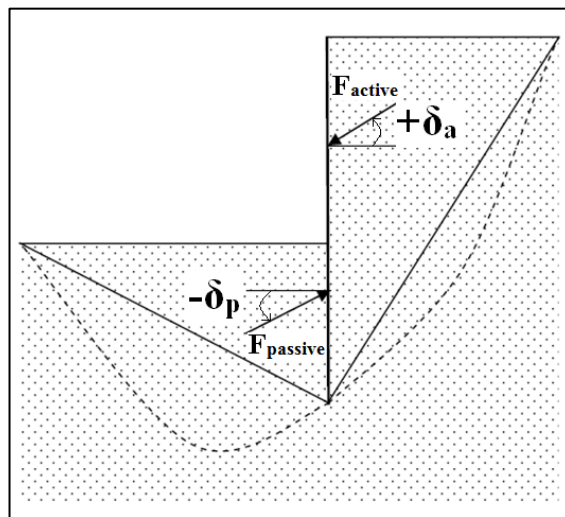


Figure 17: Direction of the wall friction angle δ [15]

For smooth steel sheet pile walls it is assumed that $\delta = \text{minimum}(2/3\phi, 20^\circ)$ for straight sliding planes or $\delta = \text{minimum}(\phi - 2.5^\circ, 30^\circ)$ for curved sliding planes. These values are often also applied for diaphragm walls. It is doubted whether this is correct since the rough surface of the concrete may lead to a higher wall friction angle. However, the bentonite cake remaining between the wall and the surrounding soil could affect the friction properties adversely [18].

The CUR231 [18] indicates that for calculations with a BEF-model it is advised to use the following:

- Based on curved sliding planes: $\delta = \text{minimum}(\phi, 20^\circ)$
 - Based on straight sliding planes: $\delta = \text{minimum}(2/3\phi, 13,3^\circ)$
- For FEM calculations, $\delta = \text{minimum}(\phi, 20^\circ)$ must be chosen.

2.3.4. Dilatancy (ψ)

The dilatancy angle, ψ , determines the plastic volume expansion due to shearing. This tendency of compacted granular material to expand in volume occurs because the grains in a compacted state are interlocking and therefore do not have the freedom to move around one another. For fine grained, cohesive soils, the dilatancy angle tends to be small; it may often be assumed that ψ is equal to zero. Apart from heavily overconsolidated layers, clay soils show little dilatancy ($\psi \approx 0$). The dilatancy of sand depends on both the density and the internal friction angle. For quartz sands the order of magnitude is $\psi \approx \phi - 30^\circ$. For ϕ -values of less than 30° , however, the dilatancy angle is mostly zero. A small negative value for ψ is only realistic for extremely loose sands [8, 19].

2.3.5. Permeabilities (k_x and k_y)

Permeabilities have the dimension of velocity (unit of length per unit of time) and are of main importance for consolidation analyses and groundwater flow calculations. *Consolidation* is the dissipation of excess pore pressure with time, accompanied by volume change. The rate of consolidation (volume change with seepage) not only depends on the permeability of the soil, but also on the size of the consolidating layer. Distinction can be made between a horizontal permeability, k_x , and a vertical permeability, k_y , since in some types of soil (for example peat) there can be a significant difference between horizontal and vertical permeability. Sands have a high permeability, while clays have a low permeability [20, 21].

2.3.6. Drained/ undrained loading

Under *drained* loading conditions no excess pore pressures are generated. This is clearly the case for dry soils and also for full drainage due to high permeability (e.g. in sands and gravels) and/or a low rate of loading. Under fully drained conditions the pore pressures do not change.

Undrained behaviour is used in case of a full development of excess pore pressures. Flow of pore water can sometimes be neglected due to a low permeability (e.g. in clays) and/or a high rate of loading. Under undrained conditions there can be no volume change, since water cannot escape [20, 21].

2.3.7. Saturated and unsaturated weight (γ_{sat} and γ_{unsat})

The saturated and the unsaturated weight refer to the total unit weight of the soil skeleton including the fluid in the pores. The unsaturated weight γ_{unsat} applies to all material above the phreatic level, while the saturated weight γ_{sat} applies to all material below the phreatic level. For sands, for instance, the saturated weight is generally around 20 kN/m^3 whereas the unsaturated weight can be significantly lower, depending on the degree of saturation. In practical situations soils are never completely dry. Hence, it is advisable not to use the fully dry unit weight for γ_{unsat} [21].

2.3.8. Modulus of subgrade reaction (k_s) - Secant

The modulus of subgrade reaction, k_s , is a deformation parameter of the soil and describes the ratio between an increment of horizontal stress and an increment of wall displacement (see (Eq. 2.1)). The modulus of subgrade reaction, also referred to as the soil spring stiffness, is not a constant value but actually depends on the depth in the soil and the magnitude of the deformation. For computer programs this soil parameter is usually divided into one, two or three linear branches. The Secant definition based on the stress-displacement diagram according to CUR 166 always uses three branches with intersections at 50, 80 and 100 % of $K_a - K_p$, as indicated in Figure 18. This tri-linear relation for the soil stiffness gives a better approximation of the real behaviour than the use of a single spring stiffness constant. The slope of the different branches is defined indirectly, via the three secant moduli at the intersection points. The choice for the size of the spring stiffness constant is mostly of importance for the calculation of the displacements of the wall [16, 22, 23].

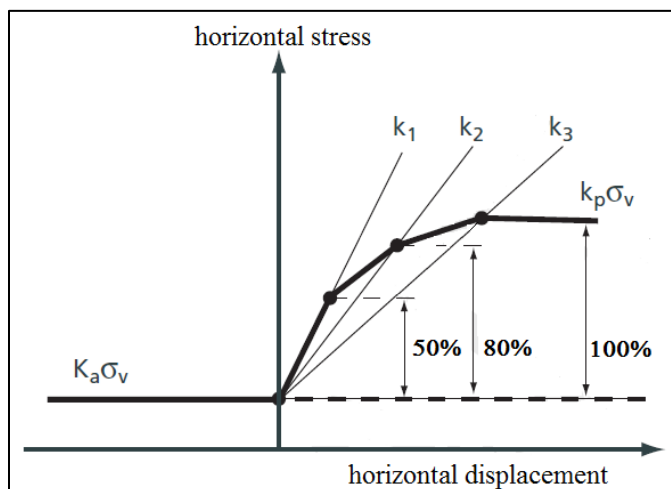


Figure 18: Non-constant value for the soil spring stiffness - approximation by 3 straight lines (CUR 166). Input via 3 secans values (k_1 , k_2 and k_3) [23]

2.3.9. Stiffness moduli (E)

The Young's modulus is the basic stiffness modulus in an elastic model. Since many soil layers exhibit non-linear behaviour in the stress-strain diagram from the very beginning of loading, the soil stiffness is described much more accurately by using three different input stiffnesses:

- The triaxial loading stiffness or secant modulus, E_{50} ,
- The triaxial unloading stiffness, E_{ur} , and
- The oedometer loading stiffness E_{oed} .

As average values for various soil types, we have $E_{ur} \approx 3 E_{50}$ and $E_{oed} \approx E_{50}$, but both very soft and very stiff soils tend to give other ratios of E_{oed}/E_{50} [8]. These above-mentioned stiffness moduli are explained in the following.

In soil mechanics the initial slope is usually indicated as E_0 and the secant modulus at 50% strength is denoted as E_{50} . For materials with a large linear elastic range it is realistic to use E_0 , but for loading of soils one generally uses E_{50} . Considering unloading problems, as in the case of tunnelling and excavations, one needs E_{ur} instead of E_{50} . For soils, both the unloading modulus, E_{ur} , and the first loading modulus, E_{50} , tend to increase with the confining pressure. Hence, deep soil layers tend to have greater stiffness than shallow layers. Moreover, the observed stiffness depends on the stress path that is followed. The stiffness is much higher for unloading and reloading than for primary loading [8]. The stiffness moduli E_0 , E_{50} and E_{ur} are depicted in the stress-strain diagram of Figure 19.

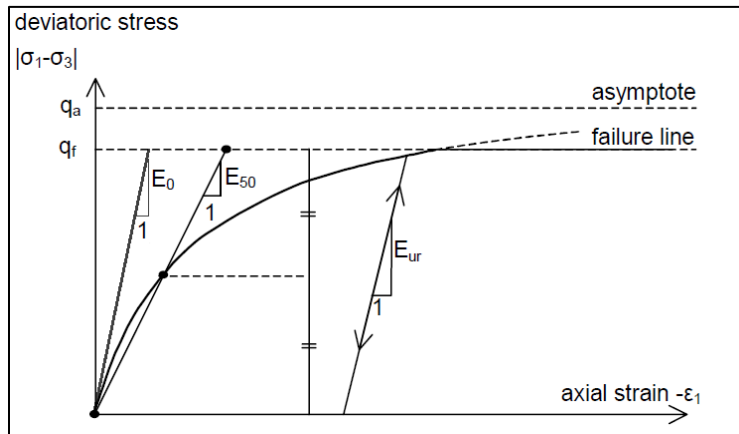


Figure 19: Hyperbolic stress-strain relation in primary loading for a standard drained triaxial test [8]

The oedometer modulus E_{oed} characterizes the soil stiffness in case of one-dimensional compression. The oedometer modulus E_{oed} relates to the Young's modulus, according to Hooke's law of isotropic elasticity, involving the Poisson's ratio ν :

$$E_{oed} = \frac{(1-\nu)E}{(1-2\nu)(1+\nu)} \quad (Eq. 2.11)$$

The amount of stress-dependency of the stiffness moduli is taken into account by means of a power law, using the parameter m . The formulas, including this power of soil hardening m , will not be dealt with further in this report, but instead reference is made to [8]. For a certain stress level the stiffness moduli are given as E_{50}^{ref} , E_{ur}^{ref} and E_{oed}^{ref} . This m -value may vary between 0 and 1 (gravel: 0.5; sand: 0.55-0.75; mud: 0.75; clay: 1.0) [24, 41].

2.3.10. OCR and POP

In order to determine the soil pressure it is important to take into account the loading history of the soil. Higher occurring loads in the past may have caused a reduction of vertical stresses, while the horizontal stresses remained significantly higher. This is called overconsolidation. If a material is overconsolidated, information is required about the Over-Consolidation Ratio (OCR):

$$OCR = \frac{\sigma_p}{\sigma_{yy}^{i0}} \quad (Eq. 2.12)$$

Where:

σ_p The greatest effective vertical stress previously reached [kN/m²]
 σ_{yy}^{i0} The in-situ effective vertical stress [kN/m²]

One identifies:

- Lower consolidated soil if $OCR < 1$
- Normally consolidated soil if $OCR = 1$ and
- Overconsolidated soil if $OCR > 1$.

It is also possible to specify the initial stress state using the Pre-Overburden Pressure (POP) as an alternative to prescribe the over-consolidation ratio. The Pre-Overburden Pressure is defined by:

$$POP = \left| \sigma_p - \sigma_{yy}^{i0} \right| \quad (Eq. 2.13)$$

These two ways of specifying the vertical pre-consolidation stress are illustrated in Figure 20.

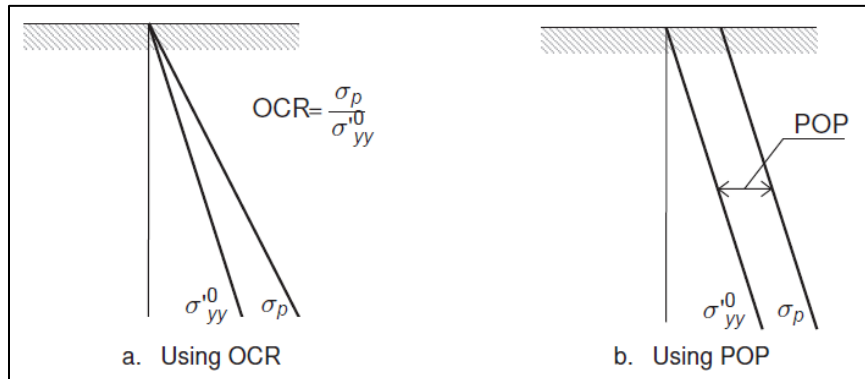


Figure 20: Illustration of vertical pre-consolidation stress in relation to the in-situ vertical stress [8]

2.4. Calculation software

In order to investigate the soil-structure interaction, two calculation software programs will be used during this research, in particular:

- PCSheetPileWall (Version 1.36) – a discrete model and;
- Plaxis 2D (Version 8) – a continuous model.

The geometric and physical nonlinearities are taken care of by the software programs. In case of geometric nonlinearity the force distribution is influenced by the deformation; here the equilibrium of forces is based on the deformed geometry of the structure. The physical nonlinearity concerns a changing bending stiffness EI as the load increases. In PCSheetPileWall, both the geometric and physical nonlinearity are included by the program itself. However, this is not totally the case with Plaxis 2D. This

program takes the geometric nonlinearity automatically into account, but does not allow for the physical nonlinearity. In Plaxis 2D the varying bending stiffness for structural elements subjected to bending should be implemented manually. The element is divided into parts, where each part is considered to behave linear-elastic (with a constant EI). A brief description with the capabilities of both programs will be given in the sections 2.4.1 and 2.4.2.

2.4.1. PCSheetPileWall

PCSheetPileWall is a discrete numerical model based on the BEF-method. The diaphragm wall is modelled as a beam supported by uncoupled elastic springs representing the soil stiffness. One of the most important features of this program is that it is capable of including the variable bending stiffness of the diaphragm wall in the soil-structure interaction. Based on the properties of the reinforced concrete diaphragm wall and the occurring bending moment, the *cracked* bending stiffness is calculated by the program. Besides the non-linear behaviour of the soil, the behaviour of the diaphragm wall therefore too becomes non-linear.

The diaphragm wall can consist out of more than one section in vertical direction, each with different moment of inertia and elastic modulus. For each section the bending moment capacity can be represented by an M-(N)- κ diagram for the SLS and ULS. For the determination of the bending stiffness of the diaphragm wall the following parameters are of great importance:

- The wall thickness;
- The amount of reinforcement;
- The concrete cover;
- The concrete quality;
- The reinforcing steel properties;
- Inclusion of the normal force due to self-weight of the wall;
- Inclusion of the reinforcement holes;
- Inclusion of eccentricity shear forces by soil (due to friction wall-soil). The vertical shear forces along the diaphragm wall have an eccentricity related to the heart of the concrete cross-section. Due to this eccentricity extra moments are exerted onto the diaphragm wall.

In this program it is only possible to draw one diaphragm wall where at both sides the surface level, groundwater level, soil layers, loading, anchors/struts and/or supports (spring supports, fixed supports, clamped connection) should be defined for each construction phase. The soil properties of each soil layer are defined by: γ , ϕ , δ , c and OCR. The soil stiffness (non-linear spring behaviour) is modelled by means of the tri-linear stiffness model as discussed in section 2.3.8 with k_1 , k_2 and k_3 (see Figure 18). As stated before, the diaphragm wall stiffness is determined as a function of the occurring bending moment.

The output of the calculations consist of the following results for each construction phase:

- The force distribution in the wall (M- and V-distribution);
- The lateral wall displacements;
- The pressures against the wall (waterpressures and (effective) soil stresses);
- The reinforcement (tensile) stresses;
- The lateral stiffness over the wall height (EI-distribution);
- The cracked and uncracked zones over the wall height. See Figure 21.

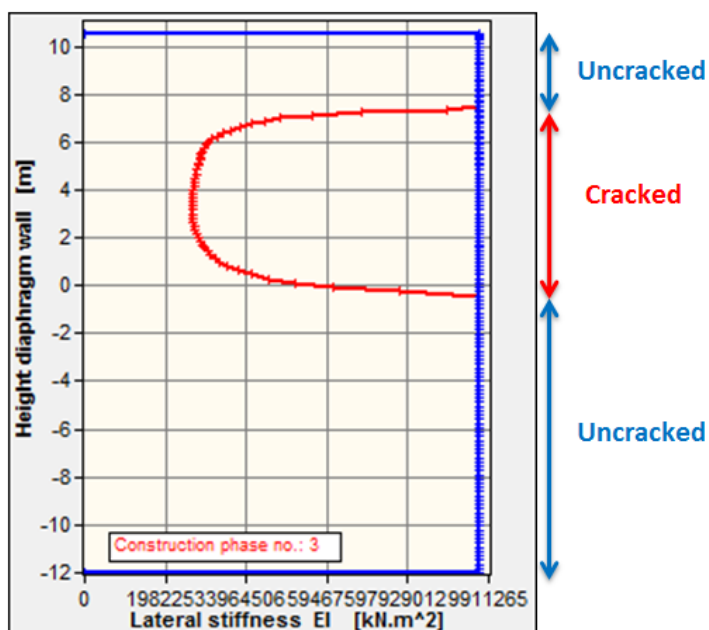


Figure 21: The cracked and uncracked zones over the wall height as determined by PCSheetPileWall

2.4.2. Plaxis 2D

Plaxis is a finite element program specifically developed to perform deformation and stability analyses in geotechnical engineering projects. It is the most widely used finite element program in the Dutch geotechnical engineering field. Through a system of coupled ordinary and partial differential equations, one can describe the equilibrium of stresses in and the deformation of the soil. This also holds for the bending behaviour of structural elements. With Plaxis 2D the soil displacements can be calculated for any loading and geological profile. Real situations may be modelled either by a Plane Strain or an Axisymmetric model. A plane strain model is used in case one dimension is relatively long compared to the other dimensions, while an axisymmetric model is used for circular structures. The program makes use of mesh elements which can be refined. This refinement is especially important in areas where large stress concentrations or large deformation gradients are expected. The finer the mesh, the more accurate the results. For the simulation of the soil behaviour Plaxis 2D has the following material models: Linear elastic, Mohr-Coulomb, Soft Soil, Hardening Soil, Soft Soil Creep, Jointed Rock and User-Defined model. For a detailed description of the material models reference is made to the Plaxis manuals [8] and [21]. These models have already been described briefly in section 2.2. In the context of this research the following material models are used: LE- and HS-model.

2.4.2.1. Finite element analysis

The possibilities of the program are discussed systematically based on the following structure:

▪ Input geometry model & assignation constitutive model

For the analysis it is important to create a geometry model first, which is a 2D-representation of the real three-dimensional problem. The geometry model includes a representative division of the subsoil into distinct soil layers, structural objects, construction stages and loading. The dimensions of the model must be sufficiently large such that the boundaries do not have any influence on the results of the problem to be studied. In order to simulate the behaviour of the soil, a suitable soil model and appropriate material parameters must be assigned to the geometry. As mentioned before, it is possible to choose between different constitutive models in Plaxis. The difference between these models lies in the manner in which the material behaviour is described in terms of stiffness and strength. A choice can be made between

simple soil stiffness behaviour by means of the e.g. MC-model or a more complex soil stiffness behaviour represented by e.g. the HS-model.

▪ **Mesh generation**

After the creation of the geometry model, the finite element model (or mesh) is generated composed of triangular elements. A choice can be made between 15-node and 6-node elements. Meshes composed of 15-node elements are actually much finer and provide a more accurate calculation of stresses and failure loads compared to meshes composed of 6-node elements. If necessary, the mesh can be optimised by performing global or local refinements. In addition to the triangular elements, which are generally used to model the soil, plate elements and interface elements may be generated to model the structural behaviour and soil-structure interaction.

Plate elements are used to simulate the behaviour of structural elements, which are presented as beam elements with elastic behaviour. The behaviour of these elements is defined by using a bending stiffness (EI) and normal stiffness (EA), from which an equivalent plate thickness can be calculated:

$$d_{eq} = \sqrt{12 \frac{EI}{EA}}$$

Where:

| | | |
|----------|----------------------------|-------------------------------------|
| d_{eq} | Equivalent plate thickness | [m] |
| EI | Bending stiffness | [kNm ² /m ³] |
| EA | Normal stiffness | [kN/m ³] |

Interface elements are applied between the soil elements and the plate elements in order to model the soil-structure interaction. With this the slip behaviour and the load transfer between the soil and the structure is described. The characteristics of the interface elements are defined by the structure and the soil. In general, for real soil-structure interaction the interface is weaker and more flexible than the associated soil layer, implying that the interface strength R_{inter} should be less than 1. In case the interface should not influence the strength of the surrounding soil it holds that $R_{inter} = 1$ (no reduced strength properties). In the absence of detailed information the properties of the interface are linked to the adjacent soil, and the interface strength is estimated to be:

- $R_{inter} = 0,50$ for clay and peat
- $R_{inter} = 0,67$ for sand

▪ **Finite element calculation:**

The finite element analysis consists of a number of calculation phases. The purpose of these calculation phases is to create a stress state which approximates the actual situation as close as possible, thereby making a distinction between the pore pressures and the effective (horizontal and vertical) stresses. The initial stress state, the so-called K_0 -procedure, is an important part of the non-linear finite element analysis. The building up of the calculation phases is of particular importance for the soil deformations, and therefore also affect the structural elements.

❖ **K_0 -procedure (Initial conditions)**

The K_0 -procedure for the generation of initial effective stress state does not take external loads and weights of structural elements into account. All loads and structural objects which are to be applied in a later stage and are not present in the initial situation, are therefore de-activated and have no effect in the initial configuration. The initial stresses in a soil body are influenced by the weight of the material and the history of its formation. By selecting $\Sigma Mweight = 1.0$ in Plaxis the full soil weight and water pressures are activated for the generation of the initial effective stresses. When using the Hardening Soil model and defining a normally consolidated initial stress state it holds that: $OCR = 1.0$ and $POP = 0.0$.

❖ **Staged construction**

After generation of the finite element model, the actual finite element calculation can be executed. Just like in the engineering practice where a project is divided into project phases, similarly the calculation process in Plaxis is divided into calculation phases using the *Staged Construction*. The initial stress generation (K_0 -procedure) is the initial construction phase, which is followed by other defined construction phases where the sequence of the types of loading and construction stages are assigned to. Staged construction enables an accurate and realistic simulation of various loading, construction and excavation processes; by means of the staged construction it is possible to activate or deactivate the weight, stiffness and strength of selected components of the finite element model. With this option it is also possible to improve the accuracy of previous computational results. The finite element calculations in Plaxis can be distinguished into three basic types of calculations:

- *Plastic calculation*: This calculation type is selected to carry out an elastic-plastic deformation analysis where it is not necessary to take the decay of excess pore pressures with time into account. This type of calculation is appropriate in most practical geotechnical applications. In case of a fully drained analysis, an assessment of settlements on the long term is possible. This gives a reasonably accurate prediction of the final situation, although the precise loading history is not followed and the process of consolidation is not dealt with explicitly.
- *Consolidation analysis*: This calculation type is selected when it is necessary to analyse the development or dissipation of excess pore pressures in water-saturated clay-type soils as a function of time.
- *Phi-c reduction (safety analysis)*: This calculation type is selected when it is desired to calculate a global safety factor for the situation at hand. The safety analysis can be executed by reducing the strength parameters of the soil.

For this research the Plastic Calculation is considered.

▪ **Output**

The output results in Plaxis 2D concern the following for the:

- Soil: Deformations and stresses;
- Structural elements: Structural displacements and forces (axial forces, shear forces and bending moments);
- Interfaces: Stresses (effective normal stress, shear stress, pore pressures).

2.4.2.2. Choice of constitutive model

The choice of a constitutive model depends on many factors but, in general, it is related to the type of analysis that needs to be performed, expected precision of predictions and available knowledge of soil.

Geo-engineering analyses can be distinguished into 2 groups:

- Bearing capacity and slope/wall stability analyses. These are related to the ULS-analysis, using basic linear models e.g. MC-model (but this is not a rule) and;
- Deformation analyses. These are related to the SLS-analysis, using advanced non-linear constitutive models e.g. HS-model.

Deformation analyses or situations where differences in stiffness play a significant role in the distribution of forces, e.g. due to incorporation of structural elements in a weir, require a more advanced constitutive model. In such cases the HS-model is preferred above the MC-model. It should be noted that the HS-model requires more detailed data. If these data are not available the MC-model may be applied. In that case, however, the uncertainties in the finite element calculation with regard to the bending moments in the retaining wall can be quite large.

In this research the emphasis lies mainly on the deformation analysis, where a good prediction of the occurring displacements is required. As the soil displacements will affect the bending stiffness and thus

the force distribution in the diaphragm wall and vice versa, the urge for a realistic displacement field is of great importance. Not only this, but also the fact that the geotechnical profile of this project consists mostly of sand layers, led to the choice for the HS-model as representative soil model throughout this research. In this research the LE-model will be used for structural elements (foundation and diaphragm wall) and will not be described explicitly, whereas the HS-model will be dealt with in more detail in section 2.4.2.4.

2.4.2.3. Linear Elastic Model (LE)

As stated before the LE-model is very limited for the simulation of soil behaviour. However, it is used for stiff structures in the soil. The following model parameters must be applied in case the LE- model is used for:

- Soil: E and ν
- Structural element: EI, EA, w and ν .

2.4.2.4. Hardening Soil Model (HS)

The HS-model is an advanced model for simulating the behaviour of different types of soil, both soft soils and stiff soils. In this model the primary load creates both elastic (recoverable by unloading) and plastic (irrecoverable by unloading) deformations. This elasto-plastic soil model is represented by a hyperbolic stress-strain relationship as depicted in Figure 22, resulting in more realistic displacement fields compared to for instance the linear-elastic perfectly-plastic MC-model. The MC-model is ideal for a stability test, but the displacements obtained are not realistic because of the constant stiffness. Figure 22 represents the stress-strain relationship for the MC-model, the HS-model and real soil.

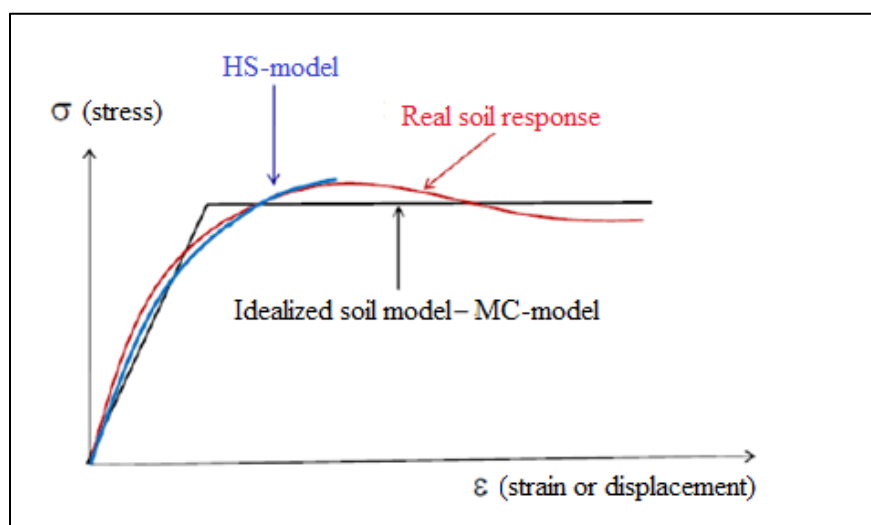


Figure 22: Comparison of HS- and MC-model with real soil response [26]

The advantage of the HS-model over the MC-model is not only the use of a hyperbolic stress-strain curve instead of a bi-linear curve, but also the control of stress level dependency. This means that the stiffness moduli increase with pressure. For real soils the stiffness depends on the stress level. With the HS-model the real soil behaviour is approximated more accurately by incorporating a combination of three different stress-dependent stiffness moduli, namely: the triaxial loading stiffness (E_{50}), the triaxial unloading-reloading stiffness (E_{ur}), and the oedometer loading modulus (E_{oed}), which have already been dealt with in section 2.3.9.

The features of the HS-model are [25]:

- Densification, i.e. a decrease of voids volume in soil due to plastic deformations,
- Stress dependent soil stiffness, i.e. commonly observed phenomena of increasing stiffness modules with increasing confining stress (also related to increasing depth);
- Soil stress history, i.e. accounting for preconsolidation effects;
- Plastic yielding, i.e. development of irreversible strains with reaching a yield criterion;
- Dilatancy, i.e. an occurrence of negative volumetric strains during shearing.

Although the HS model can be considered as an advanced soil model which is able to faithfully approximate complex soil behaviour, it includes some limitations related to specific behaviour observed for certain soils. These are:

- The model is not able to reproduce softening effects associated with soil dilatancy and soil destructureation which can be observed, for instance, in sensitive soils.
- The model is not capable to reproduce hysteretic soil behaviour observed during cycling loading [25].

The soil model parameters applicable for the HS-model can be distinguished into:

- The stiffness parameters:

E_{50}^{ref} : Secant modulus 50% strength [kN/m²]

E_{oed}^{ref} : Oedometric modulus [kN/m²]

E_{ur}^{ref} : Unloading-reloading modulus [kN/m²]

m : Power for stress-level dependency of stiffness [-]

- The strength parameters:

c : Cohesion [kN/m²]

ϕ : Internal friction angle [°]

ψ : Dilatancy angle [°]

A reasonable assumption for sand is that $E_{oed}^{ref} = E_{50}^{ref}$. For clay E_{oed}^{ref} is much lower than E_{50}^{ref} .

3. THE M-(N)-κ DIAGRAM

3.1. Introduction

A structure must provide sufficient resistance to stresses and deformations which may occur during its lifetime. The resistance to loads and deformations, are expressed in terms of the strength and the stiffness, respectively.

The bending stiffness EI is the resistance to a curvature (κ) when a structural component is loaded with a bending moment (M) and possibly an axial compressive force (N'_c). The relationship between M and κ , whether or not combined with an axial compressive force, is expressed by means of M-(N)- κ diagrams

where it holds that $\tan \alpha = \frac{M}{\kappa} = EI$. The determination of the M-(N)- κ diagram is based on the nonlinear

theory of elasticity, assuming a nonlinear relationship between moment and curvature, or stress and strain. As stated in [38], simple piece-wise linear (bilinear or trilinear) bending moment-curvature relationships

have been used to idealize the actual nonlinear relationship for various concrete elements: beams, columns, walls (see Figure 23). In order to determine the bending stiffness of a reinforced concrete structure, knowledge of the structural behaviour in the different loading phases is required. For reinforced concrete the bending stiffness can vary considerably. There appears to be a large difference in the bending stiffness of an uncracked and a cracked concrete cross-section. As soon as the concrete has cracked, the bending stiffness decreases with increasing deformation! Due to a varying bending moment, the structure contains a variable bending stiffness (EI_{var}) over its length;

every bending moment has a different EI belonging to it.

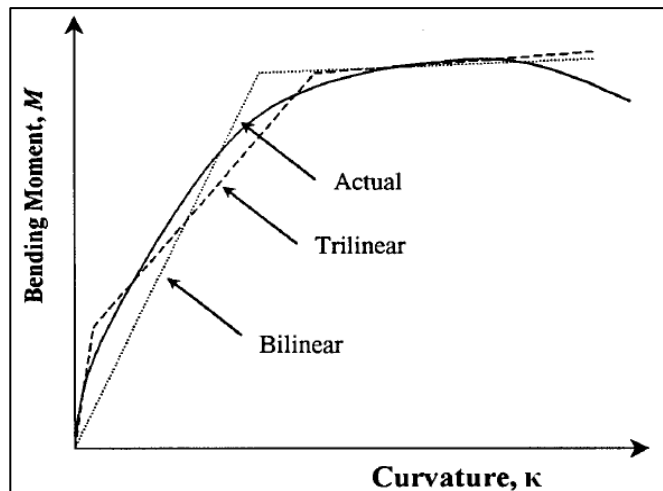


Figure 23: Idealization of the actual nonlinear bending moment – curvature relationship [38]

To put it briefly, the M-(N)- κ diagram is a simplified representation of the varying bending stiffness of a reinforced concrete structure, or in other words the resistance of a concrete cross-section to deformation in the different loading phases. To determine the force distribution EI -values of structural elements loaded in the ULS are applied. For deformation calculations the EI -values of structural elements loaded in the SLS are applicable. The basic assumptions for calculating M-(N)- κ diagrams for the SLS are different from those used for the ULS; the material and load factors play a major role. The M-(N)- κ diagram in the ULS is based on 4 loading phases, while for the SLS it usually suffices to consider only 2 loading phases.

The full derivation of the M-(N)- κ diagram is very laborious. In order to provide insight the successive phases in an M-(N)- κ diagram are dealt with by means of the stress and strain diagrams, without the corresponding formulas. For more detailed information reference is made to [42] and [43]. To determine the M-(N)- κ diagram, the following data are required:

- The dimensions of the cross-section;
- The reinforcement ratio;
- The concrete quality;
- The reinforcing steel grade.

The presence of N'_c has a favourable influence on the EI. Because of N'_c the concrete cross-section is less likely to crack, resulting in a greater EI. A higher stiffness leads to lower deformations. Therefore, it is a better criterion to consider an M- κ diagram instead of an M-N- κ diagram for EI-distributions required for deformation calculations.

3.2. Relation Moment – Curvature

The relation between the moment (M) and the curvature (κ) is the bending stiffness (EI). From mechanics it is known that κ is the reciprocal value of the radius of curvature (ρ), in formula:

$$\kappa = \frac{1}{\rho} = \frac{M}{EI} \quad (\text{Eq. 3.1})$$

The derivation of this formula is done based on Figure 24, showing a random beam-element loaded in bending. The cross-section is subject to the Bernoulli beam theory (“plane sections remain plane after bending”) and the moment is constant over the length v . Because of the curvature the element will shorten at the top side and extend at the bottom.

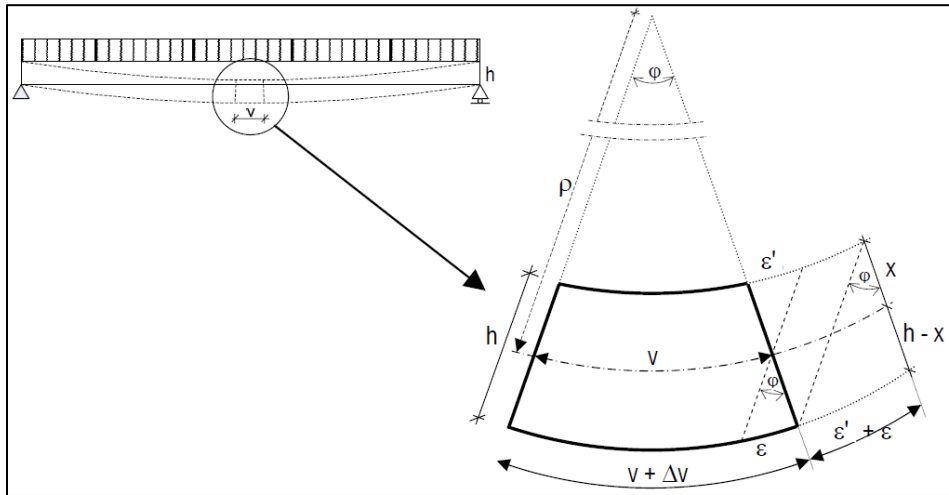


Figure 24: Beam loaded in bending with an enlarged view of a random beam-element

Similarity of triangles results in:

$$\frac{h-x}{\rho} = \frac{\Delta v}{v}, \text{ with } \frac{\Delta v}{v} = \varepsilon \text{ (specific elongation of bottom fibre)} \Rightarrow \varepsilon = \frac{h-x}{\rho} \text{ and } \kappa = \frac{1}{\rho} = \frac{\varepsilon}{h-x}$$

In a similar way the curvature for the top fibre can be deduced, so over height x :

$$\kappa = \frac{1}{\rho} = \frac{\varepsilon'}{x}$$

Since both curvatures are the same, it holds that:

$$\kappa = \frac{1}{\rho} = \frac{\varepsilon' + \varepsilon}{h}$$

The bending stress in the bottom fibre becomes:

$$\sigma_b = \frac{M}{W} = \frac{M \cdot e_b}{I} \Leftrightarrow \sigma = \frac{M \cdot (h-x)}{I}$$

Considering Hooke's law with $\varepsilon = \frac{\sigma}{E}$ and σ_b , it can be derived that the curvature is equal to:

$$\kappa = \frac{1}{\rho} = \frac{\varepsilon}{h-x} = \frac{\sigma}{E(h-x)} = \frac{M(h-x)}{EI(h-x)} = \frac{M}{EI}$$

With this, the relation between moment and curvature has been proven.

3.3. The loading phases

In concrete structures the bending stiffness EI is very important. Just like with other materials it is used to determine the deformation and deflection (SLS). For statically indeterminate structures (ULS) the stiffness ratio of the connecting parts is of more importance than the absolute value of EI. Unlike steel, the EI is not constant for concrete. In a reinforced concrete structure that is loaded to failure, the following parts can be distinguished: uncracked parts, cracked parts, parts where the steel yields, parts where concrete crushes and parts that have failed. The connecting parts thus have an EI which varies! In order to have a good prediction of the structural behaviour, the material behaviour of the concrete and the reinforcement in terms of the σ - ε diagrams is of importance. The required σ - ε diagrams in case of the ULS are given in Figure 25.

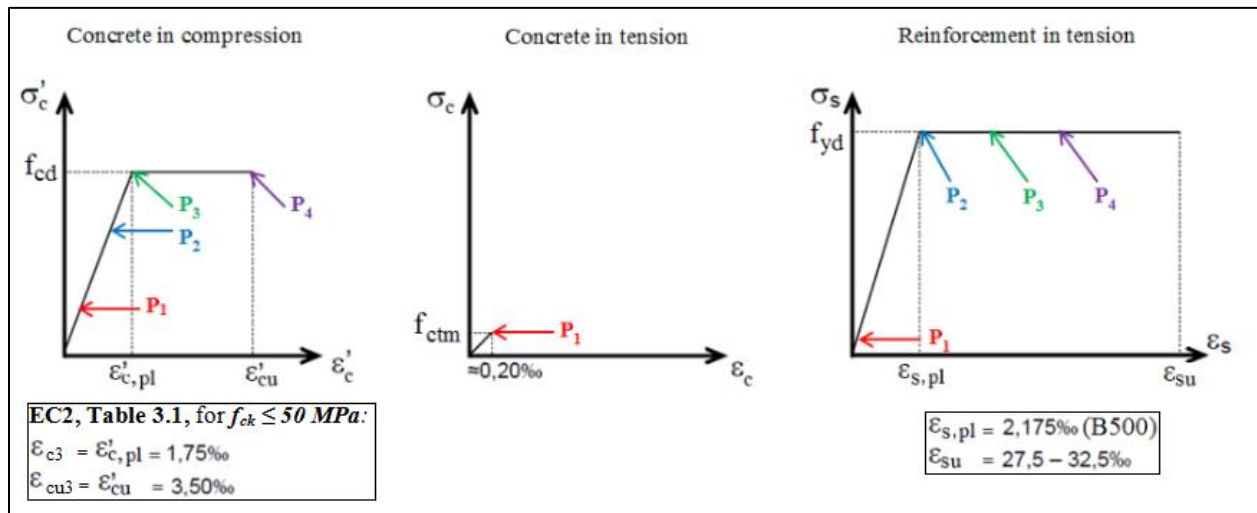


Figure 25: σ - ε diagrams for concrete (compression and tension) and reinforcement steel in the ULS (Note: The diagrams are not on scale)

To determine the M-(N)- κ diagram 4 loading phases are considered from the moment of loading till the moment of failure of the reinforced concrete structure. The 4 corresponding critical points P₁, P₂, P₃ and P₄ are indicated in each of the σ - ε diagrams of the reinforcing steel and the concrete as depicted in Figure 25. The following 4 loading phases are distinguished in the M-(N)- κ diagram:

1. The **cracking moment M_r**, with the accompanying curvature κ_r .
The (mean) tensile strength of the concrete has been reached and the first crack appears ($\sigma_c = f_{ctm}$).
2. The **yield moment M_e**, with the accompanying curvature κ_e .
The (tensile) reinforcement starts to yield ($\sigma_s = f_{yd}$).
3. The **crushing moment M_{pl}**, with the accompanying curvature κ_{pl} .
The concrete in the compression zone starts to crush ($\varepsilon'_{c,pl} = 1,75\%$).

4. The **ultimate moment** M_u , with the accompanying curvature κ_u .
The concrete has reached its ultimate compressive strain ($\varepsilon'_{cu} = 3.5\text{‰}$).

This order of the loading phases is common. However, the points P_2 and P_3 can appear in reversed order; the reinforcement does not necessarily have to yield before the concrete starts to crush. This depends on the applied amount of reinforcement. However, for a ductile failure it is necessary that the reinforcement yields before the concrete compression zone fails, thus before reaching point P_4 . This can be achieved by applying the maximum reinforcement ratio ($\rho_{l,max}$).

A short description of the 4 loading phases is given in the following, with reference to Figure 25, Figure 27 and Figure 28:

- **P₁**: In this phase the structure behaves in a linear elastic manner. The neutral axis is situated just below the centre of the concrete cross-section, because steel has a higher E-modulus than concrete. Upon reaching the cracking moment M_r , the concrete at the tension side starts to crack. Here the maximum tensile strength of concrete has been reached: $\sigma_c = f_{ctm}$.
- **P₂**: As the load increases, the structure will crack further at the tension side. At the cracks the tensile force is transferred into the steel because the concrete is no longer able to take up the tensile stresses. However, in between the cracks the tensile force can be transferred from the steel to the concrete. The influence of the uncracked stiff concrete parts, in between the cracks, on the stiffness of the structure is the so-called tension-stiffening. These uncracked concrete parts have a substantial influence on the stiffness of the structure. Upon further loading the reinforcing steel will start to yield: $\sigma_s = f_{yd}$. The corresponding strain in for instance reinforcing steel B500 is: $\varepsilon_{s,pl} = f_{yd} / E_s = 435 / 2 \cdot 10^5 = 2.175\text{‰}$ for the ULS. Since f_{ctm} has already been exceeded and the concrete is cracked, being unable to transfer tensile stresses, the σ - ε diagram for concrete in tension is no longer needed. Because the concrete at the tension side is considered to be cracked and only the reinforcement takes up the tensile force, the neutral axis will shift upwards. This results in a decrease of the concrete compression zone height (x) compared to phase P_1 .
- **P₃**: As the load is increased further, the concrete will start crushing in the outmost compression fibres, where the maximum concrete compressive stress has been reached ($\sigma'_c = f_{cd}$) with a corresponding concrete compressive strain: $\varepsilon_{c3} = \varepsilon'_{c,pl} = 1,75\text{‰}$ for normal concrete, thus $\leq C50/60$. This does not imply that the structure has failed already. The reinforcing steel was already yielding and this will remain like this. The steel stress will not become greater than f_{yd} , but the strain will increase (P_3 lies further than P_2 on the horizontal branch in the σ - ε diagram of the reinforcing steel in Figure 25). The steel undergoes a plastic deformation and the strain in the steel can increase up to about 3% ($\approx 30\text{‰}$). The concrete compressive zone is reduced further, because the cracks are going 'deeper', resulting in a lower x compared to phase P_2 .
- **P₄**: Increasing the load even more results in crushing of many more concrete fibres at the outer compression side and in the layers just below it. The reinforcing steel, which has been yielding for a while, will obviously remain yielding, whereas the strain in the steel increases further. As soon as the ultimate concrete compressive strain $\varepsilon_{cu3} = \varepsilon'_{cu} = 3.5\text{‰}$ (for normal concrete, thus $\leq C50/60$) is reached in the outmost compression fibre, a structural failure is considered. Here one finds f_{cd} acting over $\frac{1}{2} x$. The limit load bearing capacity M_u is reached. Further increase of the load, while maintaining a proper construction, is impossible. So, this is the final stage. The calculation of the flexural tensile reinforcement in a structure is based on this stage. The distance x has decreased further compared to phase P_3 .

3.4. M-(N)-κ diagram ULS: principle

In this section the principle for determining the M-κ diagram and the M-N-κ diagram in the ULS is treated. The 4 loading phases for the M-κ diagram and the M-N-κ diagram are depicted in Figure 27 and Figure 28, respectively. The ε- and σ-diagrams in each of the loading phases are depicted in these figures and commented on by means of Table 1. In Figure 27 one has considered only tension reinforcement in determining the M-κ diagram, whereas in Figure 28 the determination of the M-N-κ diagram is based on two-sided reinforcement (tension reinforcement and compression reinforcement). In case of the combination bending and axial compressive force it is usual to apply symmetrical reinforcement out of practical considerations. This prevents errors on the construction site (improper placement of the reinforcement cage) which could lead to safety issues.

In general, the procedure for determining the M-(N)-κ diagram consists of calculating the internal bending moment and the corresponding curvature for each loading phase. The procedure for each critical phase P₁, P₂, P₃ and P₄ is as follows:

- **Determine x:** The height of the concrete compression zone (x) is determined from the equilibrium of horizontal forces: ΣH = 0. It can be noted that x will decrease with each loading phase: $x_{unscr.} > x_e > x_{pl} > x_u$;
- **Determine ε and κ:** If x is known, the strains ε in the steel and concrete can be calculated by using the similarity of triangles theorem. With the calculated strains the curvature κ can now be determined, see Figure 26;
- **Determine M:** The internal bending moment in each phase is determined by the product of the internal forces in the steel and concrete, and if applicable the external compressive force N'c, with their corresponding distances to the neutral axis. Note that the bending moment will increase in each phase. The cracked zone progresses upwards into the concrete compression zone during this process resulting in an upward shift of the neutral axis. Because of this the internal lever arm will increase leading to a higher internal bending moment.

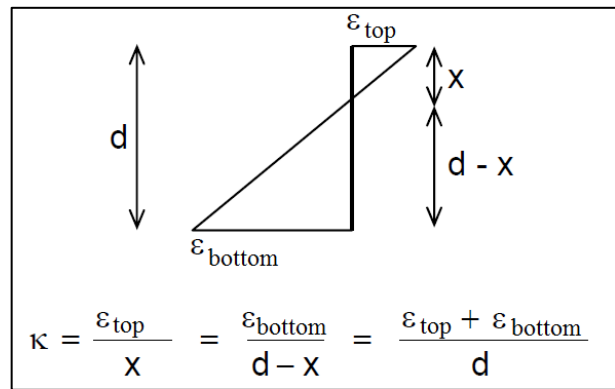


Figure 26: Determining the curvature using the ε-diagram

| Loading phase | Moment | ε - diagram | σ - diagram | Comments |
|----------------|-----------------|---|--|--|
| P ₁ | M _r | ε _s << ε _{s,pl} ε _{c,max} is reached ε' _c << 1.75‰ | σ _s << f _{yd} σ _c = f _{ctm} σ' _c << f _{cd} | No yielding of steel. Maximum concrete tensile strength is reached. Very small concrete compressive stress. |
| P ₂ | M _e | ε _s = ε _{s,pl} ε _c no longer of importance ε' _c < 1.75‰ | σ _s = f _{yd} σ _c >> f _{ctm} σ' _c < f _{cd} | Yielding of steel. Concrete is cracked and cannot transfer tensile stresses. Maximum concrete compressive stress not reached yet. |
| P ₃ | M _{pl} | ε _s > ε _{s,pl} ε _{c3} = ε' _{c,pl} = 1.75‰ | σ _s = f _{yd} σ' _c = f _{cd} | Steel is still yielding, but tensile force remains constant. Maximum concrete compressive stress is reached. |
| P ₄ | M _u | ε _s >> ε _{s,pl} ε _{cu3} = ε' _{cu} = 3.50‰ | σ _s = f _{yd} σ' _c = f _{cd} | Steel is still yielding, but tensile force remains constant. Ultimate concrete compressive strain is reached; maximum concrete compressive stress is reached in many more fibres of compression zone (½ x). |

Table 1: The occurring strains and stresses in the 4 loading phases

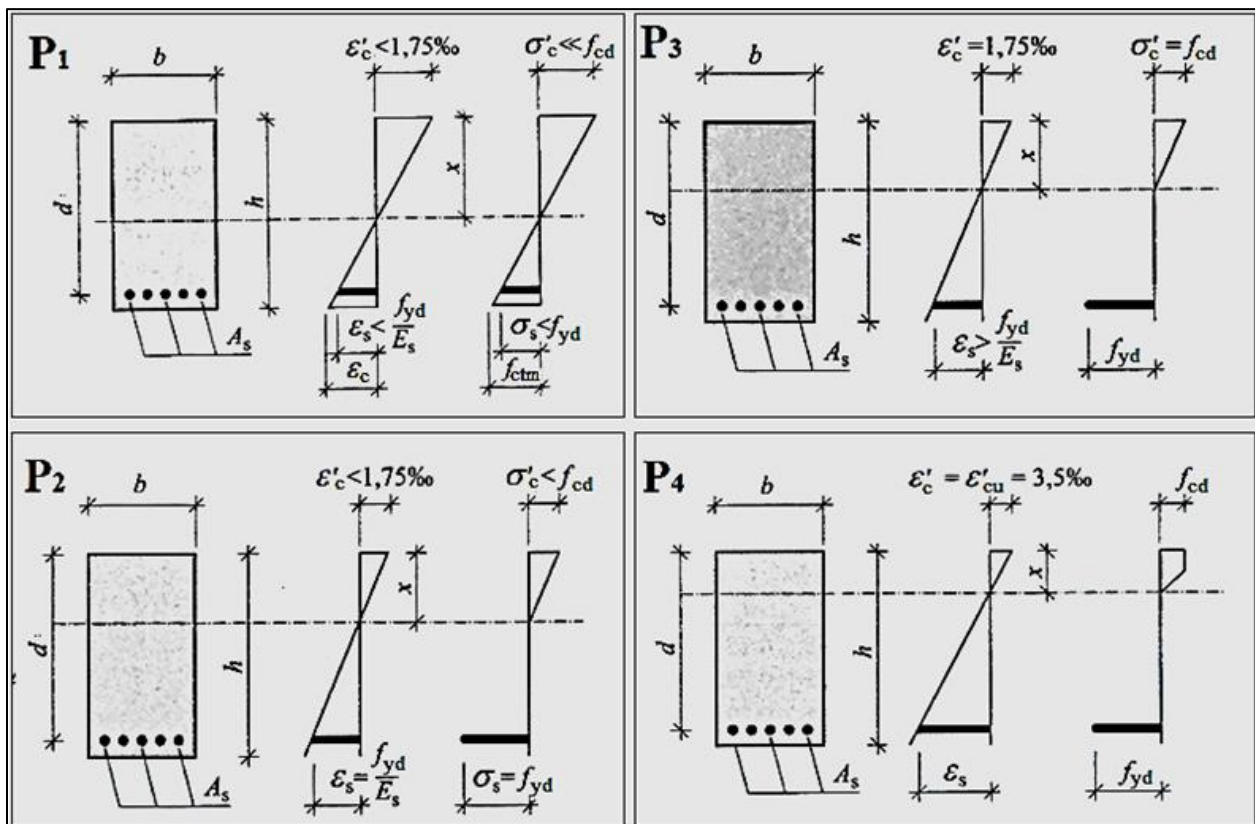


Figure 27: The 4 loading phases to determine the $M-k$ diagram in the ULS, with the occurring strains and stresses

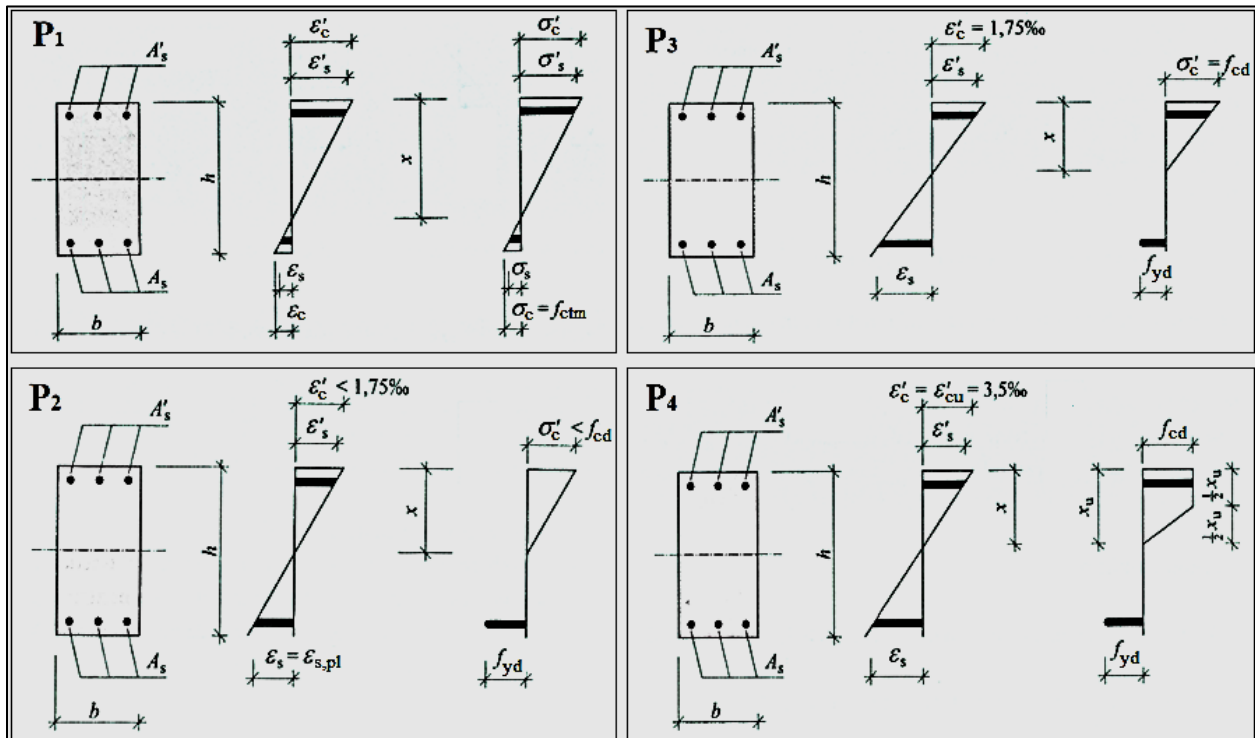


Figure 28: The 4 loading phases to determine the $M-N-k$ diagram in the ULS, with the occurring strains and stresses

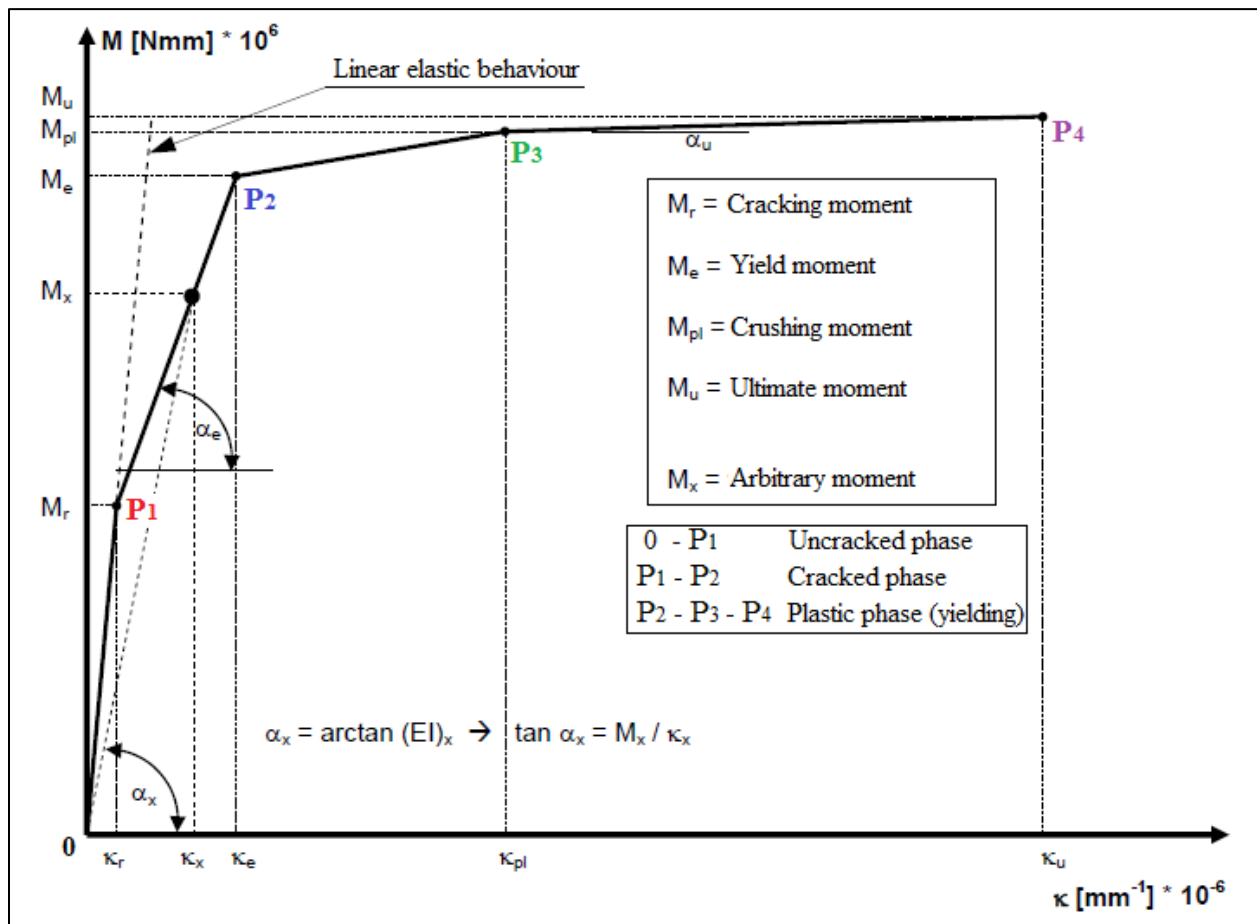


Figure 29: The M-(N)-κ diagram for the ULS

After calculating the bending moments with their corresponding curvatures in each of the 4 loading phases, these can be plotted in the M-(N)-κ diagram. See Figure 29. From the moment of loading till the moment of failure of the structure, the M-(N)-κ diagram can be well approximated by means of 4 straight lines which connect the points M_r , M_e , M_{pl} and M_u . By means of the M-(N)-κ diagram one can determine the bending stiffness EI of a reinforced concrete structure at an arbitrary bending moment (M_x). From the origin a line is drawn to M_x and the corresponding curvature κ_x is read off. The bending stiffness $(EI)_x$, which is the slope of the line, can now be determined. For an arbitrary moment the bending stiffness

becomes: $(EI)_x = \tan(\alpha_x) = \frac{M_x}{\kappa_x}$. By definition the slope is taken from the line that starts from the

origin and not from, for instance the line in the M-(N)-κ diagram with an angle of inclination α_e . Otherwise, the EI would be constant for the branch P_1 - P_2 , implying that every cracked part of the structure has the same EI which is not very likely. The EI derived for the branch P_3 - P_4 , between M_{pl} and M_u , would in that case be reduced to an absolute minimum (α_u). Of course, it is obvious that as long as the moment has not reached M_r , the bending stiffness EI remains constant for the uncracked concrete cross-section. Logically, in the uncracked phase the EI is also the largest. From Figure 29 it is clear that the bending stiffness EI decreases as the load is increased. The reason behind this phenomenon is the increasing crack formation and the yielding of the reinforcement from a certain point onward.

Once again, the points P_2 and P_3 can appear in reversed order. This implies that concrete crushing (M_{pl}) can occur before yielding of the reinforcement (M_e). Therefore, it is important to calculate and check the strains of the steel and the concrete for each loading phase (see Table 1). At a relatively low

reinforcement ratio it is usual that yielding of the steel (M_e) occurs before the concrete crushing (M_{pl}), while at a high reinforcement ratio M_{pl} is obtained before M_e . In determining the M-N- κ diagram, yielding of the tension reinforcement will occur first in case of small compressive forces and relatively large bending moments, while in case of large compressive forces and relatively small bending moments crushing of the concrete will be obtained before yielding of the steel.

As an alternative to determine EI with the M-(N)- κ diagram it is also possible for sections with a rectangular cross-section to determine EI in the ULS from: $EI = E_f \cdot I$ ($I = \frac{1}{12}bh^3$), where E_f is the fictitious modulus of elasticity according to *Table NB-1 of the National Annex to NEN-EN 1992-1-1* [40]. In this table one does not only find E_f for elements subjected to pure bending, but also for elements loaded by both a bending moment and an axial force. Since in reality the cross-section is cracked, E_f is just a ‘calculation tool’, a fictitious number.

In this research the influence of tension-stiffening (the positive contribution of the stiff uncracked concrete parts between the cracks) on the overall bending stiffness of the structure is taken into account. This implies that according to Figure 30 the path to follow starts from the origin to ①-③. If the tension-stiffening (shaded area) is not considered, this signifies that as soon as the first crack occurs the tension reinforcement takes over the total tensile force and the contribution of the tensile strength of the concrete in the stiff uncracked concrete sections is totally neglected. In that case the path from the origin to ①-②-③ has to be followed. Since this is not very realistic in practice (and it has also not been established by research) that after the first crack the curvature increases excessively, it is more likely to apply the diagram with tension stiffening. For a clear understanding Figure 30 shows a beam subjected to bending, where due to crack formation one can distinguish sections with an uncracked stiffness and sections with a cracked stiffness with or without the contribution of tension-stiffening.

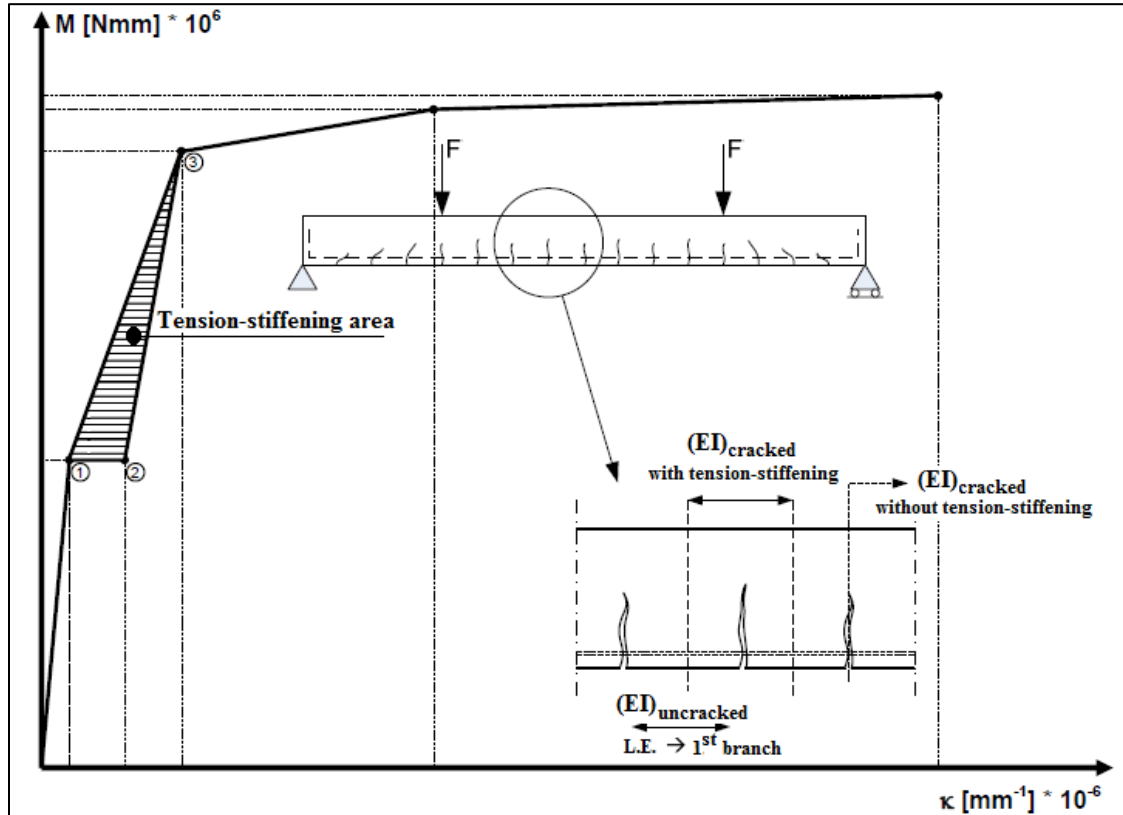


Figure 30: The influence of tension-stiffening on the bending stiffness

3.5. M-(N)-κ diagram SLS: principle

For 1st-order calculations in the ULS it is often not important what the absolute value of EI is. The ratio of the bending stiffnesses of the connecting parts is usually more important, and therefore in that case the EI of the uncracked section may be applied. However, if the absolute value of the EI plays an important role, such as for deformations and 2nd-order effects then the "real" EI obtained from the M-(N)-κ diagram must be taken into account. The 2nd-order effect, also referred to as "geometric nonlinearity", occurs when structural deformations influence the load distribution causing additional stresses. If the element also cracks, the rigidity will decrease causing even greater deformations. So, in addition to the geometric nonlinearity, one also has to deal with the physical nonlinearity of the structure.

The previous section dealt with the situation in the ULS, so for calculations on strength and the associated bending stiffness EI. If the bending stiffness EI is required to determine displacements and deformations, M-(N)-κ diagrams can be made for the SLS. The absolute value of EI will then be of greater importance than the ratio of bending stiffnesses of connecting parts. Constructing an M-(N)-κ diagram for the SLS goes in a similar way as for the ULS, with the difference that for the SLS characteristic values are to be used. In the SLS the material and load factors are equal to 1.0, as for the ULS these are > 1.0. For instance, for the concrete f_{cd} is replaced by f_{ck} and for the reinforcing steel f_{yd} is replaced by f_{yk} in the SLS.

The required σ - ε diagrams in case of the SLS are given in Figure 31. In the SLS distinction is made between short-term and long-term loading, where for the long-term loading the effect of creep (i.e. the increasing deformation of concrete in time at a constant load) is included. According to *NEN-EN 1992-1-1(EN)*, clause 7.4.3 (5) the total deformation, including creep may be calculated using an effective modulus of elasticity: $E_{c,eff} = E_{cm;\infty} = \frac{E_{cm}}{1 + \varphi(\infty, t_0)}$ [36, 37]. The creep coefficient $\varphi(\infty, t_0)$ has to be

obtained from EC2, Figure 3.1.

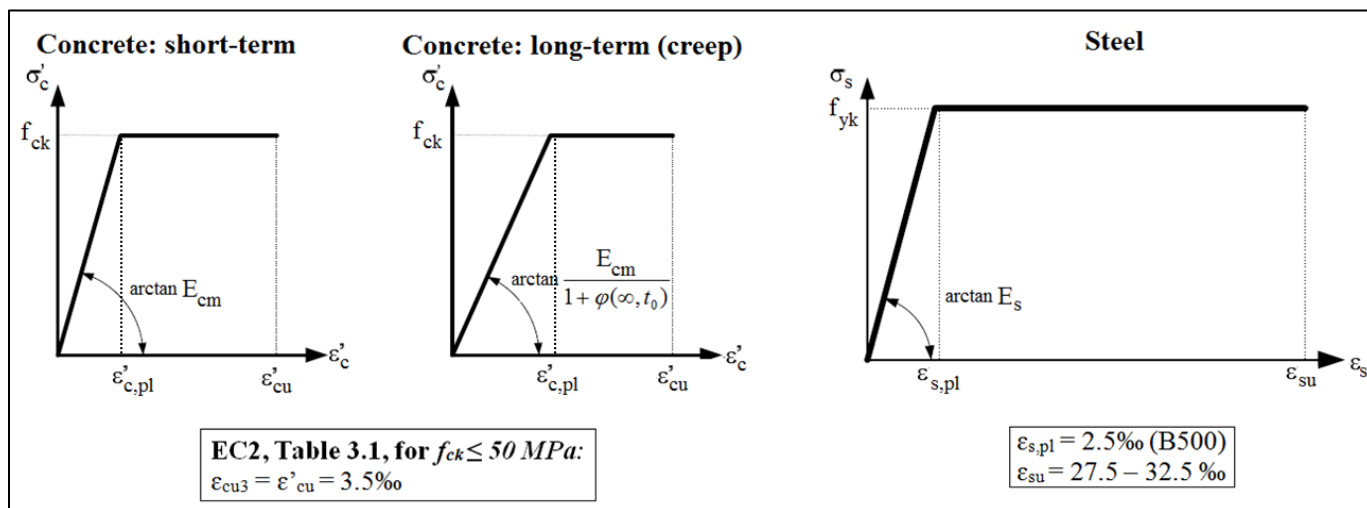


Figure 31: $\sigma - \varepsilon$ - diagrams for concrete in SLS (short-term and long-term) and for reinforcing steel in SLS

For strength calculations in the ULS $\varepsilon'_{c,pl}$ is an invariable (1.75‰ for normal concrete, thus $\leq C50/60$). In the SLS, this value depends on the E-modulus of the concrete (E_{cm} in EC2, Table 3.1). The crushing strain of concrete can be derived for:

- Short-term loading: $\varepsilon'_{c,pl} (short) = \frac{f_{ck}}{E_{cm}}$;

- Long-term loading: $\varepsilon'_{c,pl}(long) = \frac{f_{ck}}{E_{cm;\infty}} = (1 + \varphi(\infty, t_0)) \times \varepsilon'_{c,pl}(short)$. In case of creep the crushing strain of concrete is enlarged by the term $(1 + \varphi(\infty, t_0))$.

For the SLS reinforcing steel B500 will yield at a strain: $\varepsilon_{s,pl} = f_{yk} / E_s = 500 / 2 \cdot 10^5 = 2.5 \text{‰}$.

See Figure 32: It is worth mentioning that according to the now withdrawn standard NEN6720 (VBC 1995), the E-modulus of concrete, including creep, was determined by: $E'_{b\infty} = \frac{E'_b}{1 + \frac{3}{4}\varphi}$ with a maximum

value for the creep coefficient φ_{max} conformable to NEN6720, Table 8.

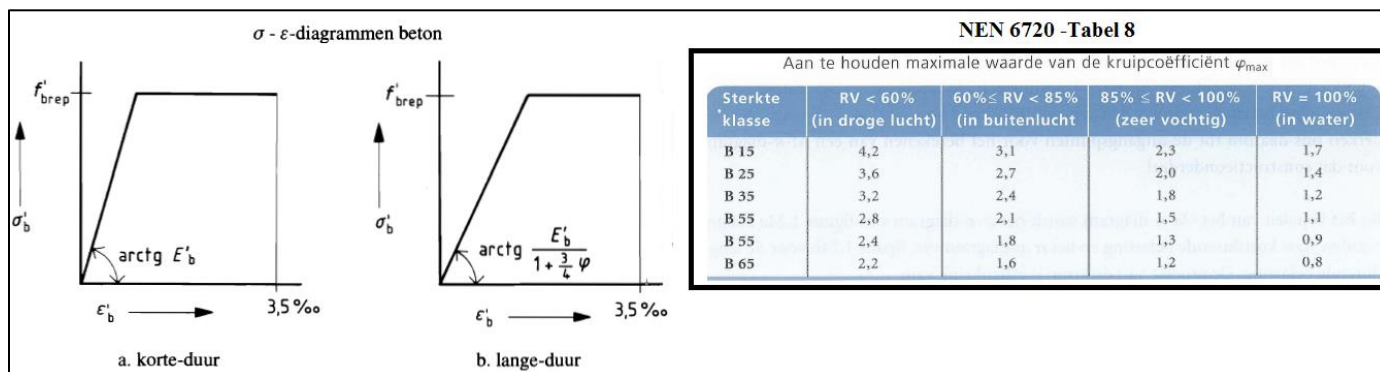


Figure 32: The E-modulus of concrete on long-term (creep) according to withdrawn standard NEN6720 (VBC 1995)

The M-(N)-κ diagram for the ULS consists of 4 points. For the SLS this is not sufficient, because due to the influence of creep the deformation will increase in the long term. Therefore, an M-(N)-κ diagram for both the short-and long-term are made for the SLS. The diagrams for short-term loading and long-term loading are used to determine the instantaneous deformations and the deformation in the final state, respectively. Both diagrams are shown schematically in Figure 33. For each of these diagrams it suffices to consider 2 points, namely the cracking moment M_r and the yield moment M_e (or, as already mentioned earlier, in case of a high reinforcement ratio the crushing moment M_{pl} can occur before the yield moment M_e). In general these 2 points are enough, but in case this proves to be insufficient, the M-(N)-κ diagram must be extended. In Figure 33 the cracking moment and yield moment on short-term are referred to as M_r and M_e , respectively. For the long-term loading these are referred to as M_{rt} and M_{et} . Usually the ultimate moment M_u in the ULS is smaller than the yield moment M_e or M_{et} in the SLS.

In Figure 33 one accordingly distinguishes the bending stiffnesses: $(EI)_{I,0}$, $(EI)_{II,0}$, $(EI)_{I,\infty}$ and $(EI)_{II,\infty}$ for the SLS, where the following subscripts have been used:

- I = uncracked stage
- II = cracked stage
- 0 = short-term loading
- ∞ = long-term loading

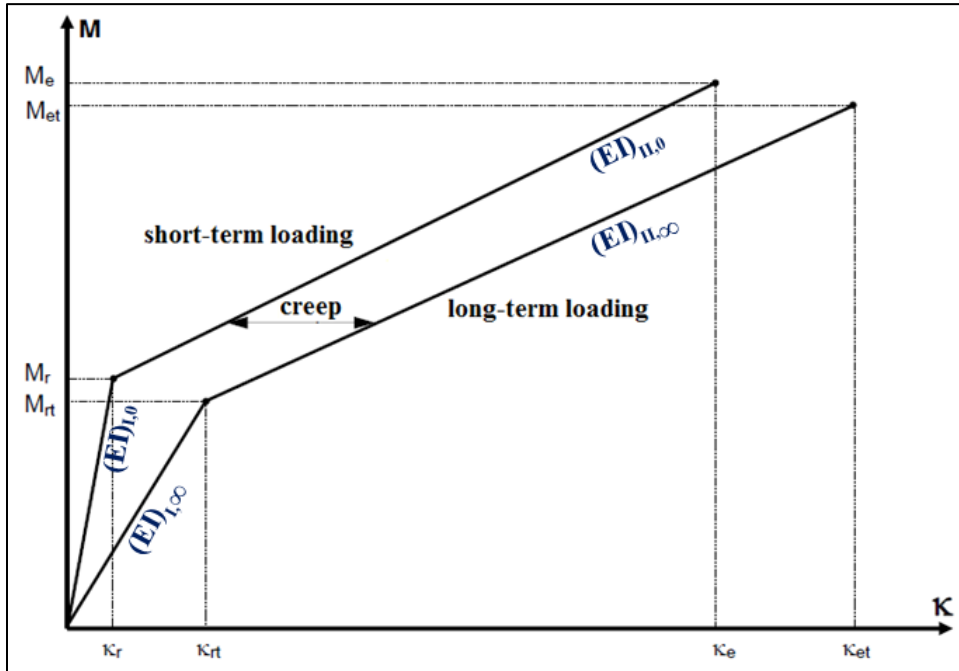


Figure 33: The M-(N)-κ diagram for the SLS

In this research the deformations of the structure are determined by considering :

- An uncracked structure with constant bending stiffness: $EI_{un\text{cr}}$
- A fully cracked structure with constant bending stiffness: $EI_{\text{cr}} (= 1/3 \times EI_{un\text{cr}})$
- A structure with variable bending stiffness over the entire span: EI_{var}

The instantaneous deformations are determined based on EI_{var} obtained from the M-(N)-κ diagram for the SLS short-term loading (so, $(EI)_{i,0}$ and $(EI)_{ii,0}$). As described in section 3.5, determination of instantaneous deformations due to the fully cracked stiffness EI_{cr} is based on EC2, Equation (7.20):

$$E_{c,\text{eff}} = \frac{E_{cm}}{1 + \varphi(\infty, t_0)}$$

With a practical creep coefficient $\varphi(\infty, t_0) \approx 2$ the bending stiffness of a fully cracked

cross-section is estimated to be 1/3 of the uncracked stiffness. It should be clear that this formula is defined for calculating the total deformation including creep, thus for long-term loading. **So, it can be stated that for deformation calculations based on the fully cracked stiffness EI_{cr} , the effect of creep on the structure has been taken into account.**

3.6. Characteristics in M-(N)-κ diagram

As discussed before there are 4 important points in an M-(N)-κ diagram: M_r , M_e , M_{pl} and M_u . In this section both the influence of the reinforcement ratio (ρ_l) and an axial compressive force (N') on the M-(N)-κ diagram are dealt with.

Influence reinforcement ratio (ρ_l)

Depending on the reinforcement ratio M_e and M_{pl} can appear in reversed order. For reinforced concrete elements a minimum and a maximum reinforcement ratio are prescribed in the standards:

- The minimum reinforcement ratio ($\rho_{l,min}$) is required to prevent brittle failure of concrete by steel rupture (brittle fracture). After cracking of the concrete the reinforcing steel should be able to take up the total tensile force. Insufficient reinforcement will otherwise lead to a sudden and brittle failure. With $\rho_{l,min}$ it is ensured that M_r in the governing cross-section is taken up, it holds that: $M_r \leq M_u$;
- The maximum reinforcement ratio ($\rho_{l,max}$) is required to ensure ductile failure, thus yielding of the steel before compression failure of the concrete, ensuring sufficient rotation capacity at ULS (ductile fracture). The ductility, however, is reduced by increasing the amount of reinforcement. Increasing the reinforcement ratio decidedly stiffens the section against rotation, which can lead to failure of the concrete compression zone without occurrence of preceding (large) deformations or cracks ('no warning of imminent collapse'). The upper limit is also required to avoid congestion of reinforcement, which may cause insufficient compaction or poor bond between reinforcement and concrete.

Figure 34 depicts an M-κ diagram for a reinforced concrete section with ρ_l as the only variable. The first branch, the uncracked section, goes until the (fictitious) cracking moment M_r . For convenience's sake this point is kept constant as starting point for the next phase at every ρ_l . In reality, there are (minor) differences between the cracking moments, since the calculation takes place with an n-weighted cross-section ($n = E_s/E_c$) taking the influence of the reinforcement into account. More reinforcement results in a higher moment of inertia, but compared to M_e , M_{pl} and M_u the differences in M_r can be neglected.

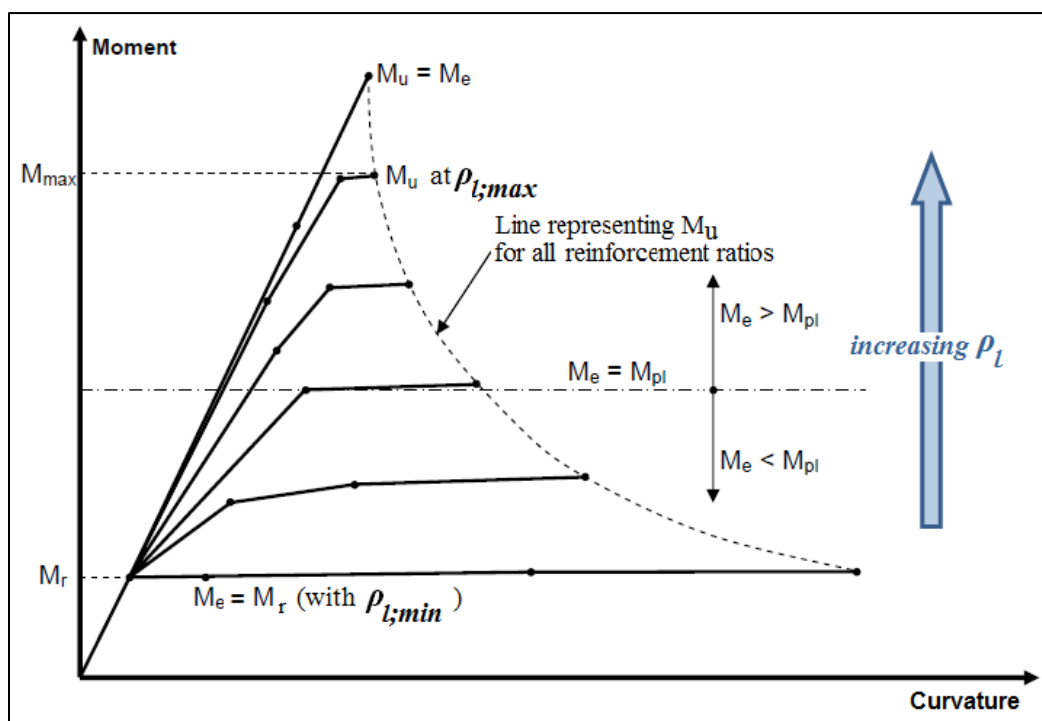


Figure 34: The M-(N)-κ diagram with reinforcement ratio (ρ_l) as variable

The following details can be noted in the diagram of Figure 34:

- With a decreasing ρ_l , the difference between M_u and M_r becomes smaller. To avoid brittle fracture, it is therefore necessary to define a $\rho_{l,min}$;
- With an increasing ρ_l , the 'horizontal' branch between M_c/M_{pl} and M_u becomes smaller. The yield path becomes smaller and at a very high reinforcement ratio there will be no yielding at all. This form of failure is also undesirable and therefore a $\rho_{l,max}$ must be defined;
- With an increasing ρ_l , the tension-stiffening effect reduces. Eventually, the points origin-①-③ as shown in Figure 30 are lying approximately on one line and there is no shaded area anymore;
- The ability to deform plastically increases with a decreasing ρ_l .

In Figure 34 the (almost) horizontal branch represents the curvature distance between $M_e - M_u$ or between $M_{pl} - M_u$. The dividing line is shown in the middle of the diagram; on this line it holds that $M_e = M_{pl}$. Below this line the yielding of the reinforcement will always occur before the crushing of concrete, so $M_e < M_{pl}$. While above this line the opposite holds; the concrete will crush before the reinforcement yields, so $M_{pl} < M_e$. Often $M-\kappa$ diagrams are based on the situation where yielding of the reinforcement occurs first, but this only holds for relatively low reinforcement ratios.

The "horizontal" branch in the $M-\kappa$ diagram actually determines the reserve that the structure possesses before collapsing, the so-called "rotational capacity" (the ability to deform). The longer this branch, the more a structure can deform. After all, the horizontal branch represents an increase in the curvature. The longest branch is found at the bottom of the diagram, where the reinforcement ratio is minimal ($\rho_{l,min}$). It is precisely enough to take up the cracking moment.

At the top of the diagram one finds a point without a horizontal branch. This is the point where at the same time the reinforcement yields and the bending moment capacity of the structure is reached, so $M_e = M_u$. One of the principles in the safety philosophy of concrete structures is that the reinforcement should yield (deform) before compression failure of the concrete occurs. This condition can be expressed in a limit for the maximum height x_u of the concrete compression zone and the maximum reinforcement ratio $\rho_{l,max}$ ensuing from this height. For normal concrete (thus $\leq C50/60$) and reinforcing steel B500, the maximum compressive zone $x_u = 0.448 d$ according to [42].

Influence axial compressive force (N'_c)

An axial compressive force (N'_c) causes a reduction of the tensile stress in the concrete cross-section. The compressive stress (indirectly) provides for an increase in the stiffness of the element. This is clearly seen in Figure 35, when comparing the case $N = 0$ with $N \neq 0$ kN. The presence of an axial compressive force in the cracked cross-section leads to an increased bending stiffness EI , which is clearly reflected by the steepening of the slope of branches ①-② and ②-③ with increasing N . The "enlarged view" in Figure 35 also shows that an increased N leads to an increased cracking moment M_r and a shorter yield path. The presence of a higher N shows more brittle behaviour, reflected by a shorter 'horizontal branch'(③-④). The stiffness of the uncracked cross-section remains constant, regardless of whether or not the element is loaded by an axial compressive force. For deformation calculations it is safer to assume a lower bending stiffness. Therefore, it is preferred to use $M-\kappa$ diagrams ($N'_c = 0$) above $M-N-\kappa$ diagrams in calculating deformations.

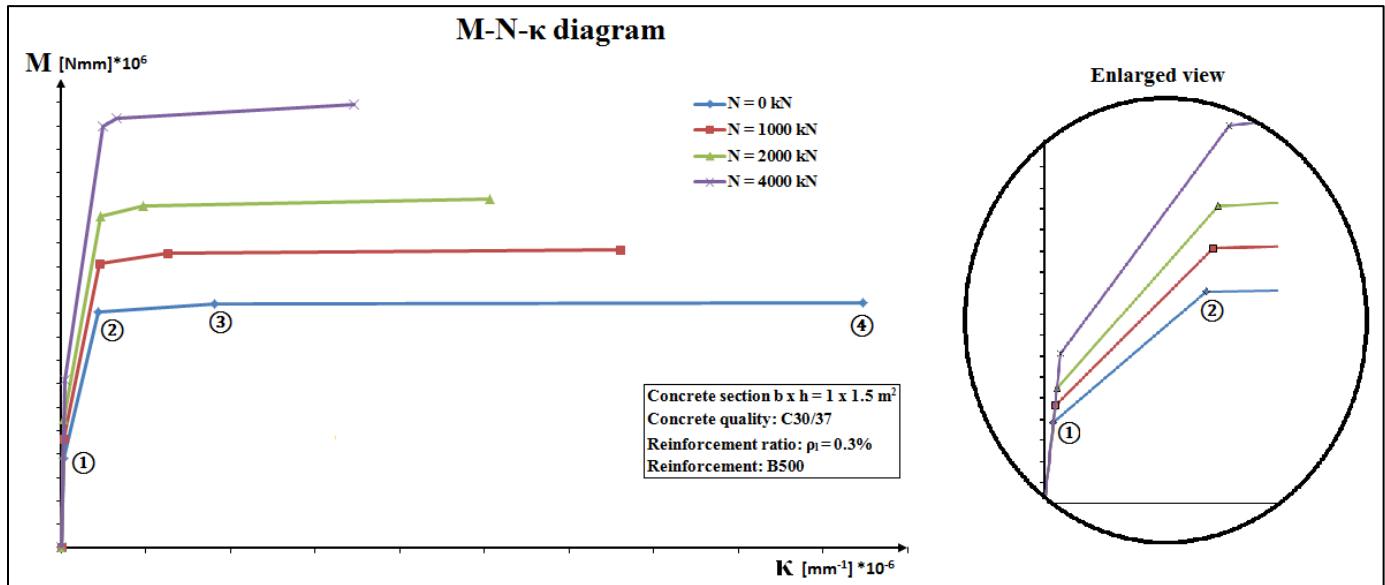


Figure 35: The M-N-κ diagram with normal compressive force ($N = N'$) as variable

3.7. EC2: Minimum and maximum reinforcement ratio diaphragm walls

In order to prevent brittle failure by steel rupture and to ensure sufficient ductility, a minimum reinforcement ratio ($\rho_{l,\min}$) and a maximum reinforcement ratio ($\rho_{l,\max}$) are required, respectively.

EC2, clause 9.6.2 states the following for the vertical reinforcement applied in reinforced concrete walls with a length to thickness ratio of 4 or more:

- The maximum area of reinforcement for walls outside laps is: $A_{sv,\max} = 0.04A_c$. However, this area can be increased provided that the concrete can be placed and compacted sufficiently;
- The minimum area of vertical reinforcement in walls is given by: $A_{sv,\min} = 0.002A_c$. Half of this area should be located at each face. The distance between two adjacent vertical bars should not exceed the lesser of either three times the wall thickness or 400 mm.

A_c represents the total cross-sectional area of concrete. If the reinforcement ratio is defined based on A_c one finds $\rho_{l,\min} = 0.2\%$ and $\rho_{l,\max} = 4\%$ for a diaphragm wall.

3.8. Software programs using M-N-κ diagram: PCSheetPileWall

The bending stiffness EI of diaphragm walls is not constant over the height, but it varies as a function of the magnitude of the *occurring bending moment and the amount of reinforcement*. As soon as the cracking moment M_r has been exceeded, the wall stiffness decreases at an increasing bending moment. The stiffness which is reached in each stage of construction depends on the calculated moment. However, if the wall stiffness is adjusted, this in its turn influences the calculated moment again. In order to gain a clear insight into the actual occurring moment distribution of the wall, it is necessary to apply the reduced bending stiffness following from an M-N-κ diagram, based on the amount of reinforcement.

Currently, there are almost no retaining wall calculation programs available in which the reinforced concrete wall stiffness is included based on the bending moment. The only known exception is formed by the program PCSheetPileWall, where the use of M-κ diagrams is supported with or without an axial force.

Optionally, creep effects can be considered while effects of unloading with respect to a previous construction phase are taken into account automatically.

It is most realistic to calculate the bending moment in a diaphragm wall using an "interaction" model in which the soil behaviour is also taken into account. The wall deformation depends on both the soil stiffness (k_s) and the wall stiffness (EI). A reduced wall stiffness results in greater wall deformations, but on the other hand the deformations on their turn influence the wall stiffness. For geotechnical structures the influence of the soil behaviour on the M and EI of the wall is accounted for by means of the:

- Elastic foundation model, representing the soil stiffness using elastic springs. PCSheetPileWall is based on this model;
- Finite element model, which gives a very realistic representation of the soil behaviour. In this research the program Plaxis 2D will be used. This model gives a more accurate prediction of the soil-wall interaction. The only drawback of this program is that the variable stiffness over the wall height can not be taken into account automatically, thus it is not based on the M - N - κ diagram. The varying stiffnesses (cracked and uncracked stiffnesses) must be entered manually for the various sections.

4. DESIGN STANDARDS: CRACKED VS. UNCRACKED BENDING STIFFNESS

4.1. EC2: Behaviour of not fully cracked member

As long as the occurring moment in a reinforced concrete member does not exceed the cracking moment (M_r), the member is in the uncracked condition behaving in a linear elastic manner represented by the uncracked stiffness (EI_{uncr}). When the bending moment in a cross-section reaches M_r , flexural cracks form in the outermost layers of the tension zone. As the bending moment increases the cracks start propagating. The section becomes fully cracked, when the flexural cracks reach the neutral axis, rendering the entire tension zone ineffective in resisting the bending moment. Due to cracking the bending stiffness has decreased to the so-called cracked bending stiffness (EI_{cr}), which is assumed to be $1/3EI_{\text{uncr}}$. The background concerning this approach for the cracked bending stiffness is explained in section 4.2. In practice it is more common to find members consisting of cracked and uncracked zones instead of a totally uncracked or fully cracked member. This implies the existence of an actual variable bending stiffness (EI_{var}) along the reinforced concrete member. The decreased bending stiffnesses in the cracked zones will lead to greater deformations of the concrete member as a whole.

In structural design deformation calculations are complicated by the non-linear behaviour of concrete. The deformation calculations in Eurocode 2 (EC2) are based on the determination of the curvatures and deflections of a concrete beam corresponding to its uncracked and fully-cracked conditions. EC2 states in clause 7.4.3 that:

“Members which are expected to crack, but may not be fully cracked, will behave in a manner intermediate between the uncracked and fully cracked conditions”.

EC2, Equation (7.18) requires the calculation of a deformation value which is a weighted average of the uncracked and fully-cracked state of the member:

$$\alpha = \zeta\alpha_{\text{II}} + (1 - \zeta)\alpha_1 \quad (\text{Eq. 4.1})$$

Where:

- α The considered deformation parameter, e.g. a strain, curvature, rotation or deflection
- $\alpha_1, \alpha_{\text{II}}$ Values of the deformation parameter calculated for the uncracked and fully cracked conditions, respectively
- ζ Distribution coefficient allowing tension stiffening, where in case of pure bending it holds:

$$\zeta = 1 - \beta \left(\frac{M_r}{M} \right)^2 \quad (\text{Eq. 4.2})$$

With:

$\zeta = 0$ for uncracked sections

β is a coefficient taking account of the duration loading or repeated loading
 = 1.0 for short-term (instantaneous) loading
 = 0.5 for sustained loads or many cycles of repeated loading

M_r is the cracking moment

M is the maximum service moment

Figure 36 represents the moment-curvature relation in a reinforced concrete section under pure bending just before yielding of the reinforcement. The curvature is given by $\kappa = 1/r$. The slope of the $1/r_I$ – and $1/r_{II}$ – curve represent the stiffnesses EI_{uncr} and EI_{cr} , respectively.

According to EC2 the actual EI_{var} along the reinforced concrete member can be calculated by interpolating between the two extremes, namely the uncracked stiffness (EI_{uncr}) and the fully cracked stiffness (EI_{cr}). Analogous to (Eq. 4.1), the actual varying bending stiffness for a cracked structure can be found from:

$$EI_{var} = \zeta \cdot (EI_{cr}) + (1 - \zeta) \cdot (EI_{uncr}) \quad (Eq. 4.3)$$

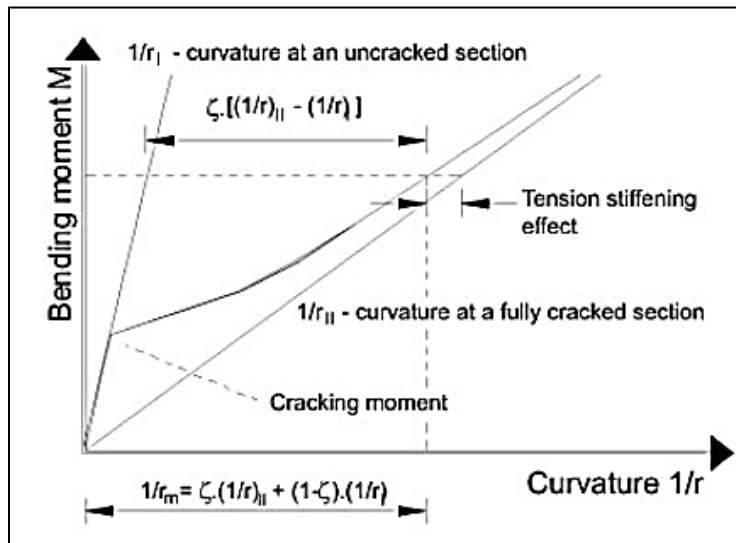


Figure 36: Moment-curvature relation in a reinforced concrete section under pure bending before reinforcement yielding [34]

4.2. EC2 & ACI 318-05: Fully cracked bending stiffness

The in-plane bending stiffness (EI) of a concrete element is the product of two variables, which are subject to change during the course of loading. These are:

1. The in-plane moment of inertia (I), reflecting the cross-sectional resistance to loading. The variation in the moment of inertia is associated with the cracking of concrete due to the tensile strains being greater than the cracking strain of concrete.
2. The modulus of elasticity (E_c), reflecting the material resistance to loading. The variation in the modulus of elasticity with the increasing load is caused by the non-linear stress-strain behaviour of concrete beyond the elastic limits.

In a finite element analysis the bending stiffness is basically expressed in terms of the product of the modulus of elasticity of concrete and the *moment of inertia of the gross concrete section* ($E_c I_g$). Instead of modifying cracked sections with the proper *effective moment of inertia* ($I_{c,eff}$), it is easier to modify the corresponding E_c - value by assigning an *effective modulus of elasticity for concrete* ($E_{c,eff}$) and keeping I_g constant in the analytical models. Thus, the product of $E_{c,eff}$ and I_g still reflects the same amount of reduction in stiffness due to cracking. In addition, the modification of E_c instead of I_g provides the flexibility in using any finite element software.

The bending stiffness (EI_{cr}) of a fully cracked cross-section can be approached in 2 ways, namely by means of:

1. “ $E_{c,eff}$ -approach”, defined in the EC2 (NEN-EN 1992-1-1);
2. “ $I_{c,eff}$ -approach”, defined in the ACI 318-05 and different research articles (see [28], [29], [32], [33])

▪ The $E_{c,eff}$ – approach

In this approach the effective concrete modulus ($E_{c,eff}$) is determined as a result of the non-linear behaviour and creep, while the moment of inertia of the concrete cross-section remains constant. The moment of inertia is considered to be equal to that of the uncracked section. With the exception of beams with heavy reinforcement, the gross moment of inertia (I_g) gives close values to the uncracked moment of inertia (I_{uncr}). Because of the reinforcement I_{uncr} is somewhat higher than I_g . I_g , which neglects the contribution of the reinforcement, is obtained from the following equation:

$$I_g \approx I_{uncr} = \frac{1}{12}bh^3 \quad (Eq. 4.4)$$

The uncracked stiffness is defined as:

$$EI_{uncr} = E_c I_g \quad (Eq. 4.5)$$

According to *NEN-EN 1992-1-1+C2:2011(EC2)*, clause 5.8.7.2 (4) and 7.4.3 (5) the unfavourable effect of cracking on the bending stiffness of statically indeterminate structures can be simplified by assuming a *fully cracked section*. The total deformation, including creep, can be calculated using the effective modulus of elasticity for concrete as represented by EC2, Equation (7.20):

$$E_{c,eff} = \frac{E_{cm}}{1 + \varphi(\infty, t_0)} \quad (Eq. 4.6)$$

Where:

$\varphi(\infty, t_0)$ The final value of the creep coefficient depending on the relative humidity (R.H), age loading time, concrete quality, cross-sectional dimensions and load duration

The creep coefficient can be derived using EC2, 3.1.4, Figure 3.1. As a rule of thumb the creep coefficient is assumed to be $\varphi(\infty, t_0) \approx 2$ in engineering practice. Based on this assumption the bending stiffness of a fully cracked cross-section becomes:

$$EI_{cr} = E_{c,eff} \times I_g = \frac{E_c}{1+2} \times I_g = \frac{1}{3} E_c I_g \Leftrightarrow EI_{cr} = \frac{1}{3} EI_{uncr} \quad (Eq. 4.7)$$

▪ The $I_{c,eff}$ – approach

In this approach the elasticity modulus of concrete is considered to be constant, while the moment of inertia is varying along the reinforced concrete member. The overall moment of inertia of a concrete member decreases gradually from the uncracked moment of inertia (I_{uncr}) to the fully cracked moment of inertia (I_{cr}), as flexural cracks form at discrete locations along the span. Figure 37 depicts the transformed section of a cracked rectangular section. Based on this, the moment of inertia of a section in the fully cracked condition is determined from (Eq. 4.8), which assumes that the concrete in the compression zone has a linear elastic behaviour up to the yielding of the tension reinforcement.

$$I_{cr} = \frac{1}{12}bc^3 + nA_s(d-c)^2 \quad (Eq. 4.8)$$

Where:

- b The width
- c The neutral axis depth of the fully-cracked section
- d The effective depth of the tension reinforcement
- n The modular ratio of steel to concrete (E_s/E_c)
- A_s The total cross-sectional area of longitudinal reinforcement

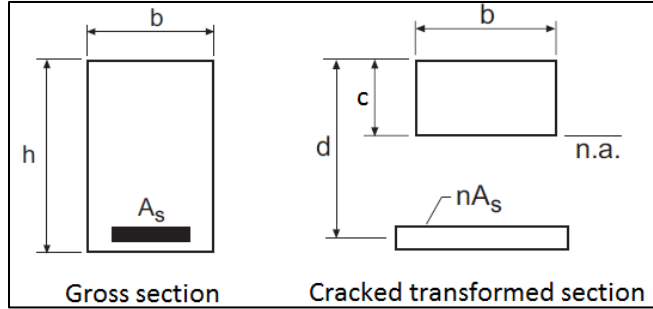


Figure 37: Gross and cracked transformed section of a rectangular beam (without compression reinforcement) [35]

To simplify the deformation calculations of not fully cracked flexural members, the concept of effective bending stiffness (EI_{eff}) is used. As the applied load or moment is increased more cracks are formed, resulting in a decrease of the tension stiffening effect (the tensile contribution of the concrete between the cracks). The decrease in the tension-stiffening of concrete leads to the gradual decrease in the moment of inertia of the concrete member. This gradual decrease is taken into consideration by the effective moment of inertia ($I_{c,eff}$) approach. If the elasticity modulus of concrete is considered constant, the effective moment of inertia can be considered uniform along the member. $I_{c,eff}$ will be a function of the moment of inertia of the uncracked section (I_{uncr}) and the moment of inertia of the cracked section (I_{cr}).

ACI 318-05, Equation (9-8) concerns the effective moment of inertia expression - also known as the Branson expression (1965) - which averages the moments of inertia of the uncracked and fully-cracked portions of a concrete flexural member:

$$I_{c,eff} = \left(\frac{M_r}{M_a}\right)^3 \cdot I_g + \left[1 - \left(\frac{M_r}{M_a}\right)^3\right] \cdot I_{cr}, \text{ or} \quad (\text{Eq. 4.9})$$

$$I_{c,eff} = I_{cr} + (I_g - I_{cr}) \cdot \left(\frac{M_r}{M_a}\right)^3, \text{ where } I_{cr} \leq I_{c,eff} \leq I_g \quad (\text{Eq. 4.10})$$

Where:

- I_g The moment of inertia of the gross concrete section, neglecting reinforcement
- I_{cr} The moment of inertia of the fully cracked section
- M_r The cracking moment
- M_a The maximum bending moment in the member
- ‘Power 3’ A constant proposed by Branson for simply supported beams to include tension stiffening of concrete and also the variations in the stiffness along beams.

Branson's expression provides accurate estimates for reinforced concrete beams with *reinforcement ratios greater than 1%*, which corresponds to an I_g/I_{cr} ratio of 3. For lower reinforcement ratios ($I_g/I_{cr} < 3$), the member response estimated by Branson's approach is stiffer than the actual response, resulting in the underprediction of the deflections. A plot of the bending moment and deflections, as the EI decreases from the uncracked condition ($E_c I_g$) to the fully cracked condition ($E_c I_{cr}$), is shown in Figure 38.

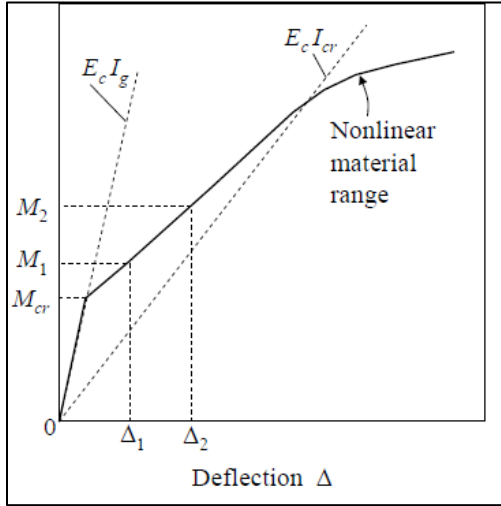


Figure 38: Increasing deflections and decreasing EI as cracking progresses [30]

The $I_{c,eff}$ provides a transition between the upper and lower limits of I_g and I_{cr} as a function of the level of cracking represented by M_a/M_{cr} . This relation is shown in Figure 39:

- If $M_a/M_{cr} < 1$, no cracking is likely and $I_{c,eff} = I_g$
- If $M_a/M_{cr} > 3$, the cracking will be extensive and $I_{c,eff} = I_{cr}$

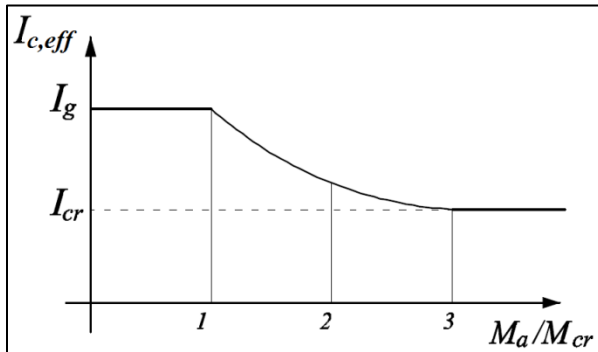


Figure 39: Variation in effective moment of inertia with occurring bending moment [31]

Branson's approach is applicable for $I_g/I_{cr} = 3$. This relation is proven to be true if substituted in the $I_{c,eff}$ formula (Eq. 4.10). In the uncracked situation with $I_{c,eff} = I_g$, one needs to find that $M_a/M_{cr} = 1$:

$$I_{c,eff} = I_{cr} + (I_g - I_{cr}) \cdot \left(\frac{M_r}{M_a}\right)^3 \xrightarrow[\substack{\text{Uncracked condition} \\ I_{c,eff} = I_g; I_{cr} = \frac{1}{3} I_g}]{I_g} I_g = \frac{1}{3} I_g + (I_g - \frac{1}{3} I_g) \cdot \left(\frac{M_r}{M_a}\right)^3$$

$$\Leftrightarrow \frac{2}{3} I_g = \frac{2}{3} I_g \cdot \left(\frac{M_r}{M_a}\right)^3 \Leftrightarrow \left(\frac{M_r}{M_a}\right)^3 = 1 \Leftrightarrow \frac{M_a}{M_r} = 1 \quad \text{OK!}$$

The bending stiffness of a fully cracked cross-section becomes:

$$EI_{cr} = E_c \times I_{c,eff} \xrightarrow[I_{c,eff}=I_{cr}=\frac{1}{3}I_g]{\text{Fully cracked}} E_c \times \frac{1}{3} I_g = \frac{1}{3} E_c I_g \Leftrightarrow EI_{cr} = \frac{1}{3} EI_{un-cr} \quad (\text{Eq. 4.11})$$

Conclusion: From both the “ $E_{c,eff}$ -approach” as the “ $I_{c,eff}$ -approach” it is found that $EI_{cr} = \frac{1}{3} EI_{un-cr}$; see (Eq. 4.7) and (Eq. 4.11). In the FEM-analysis it is easier to apply a constant moment of inertia and modify the modulus of elasticity.

4.3. Bending stiffnesses: EI_0 , EI_{var} and EI_∞

In this research the bending stiffness EI for the uncracked and fully cracked condition is calculated as the product of moment of inertia of the gross concrete section (I_g) and the modulus of elasticity of concrete (E_c), where according to [39] E_c is applied as follows in the design process:

- For SLS-calculations the mean value E_{cm} is used;
- For ULS-calculations a partial safety factor, γ_{cE} , is used to give a design value for the modulus, $E_{cd} = E_{cm}/\gamma_{cE}$ (where γ_{cE} is 1.2).
- For long-term deflection calculations E_{cm} is modified by creep to give an effective modulus, $E_{c,eff}$. This is calculated using the expression $E_{c,eff} = E_{cm}/(1 + \phi)$ where ϕ is the creep coefficient with a value typically between 1 and 3.

Because of the deformation calculations (SLS) considered in this research, it is obvious that E_{cm} has to be applied. From this point forward the bending stiffnesses considered in this report will be addressed as follows:

- EI_0 : the uncracked bending stiffness, where $EI_0 = E_{cm} \times I_g$;
- EI_∞ : the cracked bending stiffness, where $EI_\infty = E_{cm} \times \frac{1}{3} I_g$;
- EI_{var} : the variable bending stiffness, which will be determined from the M-(N)- κ diagram generated by the program PCSheetPileWall.

4.4. Additional information

Although seismic analysis is out of scope for this research, some similarity can be found with regard to approximating the cracked stiffness of the reinforced concrete walls. Mostly seismic analysis and design of reinforced concrete structures are performed based on linear response, not taking the influence of cracking and effective stiffness into account. For the design codes that do recognize the influence of cracking, the stiffness of the cracked section (EI_c) is considered to be proportional to the stiffness of the gross uncracked section (EI_g), specifying reduction factors to be applied to the stiffness of the uncracked cross section. According to Table 2 the stiffness of cracked walls should be taken as $0.35 I_g$ which is about the $1/3 I_g$ mentioned in section 4.2 for flexural concrete members.

| Element | <i>New Zealand Code</i> | <i>ACI 318S-05 Design Code</i> |
|-----------------|-------------------------|--------------------------------|
| Beams | $0.35I_g$ | $0.35 I_g$ |
| Columns | $0.40 - 0.70I_g$ | $0.70 I_g$ |
| Walls uncracked | ----- | $0.70 I_g$ |
| Walls cracked | ----- | $0.35 I_g$ |

Table 2: Reduction factors for the cracked bending stiffness used in seismic design [27]

References

- [1] Soletanche Bachy. (n.d.). [http://www.bachy-soletanche.com/SBF/sitev4_uk.nsf/technique/diaphragm-wall/\\$File/Parois%20moul%C3%A9es%20%26%20Barrettes%20va.pdf](http://www.bachy-soletanche.com/SBF/sitev4_uk.nsf/technique/diaphragm-wall/$File/Parois%20moul%C3%A9es%20%26%20Barrettes%20va.pdf). Retrieved from <http://www.bachy-soletanche.com>.
- [2] Masuda, T. (1993). *Behavior of deep excavation with diaphragm wall*. Massachusetts Institute of Technology, Department of Civil and Environmental Engineering .
- [3] CUR. (2005, September). https://books.google.nl/books?id=QS2PhGP9ys0C&pg=PA281&lpg=PA281&dq=blum+method&source=bl&ots=ShECG6-BPQ&sig=8y_cG-0F8q139jsd2mzS0Cz5vx4&hl=nl&sa=X&ei=ch0pVaGENMe9Pe6kcgf&ved=0CD8Q6AEwAw#v=onepage&q=blum%20method&f=false. Retrieved from <https://books.google.nl>.
- [4] Richards, T. (2005). Diaphragm walls. *21st Central PA Geotechnical Conference*. Pennsylvania.
- [5] Chandra, S. (2014, December 3). Modelling of soil behaviour. Retrieved from http://home.iitk.ac.in/~peeyush/mth426/Lec4_schandra.pdf
- [6] <http://mfile.narotama.ac.id/files/Civil%20Engineering/Deep%20Excavation;%20Theory%20and%20Practice/Chapter%207%20%20Stress%20And%20Deformation%20Analysis;%20Beam%20On%20Elastic%20Foundation%20Method.pdf>
- [7] CUR committee C183. (2014). *Quay walls* (2nd ed.). Rotterdam, The Netherlands: CRC Press/Balkema.
- [8] Plaxis b.v. (2002). *Plaxis version 8 - Material Models Manual*. Delft, Netherlands: A. A. Balkema Publishers.
- [9] Pervizpour, M. (2004). Soil Strength. Retrieved from <http://www.lehigh.edu/~mepa/f/ENGR-627-Lect4.pdf>
- [10] Shear Strength of Soil I. (n.d.). Retrieved from <https://www.scribd.com/doc/218776762/CE240LectW111shearstrength1>
- [11] Shear Strength of Soil. (n.d.). Retrieved from <http://www4.hcmut.edu.vn/~cnan/Principles%20of%20geotechnical%20engineering%20%28Fifth%20Edition,%20Das%29/311-363.PDF>
- [12] Shear Strength of Soils. (2001). Retrieved from <http://home.iitk.ac.in/~priyog/Shear%20Strength%20Lecture.pdf>
- [13] Yokoi, H. (1968). Relationship between Soil Cohesion and Shear. *Soil Science and Plant Nutrition*. doi:10.1080/00380768.1968.10432750
- [14] Sankar, U. (n.d.). Slope Stability and Dump Stability. Retrieved from <http://www.slideshare.net/sankarsulimella/slopestability>

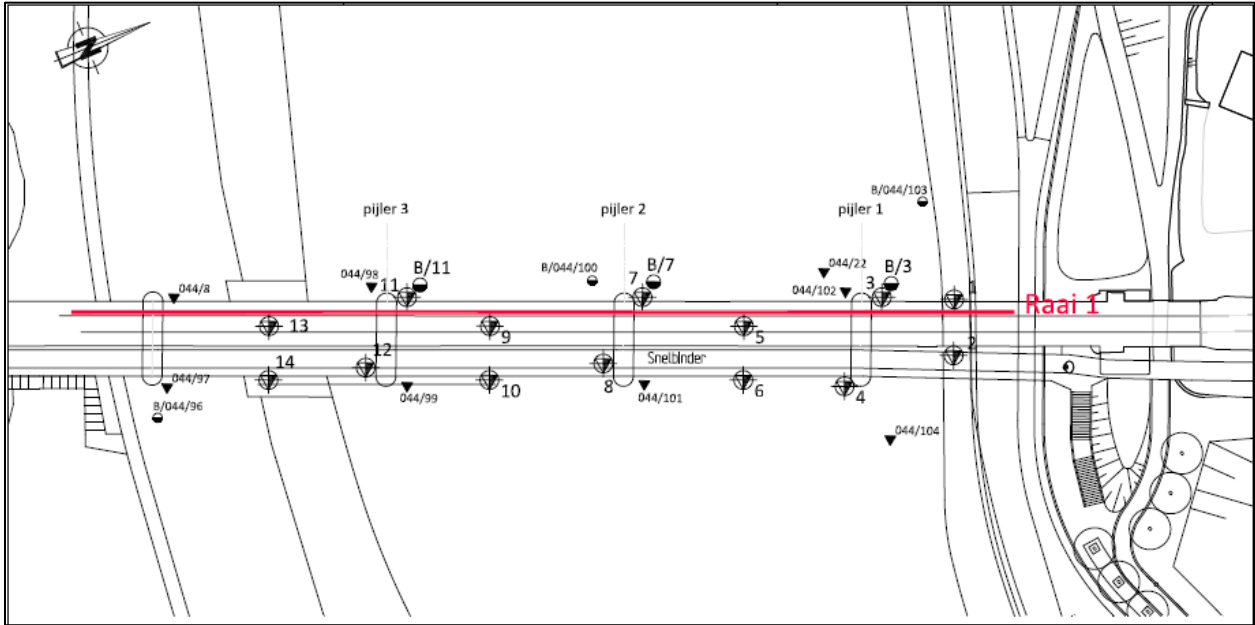
- [15] Koning, M. d. (2006). *Verticaal evenwicht van damwandconstructies*. MSc. Thesis, TU Delft, Civil Engineering and Geosciences.
- [16] Wolsink, G. (n.d.). Helpindex PScheetPileWall version 1.36. Retrieved from <http://members.ziggo.nl/wolsink/>: <http://members.ziggo.nl/wolsink/>
- [17] Verruijt, A. (2003). *Grondmechanica*. Delft, The Netherlands: Delft University Press. Retrieved from <http://geo.verruijt.net/>
- [18] COB/CUR-commissie T114/C174. (2010). *CUR/COB-rapport 231: Handboek Diepwanden-Ontwerp en Uitvoering*. Gouda: Stichting CURNET.
- [19] https://en.wikipedia.org/wiki/Dilatancy_%28granular_material%29
- [20] <http://environment.uwe.ac.uk/geocal/SoilMech/stresses/default.htm>
- [21] Plaxis b.v. (2002). *Plaxis version 8 - Reference Manual*. Delft, Netherlands: A.A. Balkema Publishers.
- [22] CUR commissie C69. (1997). *CUR-publicatie 166: Damwandconstructies*. Gouda: CUR.
- [23] Deltares. (2014). *D-Sheet Piling - User Manual: Design of diaphragm and sheet pile walls*. Delft, The Netherlands.
- [24] Józsa, V. (n.d.). *Effects of rarely analyzed soil parameters for FEM analysis of embedded retaining structures*. Budapest University of Technology and Economics, Geotechnical Department, Budapest, Hungary. Retrieved from <http://www.kiviniria.nl/eygec/papers/03%20UC%20Jozsa.pdf>
- [25] Obrzud, R. (2010). *On the use of the Hardening Soil Small Strain model in geotechnical practice*. Elmepress International. Retrieved from <http://www.geomod.ch/pdf/zsday-hard.pdf>
- [26] Ehsan, R. (2013). *A study of Geotechnical Constitutive Models using Plaxis 2D*. Retrieved from <http://www.indabook.org/d/A-Study-of-Geotechnical-Constitutive-Models-using-PLAXIS.pdf>
- [27] Burgos, M. & Pique, J.R. (2008). Effective Rigidity of Reinforced Concrete Elements in Seismic Analysis and Design. *The 14th World Conference on Earthquake Engineering*. Beijing, China. Retrieved from http://www.iitk.ac.in/nicee/wcee/article/14_05-01-0471.PDF
- [28] Kalkan, I. (2013). Deflection Prediction for Reinforced Concrete Beams Through Different Effective Moment of Inertia Expressions. *International Journal of Engineering Research and Development, Vol.5, No.1*.
- [29] Hussein, K. (2014). How Construction Errors Affect the Bearing Capacity of the Concrete Beams - Inelastic Deflection of Concrete I-Beams. *International Journal of Engineering and Advanced Technology, Volume-3, Issue-4*.
- [30] Jiravacharadet, M. (n.d.). Reinforced Concrete Design - Serviceability. Retrieved from http://www.sut.ac.th/engineering/Civil/CourseOnline/430431/RC21_Service.pdf

- [31] <http://site.iugaza.edu.ps/ssihada/files/2012/09/Serviceability.pdf>
- [32] Al-Khaleefi, A.M. & Jan, C.T. (2005). Designing for the Effect of Progressive Cracking in Reinforced Concrete Slabs. *30th Conference on OUR WORLD IN CONCRETE & STRUCTURES*. Singapore. Retrieved from <http://cipremier.com/100030020>
- [33] Su, R.K.L. & Tang, T.O. (2014). Shear and Flexural Stiffnesses of Reinforced Concrete Shear Walls Subjected to Cyclic Loading. *The Open Construction and Building Technology Journal*.
- [34] http://www.scielo.br/scielo.php?script=sci_arttext&pid=S1983-41952013000300008
- [35] <http://wp.kntu.ac.ir/beheshti/Gross%20and%20Cracked%20Moment%20of%20Inertia%20of%20Rectangular%20and%20Flanged%20Section.pdf>
- [36] NEN-EN 1992-1-1+C2 (nl). (2011). *Eurocode 2: Ontwerp en berekening van betonconstructies - Deel 1-1: Algemene regels en regels voor gebouwen*. Delft: Nederlands Normalisatie-instituut.
- [37] NEN-EN 1992-1-1 (en). (2005). *Eurocode 2: Design of concrete structures - Part 1-1: General rules and rules for buildings*. Delft: Nederlands Normalisatie-instituut.
- [38] Ibrahim, A. (2000). *Linear and Nonlinear Flexural Stiffness Models for Concrete Walls in High-Rise Buildings*. PhD dissertation, The University of British Columbia, Department of Civil Engineering, Vancouver, Canada.
- [39] Bamforth, P., Chisholm, D., Gibbs, J. & Harrison, T. (2008). *Properties of Concrete for use in Eurocode 2 - How to optimise the engineering properties of concrete in design to Eurocode 2*. Surrey: The Concrete Centre.
- [40] NEN-EN 1992-1-1+C2/NB (nl). (2011). *Nationale bijlage bij NEN-EN 1992-1-1+C2, Eurocode 2: Ontwerp en berekening van betonconstructies - Deel 1-1: Algemene regels en regels voor gebouwen*. Delft: Nederlands Normalisatie-instituut.
- [41] CUR commissie. (2012). *CUR-publicatie 166: Damwandconstructies* (Vol. 6e herziene druk). Gouda: Stichting CURNET.
- [42] Braam, C.R. & Lagendijk, P. (2008). *Cement en Beton 2 - Constructieel Gewapend Beton* (Vol. Vierde herziene druk). 's-Hertogenbosch: Cement&BetonCentrum.
- [43] Braam, C. (2010). *Cement en Beton 4 - Ontwerpen in Gewapend beton* (Vol. Tweede herziene druk). 's-Hertogenbosch: Cement&BetonCentrum.

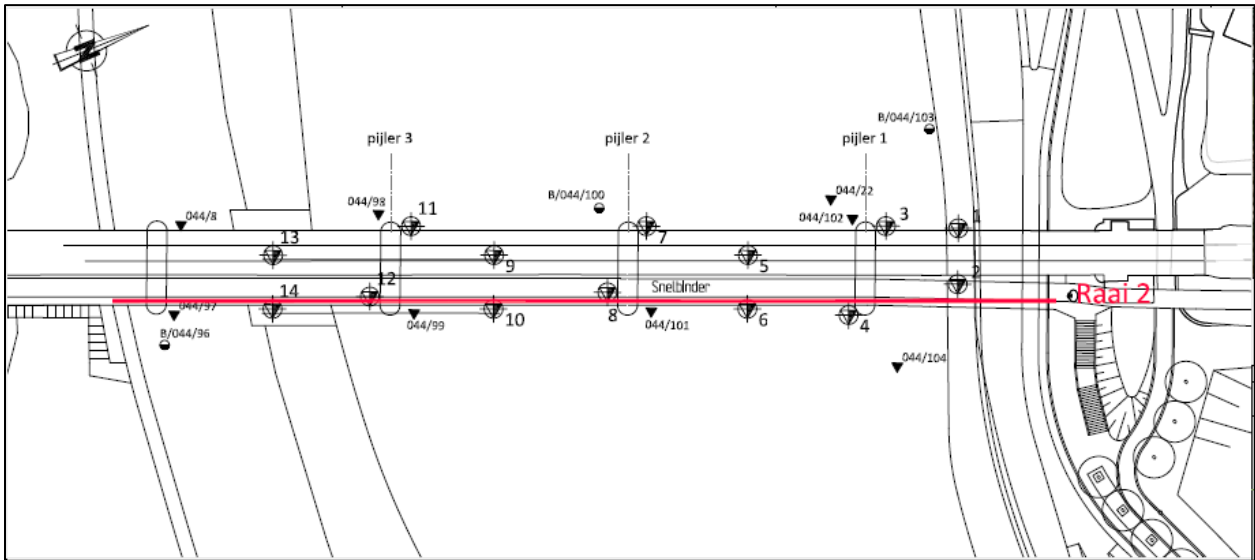
APPENDIX B

GEOTECHNICAL SOIL PROFILES

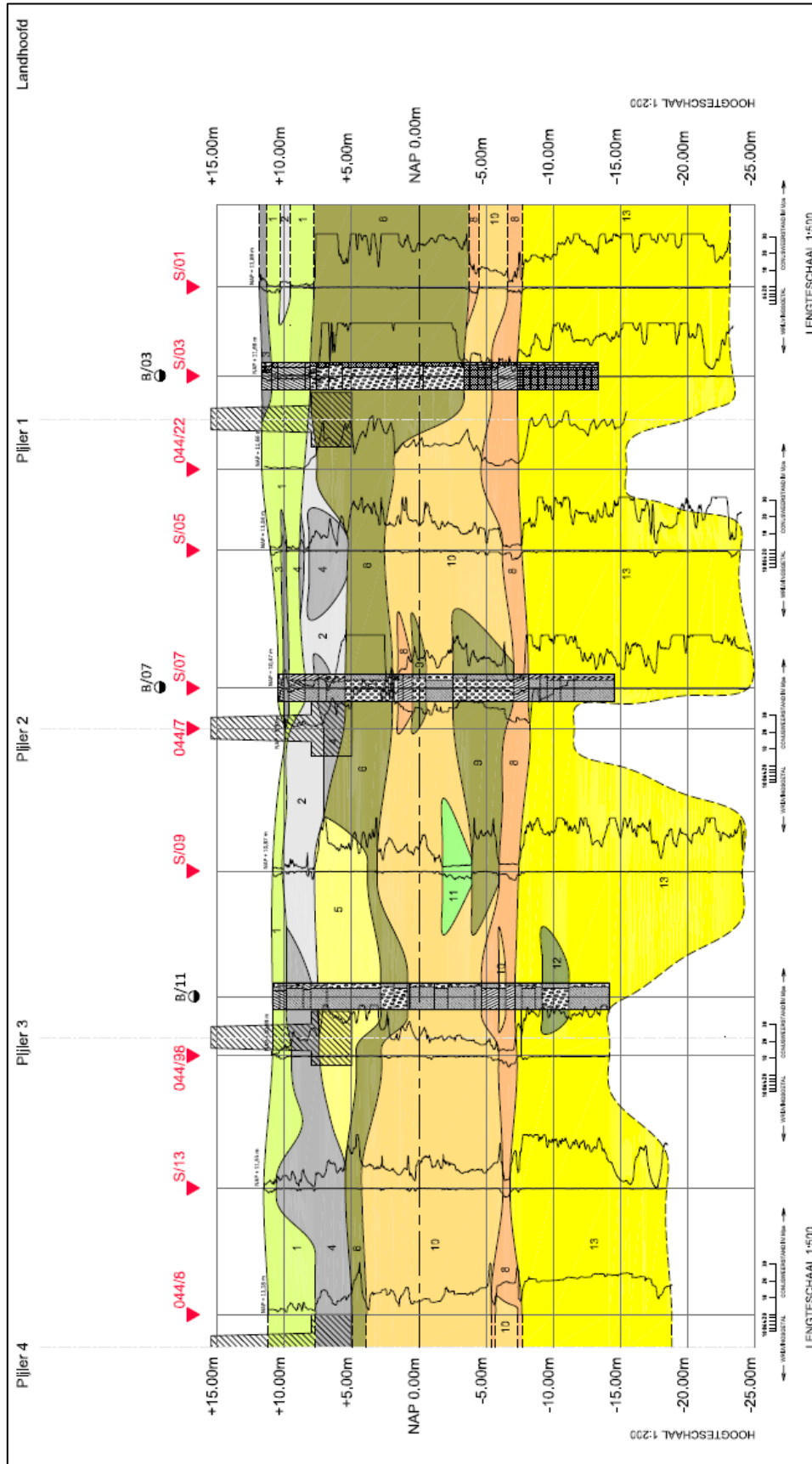
Line of direction 1



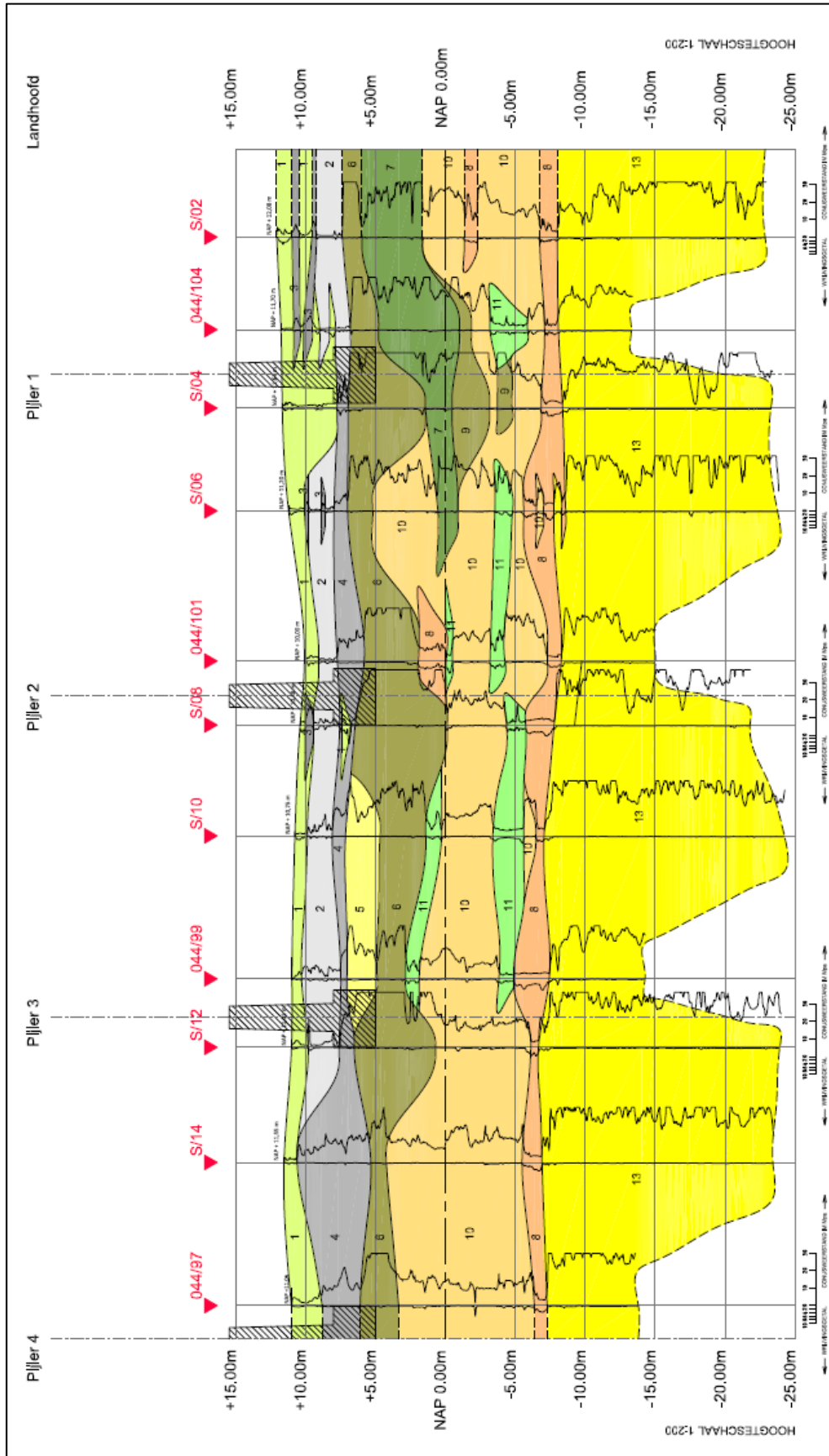
Line of direction 2



Soil profile over Line of direction 1



Soil profile over Line of direction 2



| Legenda Geologisch Profiel | Geologie | | | | | | | | |
|---|---|--|--|--|--|--|--|---|--|
| <p>1 Klei</p> <p>2 zand los</p> <p>3 zand matig vast</p> | <p>Formatie van Echteld</p> | | | | | | | | |
| <p>4 Zand matig vast</p> <p>5 Zand vast</p> <p>6 Grind matig/sterk zandig</p> <p>7 Zand met grindlagen</p> | <p>Formatie van Kreftenheye Drente</p> | | | | | | | | |
| <p>8 Leem</p> <p>9 Grind matig/sterk zandig</p> <p>10 Zand</p> <p>11 Klei</p> | <p>Formatie van Urk - Waalre</p> | | | | | | | | |
| <p>12 Grind matig/sterk zandig</p> <p>13 Zand</p> | <p>Formatie van Waalre</p> | | | | | | | | |
| <p>— — GRENS ONZEKER</p> <p> SONDERING (MOS Grondmechanica B.V)</p> <p> SONDERING</p> <p> BORING</p> | <p>LEGENDA BORINGEN</p> <table border="0"> <tr> <td> ZAND</td> <td> KLEI</td> </tr> <tr> <td> VEEN</td> <td> HOUT</td> </tr> <tr> <td> LEEH</td> <td> PUON</td> </tr> <tr> <td> GROND</td> <td></td> </tr> </table> |  ZAND |  KLEI |  VEEN |  HOUT |  LEEH |  PUON |  GROND | |
|  ZAND |  KLEI | | | | | | | | |
|  VEEN |  HOUT | | | | | | | | |
|  LEEH |  PUON | | | | | | | | |
|  GROND | | | | | | | | | |

Soil parameters, characteristic values

| nr. | Grondlaag | Grondsoort ⁽ⁱⁱ⁾ | γ_{nat} [kN/m ³] | $c_{2\%}$ [*] [kN/m ²] | $\phi_{2\%}$ [*] [graden] | $\psi^{\square(iii)}$ [graden] | E'_{50} ^{ref} [kN/m ²] | E'_{oed} ^{ref} [kN/m ²] | E'_{ur} ^{ref(v)} [kN/m ²] | m | $\gamma_{0,7}$ ^(v) | G_o^{ref} ^(vi) [kN/m ²] |
|------|----------------------------|----------------------------|--|--|---------------------------------------|-----------------------------------|--|---|---|-----|-------------------------------|---|
| 1_1 | Klei zwak zandig | | 19 | 5 | 25 | 0 | 10.000 | 10.000 | 30.000 | 0,8 | $1,0^E-04$ | 90.000 |
| 1_2 | Zand los | | 19 | 0 | 30 | 0 | 15.000 | 15.000 | 45.000 | 0,5 | $1,0^E-04$ | 90.000 |
| 1_3 | Zand matig vast | | 20 | 0 | 31 | 1 | 25.000 | 25.000 | 75.000 | 0,5 | $1,0^E-04$ | 150.000 |
| 2_4 | Zand matig vast | | 20 | 0 | 31 | 1 | 25.000 | 25.000 | 75.000 | 0,5 | $1,0^E-04$ | 150.000 |
| 2_5 | Zand vast | | 21 | 0 | 35 | 5 | 75.000 | 75.000 | 225.000 | 0,5 | $1,0^E-04$ | 450.000 |
| 2_6 | Grind matig / sterk zandig | | 21 | 0 | qc < 20 MPa : 30 | - | 60.000 | 60.000 | 180.000 | 0,5 | $1,0^E-04$ | 360.000 |
| 2_7 | Zand grindgelaagd | | 21 | 0 | qc > 20 MPa : 35 | 5 | 90.000 | 90.000 | 270.000 | 0,5 | $1,0^E-04$ | 540.000 |
| 3_8 | Leem | | 20,5 | 0 | 32,5 | 2,5 | 60.000 | 60.000 | 180.000 | 0,5 | $1,0^E-04$ | 360.000 |
| 3_9 | Grind matig / sterk zandig | | 21 | 5 | 28,5 | 0 | 15.000 | 15.000 | 45.000 | 0,7 | $1,0^E-04$ | 112.500 |
| 3_10 | Zand | | 21 | 0 | 32 | 2 | 45.000 | 45.000 | 135.000 | 0,5 | $1,0^E-04$ | 270.000 |
| 3_11 | Klei siltig | | 20 | 0 | 30 | 0 | 25.000 | 25.000 | 75.000 | 0,5 | $1,0^E-04$ | 150.000 |
| 4_12 | Grind matig / sterk zandig | | 20 | 13 | 22,5 | 0 | 5.000 | 5.000 | 15.000 | 0,8 | $1,0^E-04$ | 45.000 |
| 4_13 | Zand | | 21 | 0 | 32 | 2 | 45.000 | 45.000 | 135.000 | 0,5 | $1,0^E-04$ | 270.000 |
| | | | 21 | 0 | 32 | 2 | 30.000 | 30.000 | 90.000 | 0,5 | $1,0^E-04$ | 180.000 |
| | | | 20 | 0 | 30 | 0 | 15.000 | 15.000 | 45.000 | 0,5 | $1,0^E-04$ | 90.000 |

Opmerkingen:

(i) Aanvulzand: Aangenomen grondparameters van het zand dat is gebruikt voor het aanvullen van de ruimte boven de poer en rondom de pijler.

(ii) Zie geotechnisch lengteprofiel tek.nr. 12-045-AA1 en 12-04-AB1

(iii) $\psi = \phi - 30^\circ$

(iv) $E'_{ur}^{ref} = 3 \times E'_{50}^{ref}$

(v) $\gamma_{0,7} = 1,0E-04$

(vi) $G_o^{ref} = a \times E'_{ur}^{ref}$ met a variërend tussen 2 en 3 van stijve tot slappe grondsoorten

In deze tabel hebben de symbolen de volgende betekenis:

| | | | |
|----------------|--|----------------|--|
| γ_{nat} | : Volumiek grondgewicht onder water | $E'_{oed,ref}$ | : Tangentiële elasticiteitsmodulus uit de samendrukingsproef bij belastingen boven de grensspanning σ_g , geschaald naar de referentiespanning σ_{ref} . |
| q_c | : Conusweerstand | $E'_{ur,ref}$ | : Elasticiteitsmodulus bij ontlasten/herbelasten bij referentiespanning σ_{ref} |
| $c_{2\%}$ | : Effectieve cohesie | m | : Macht in spanningsafhankelijke stijfheidsrelatie $E = f(E_{ref}, \sigma, \sigma_{ref}, m)$ |
| $\phi_{2\%}$ | : Hoek van inwendige wrijving bij vervormingsrek $\epsilon = 2\%$ | $\gamma_{0,7}$ | : Schuifrek bij 0,722 van de maximale waarde van schuifmodulus G bij kleine rekken |
| ψ | : Dilatantiehoek | G_o^{ref} | : Schuifmodulus bij kleine rekken, geschaald naar de referentiespanning σ_{ref} |
| σ_{ref} | : Referentiespanning (= 100 kPa) | | |
| $E'_{50,ref}$ | : Secante elasticiteitsmodulus uit de triaxiaalproef E'_{50} bij 50% mobilisatie van de schuifspanning (geschaald naar de referentiespanning σ_{ref}). | | |

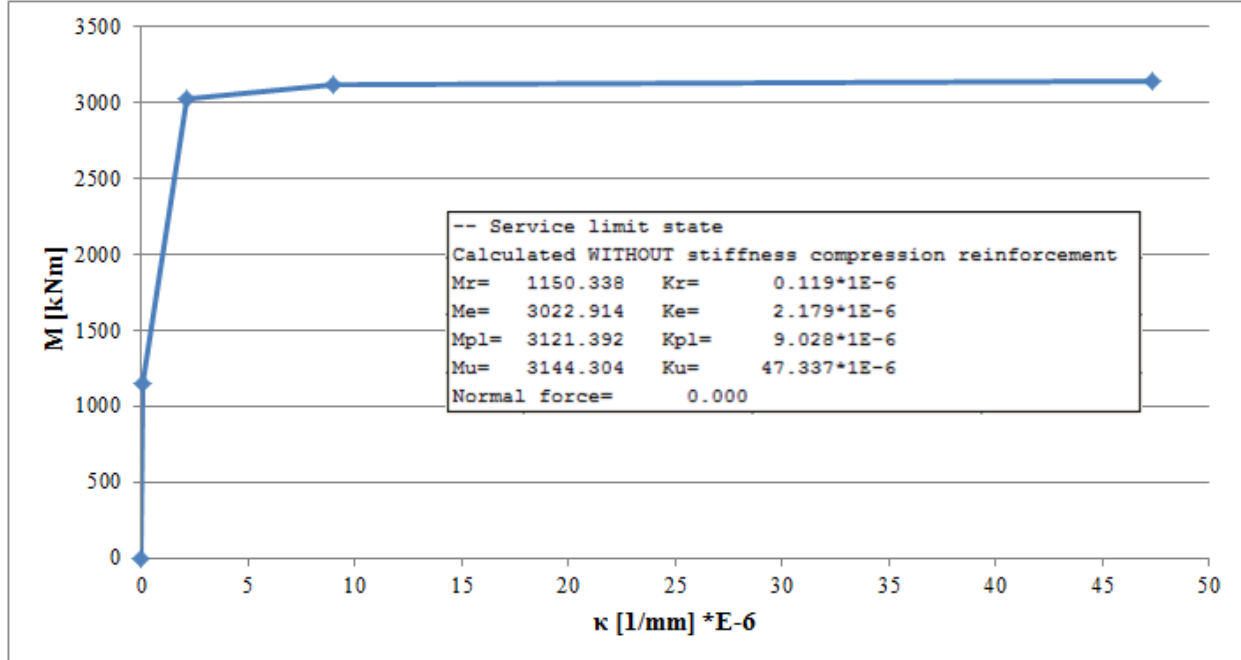
APPENDIX C1

ITERATION PROCESS RIGHT WALL

“WALLS ONLY; HINGED”

Case a: EI (κ)

M-κ diagram diaphragm walls:



Iteration process EI right wall (N = 0 kN)

| | | $M_{Ed,max}$ | κ_{Ed} | | $(EI)_{Ed,min}$ | EA | E | | | $l_{cracked}$ |
|-------------|-------------------|--------------|---------------|-----------|-------------------------------------|----------------------|----------------------|-------|-----------|---------------|
| Iteration # | | [kNm] | [1/mm] | [1/m] | [kNm ² /m ³] | [kN/m ³] | [kN/m ²] | [MPa] | Note: | [m] |
| Procedure 1 | 1 | 2400 | 1.494E-06 | 1.494E-03 | 1.61E+06 | 8.57E+06 | 5.71E+06 | 5713 | E < 11000 | 12.2 |
| | 2 | 1390 | 3.826E-07 | 3.826E-04 | 3.63E+06 | 1.94E+07 | 1.29E+07 | 12916 | E > 11000 | 6 |
| | 3 | 2050 | 1.109E-06 | 1.109E-03 | 1.85E+06 | 9.86E+06 | 6.57E+06 | 6574 | E < 11000 | 11.9 |
| | 4 | 1470 | 4.707E-07 | 4.707E-04 | 3.12E+06 | 1.67E+07 | 1.11E+07 | 11105 | E > 11000 | 6.9 |
| | 5 | 1930 | 9.767E-07 | 9.767E-04 | 1.98E+06 | 1.05E+07 | 7.03E+06 | 7026 | E < 11000 | 11.6 |
| | 6 | 1520 | 5.257E-07 | 5.257E-04 | 2.89E+06 | 1.54E+07 | 1.03E+07 | 10281 | E < 11000 | 7.4 |
| | 7 | 1850 | 8.887E-07 | 8.887E-04 | 2.08E+06 | 1.11E+07 | 7.40E+06 | 7402 | E < 11000 | 11 |
| | 8 | 1560 | 5.697E-07 | 5.697E-04 | 2.74E+06 | 1.46E+07 | 9.74E+06 | 9737 | E < 11000 | 7.8 |
| | 9 | 1820 | 8.557E-07 | 8.557E-04 | 2.13E+06 | 1.13E+07 | 7.56E+06 | 7562 | E < 11000 | 10.8 |
| | 10 | 1570 | 5.807E-07 | 5.807E-04 | 2.70E+06 | 1.44E+07 | 9.61E+06 | 9613 | E < 11000 | 8 |
| | 11 | 1830 | 8.667E-07 | 8.667E-04 | 2.11E+06 | 1.13E+07 | 7.51E+06 | 7508 | E < 11000 | 10.9 |
| | 12 | 1560 | 5.697E-07 | 5.697E-04 | 2.74E+06 | 1.46E+07 | 9.74E+06 | 9737 | E < 11000 | 7.9 |
| | 13 | 1830 | 8.667E-07 | 8.667E-04 | 2.11E+06 | 1.13E+07 | 7.51E+06 | 7508 | E < 11000 | 10.9 |
| | 14 | 1560 | 5.697E-07 | 5.697E-04 | 2.74E+06 | 1.46E+07 | 9.74E+06 | 9737 | E < 11000 | 7.9 |
| | FINAL | 1695 | 7.182E-07 | 7.182E-04 | 2.36E+06 | 1.26E+07 | 8.39E+06 | 8392 | E < 11000 | 9.4 |
| Procedure 2 | Linkerwand_check | 1390 | 3.826E-07 | 3.826E-04 | 3.63E+06 | 1.94E+07 | 1.29E+07 | 12916 | | |
| | Rechterwand_check | 2070 | 1.131E-06 | 1.131E-03 | 1.83E+06 | 9.76E+06 | 6.51E+06 | 6509 | | |

Note: $M_{Ed,max}$ is the maximum occurring moment in the cracked zone. We consider only one EI (which is the corresponding minimum EI) over this cracked height.

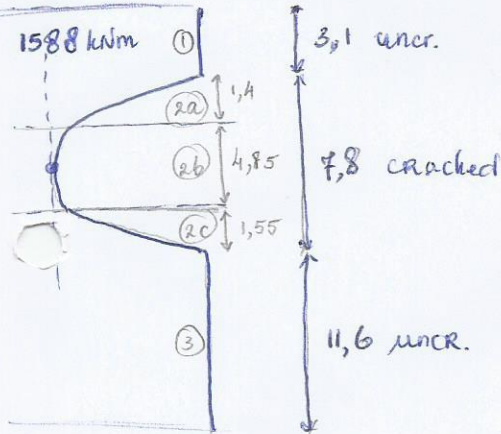
Overview iteration steps right wall (see next pages):

④ Iteration process to find cracked height & EI-distr. Right wall. (2)

- Question: What is cracked height & corresponding EI-distr. of right wall?
- Answer: Iteration process (until cracked height remains the same, $\Delta = 5\%$ allowed!)

$EI = f(M_{\text{optredend, wapening}})$
 ↑
 M-k diagram.

Left wall = partially cracked (cracked area; 3 zones) \Rightarrow Aanhouden bij elke iteratie!

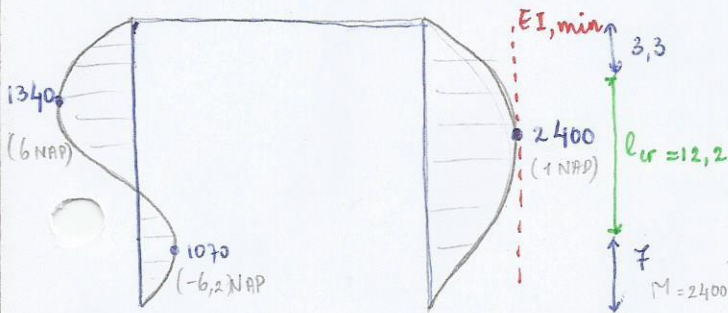


| zone | EI (kNm ² /m) | EA (kN/m) |
|------|--------------------------|--------------------|
| 1 | $9,67 \times 10^6$ | $5,16 \times 10^7$ |
| 2a | $4,71 \times 10^6$ | $2,51 \times 10^7$ |
| 2b | $2,65 \times 10^6$ | $1,41 \times 10^7$ |
| 2c | $4,59 \times 10^6$ | $2,45 \times 10^7$ |
| 3 | $9,67 \times 10^6$ | $5,16 \times 10^7$ |

$w = 0$ kN/m/m!
 $v = 0,2$

Right wall = Iteration proces to find cracked height & corresp. EI-distr.

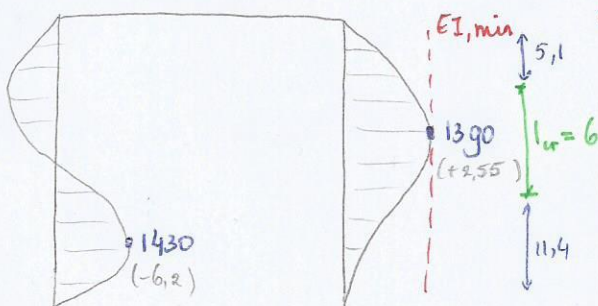
- Iteration #0 = 1st assumption \Rightarrow Right wall totally uncracked!



| zone | l(m) | from - to | EI (kNm ² /m) | EA (kN/m) |
|------|------|-----------|--------------------------|--------------------|
| 1 | 22,5 | +10,5 -12 | $9,67 \times 10^6$ | $5,16 \times 10^7$ |

$M_{\text{result}} = 2400$

- Cracked height (Ploaxis 2D) = $M > M_{cr} = (1150) + 7,2 \text{ t/m} - 5,0 \text{ m} \Rightarrow l_{cr} = 12,2 \text{ m}$
- EI cracked zone = $M_{Ed} = 2400 \Rightarrow (EI)_{Ed, \text{min}} = 1,61 \times 10^6$
 $(EA) = 8,57 \times 10^6$



- Iteration #1

| zone | l(m) | from - to | EI (kNm ² /m) | EA (kN/m) |
|------|------|------------|--------------------------|--------------------|
| 1 | 3,3 | +10,5 +7,2 | $9,67 \times 10^6$ | $5,16 \times 10^7$ |
| 2 | 12,2 | +7,2 -5,0 | $1,61 \times 10^6$ | $8,57 \times 10^6$ |
| 3 | 7 | -5,0 -12 | $9,67 \times 10^6$ | $5,16 \times 10^7$ |

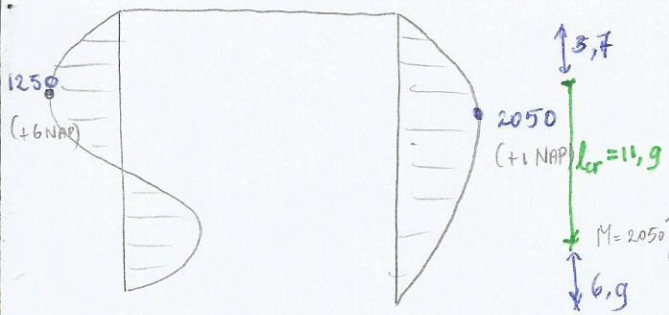
$M_{\text{result}} = 1390$

- Height cracked zone (Ploaxis 2D) = $M > M_{cr} + 5,4 \text{ t/m} - 0,6 \text{ m} \Rightarrow l_{cr} = 6 \text{ m}$
- EI cracked zone: $M_{Ed} = 1390 \Rightarrow (EI)_{Ed, \text{min}} = 3,63 \times 10^6$
 $EA = 1,94 \times 10^7$

Note: * $EI = 9,67 \times 10^6 \text{ kNm}^2/\text{m}^4$
 $EA = 5,16 \times 10^7 \text{ kN/m}^2$

Iteration # 2 :

$M_{\text{result}} = 2050$

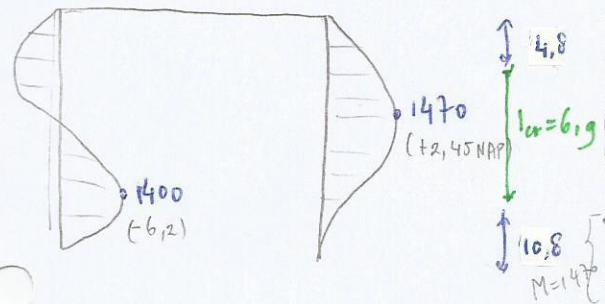


| zone | l(m) | from | to | EI (kNm ² /m ⁴) | EA (kN/m ²) |
|------|------|-------|------|--|-------------------------|
| 1 | 5,1 | +10,5 | +5,4 | * | * |
| 2 | 6 | +5,4 | -0,6 | $3,63 \times 10^6$ | $1,94 \times 10^7$ |
| 3 | 11,4 | -0,6 | -12 | * | * |

Height cracked zone = $+6,8 \text{ t/m} - 5,1 \text{ m} \Rightarrow l_{cr} = 11,9 \text{ m}$
 EI " " = $M_{Ed} = 2050 \rightarrow (EI)_{Ed, \text{min}} = 1,85 \times 10^6$
 $EA = 9,86 \times 10^6$

Iteration # 3 :

$M_{\text{result}} = 1470$

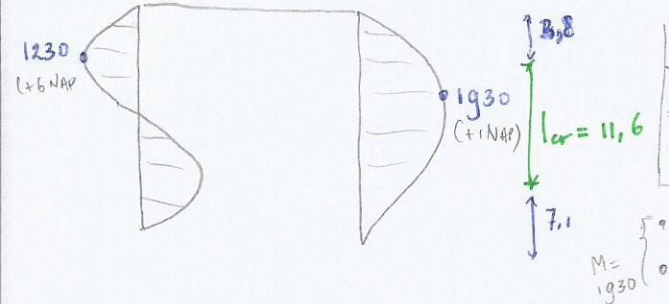


| zone | l(m) | from | to | EI (kNm ² /m ⁴) | EA (kN/m ²) |
|------|------|-------|------|--|-------------------------|
| 1 | 3,7 | +10,5 | +6,8 | * | * |
| 2 | 11,9 | +6,8 | -5,1 | $1,85 \times 10^6$ | $9,86 \times 10^6$ |
| 3 | 6,9 | -5,1 | -12 | * | * |

Height cracked zone = $+5,7 \text{ t/m} - 1,2 \text{ m} \Rightarrow l_{cr} = 6,9 \text{ m}$
 EI " " = $M_{Ed} = 1470 \rightarrow (EI)_{Ed, \text{min}} = 3,12 \times 10^6$
 $EA = 1,67 \times 10^7$

Iteration # 4 :

$M_{\text{result}} = 1930$

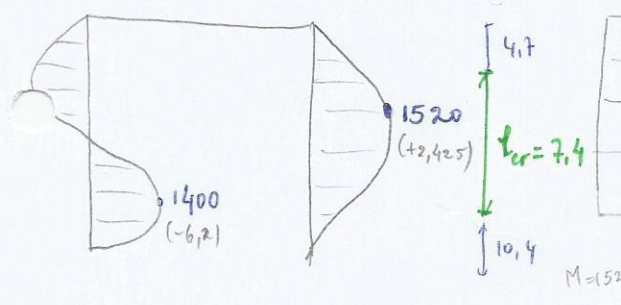


| zone | l(m) | from | to | EI (kNm ² /m ⁴) | EA (kN/m ²) |
|------|------|-------|------|--|-------------------------|
| 1 | 4,8 | +10,5 | +5,7 | * | * |
| 2 | 6,9 | +5,7 | -1,2 | $3,12 \times 10^6$ | $1,67 \times 10^7$ |
| 3 | 10,8 | -1,2 | -12 | * | * |

Height cracked zone = $+6,7 \text{ t/m} - 4,9 \text{ m} \Rightarrow l_{cr} = 11,6 \text{ m}$
 EI " " = $M_{Ed} = 1930 \rightarrow (EI)_{Ed, \text{min}} = 1,98 \times 10^6$
 $EA = 1,05 \times 10^7$

Iteration # 5 :

$M_{\text{res}} = 1520$

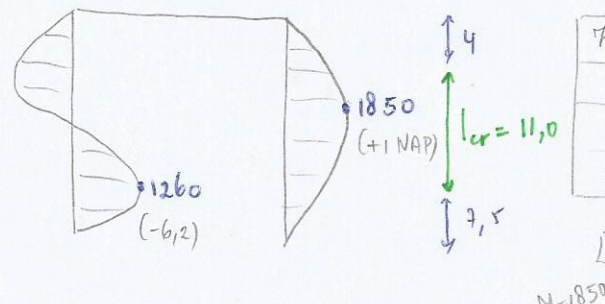


| zone | l(m) | from | to | EI | EA |
|------|------|-------|------|--------------------|--------------------|
| 1 | 3,8 | +10,5 | +6,7 | * | * |
| 2 | 11,6 | +6,7 | -4,9 | $1,98 \times 10^6$ | $1,05 \times 10^7$ |
| 3 | 7,1 | -4,9 | -12 | * | * |

Height CR zone = $+5,8 \text{ t/m} - 1,6 \text{ m} \Rightarrow l_{cr} = 7,4 \text{ m}$
 EI " " = $M_{Ed} = 1520 \rightarrow (EI)_{Ed, \text{min}} = 2,89 \times 10^6$
 $EA = 1,54 \times 10^7$

Iteration # 6 :

$M_{\text{res}} = 1850$

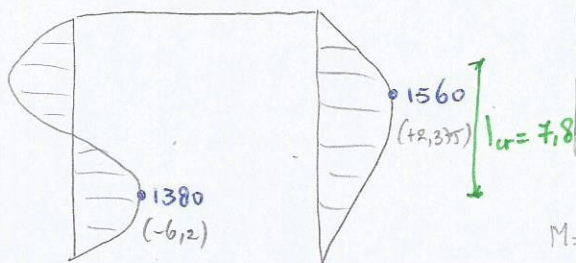


| zone | l(m) | from | to | EI | EA |
|------|------|-------|------|--------------------|--------------------|
| 1 | 4,7 | +10,5 | +5,8 | * | * |
| 2 | 7,4 | +5,8 | -1,6 | $2,89 \times 10^6$ | $1,54 \times 10^7$ |
| 3 | 10,4 | -1,6 | -12 | * | * |

Height CR zone = $+6,5 \text{ t/m} - 4,5 \text{ m} \Rightarrow l_{cr} = 11 \text{ m}$
 EI " " = $M_{Ed} = 1850 \rightarrow (EI)_{Ed, \text{min}} = 2,08 \times 10^6$
 $EA = 1,11 \times 10^7$

Iteration #7:

$M_{res} = 1560$

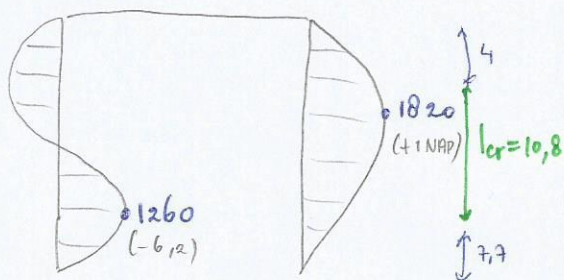


| zone | l(m) | from | to | EI | EA |
|------|------|-------|------|--------------------|--------------------|
| 1 | 4 | +10,5 | +6,5 | * | * |
| 2 | 11,0 | +6,5 | -4,5 | $2,08 \times 10^6$ | $1,11 \times 10^7$ |
| 3 | 7,5 | -4,5 | -12 | * | * |

\bullet height cr. zone = $+5,9 \text{ t/m} - 1,9 \text{ m} \Rightarrow l_{cr} = 7,8 \text{ m}$
 $M = 1560 \text{ EI}$ " " = $M_{Ed} = 1560 \rightarrow (EI)_{Ed, min} = 2,74 \times 10^6$
 $EA = 1,46 \cdot 10^7$

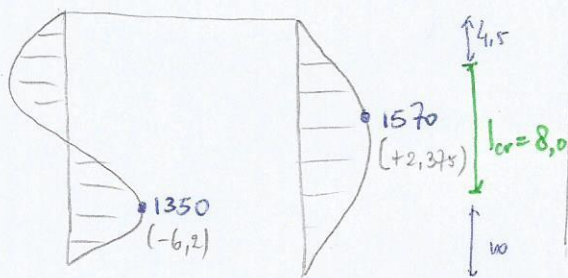
Iteration #8:

$M_{res} = 1820$



| zone | l(m) | from | to | EI | EA |
|------|------|-------|------|--------------------|--------------------|
| 1 | 4,6 | +10,5 | +5,9 | * | * |
| 2 | 7,8 | +5,9 | -1,9 | $2,74 \times 10^6$ | $1,46 \times 10^7$ |
| 3 | 10,1 | -1,9 | -12 | * | * |

\bullet height cr. zone = $+6,5 \text{ t/m} - 4,3 \text{ m} \Rightarrow l_{cr} = 10,8 \text{ m}$
 $M = 1820$
 \bullet EI cr. zone = $M_{Ed} = 1820 \rightarrow (EI)_{Ed, min} = 2,13 \times 10^6$
 $EA = 1,13 \times 10^7$



Iteration #9:

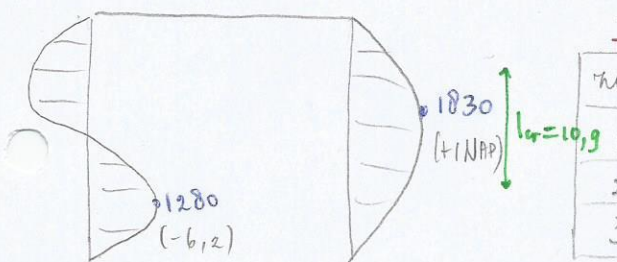
$M_{res} = 1570$

| zone | l(m) | from | to | EI | EA |
|------|------|-------|------|--------------------|--------------------|
| 1 | 4 | +10,5 | +6,5 | * | * |
| 2 | 10,8 | +6,5 | -4,3 | $2,13 \times 10^6$ | $1,13 \times 10^7$ |
| 3 | 7,7 | -4,3 | -12 | * | * |

\bullet height cr. zone = $+6,0 \text{ t/m} - 2,0 \text{ m} \Rightarrow l_{cr} = 8,0 \text{ m}$
 $M = 1570$
 \bullet EI cr. zone = $M_{Ed} = 1570 \rightarrow (EI)_{Ed, min} = 2,7 \times 10^6$
 $EA = 1,44 \times 10^7$

Iteration #10:

$M_{res} = 1830$

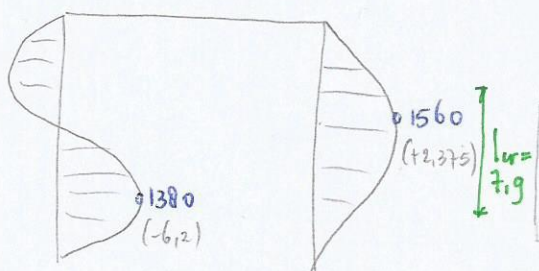


| zone | l(m) | from | to | EI | EA |
|------|------|-------|-----|-------------------|--------------------|
| 1 | 4,5 | +10,5 | +6 | * | * |
| 2 | 8 | +6 | -2 | $2,7 \times 10^6$ | $1,44 \times 10^7$ |
| 3 | 10 | -2 | -12 | * | * |

\bullet height cr. zone = $+6,5 \text{ t/m} - 4,4 \text{ m} \Rightarrow l_{cr} = 10,9 \text{ m}$
 \bullet EI cr. zone = $M_{Ed} = 1830 \rightarrow (EI)_{Ed, min} = 2,11 \times 10^6$
 $EA = 1,13 \times 10^7$

Iteration #11:

$M_{res} = 1560$

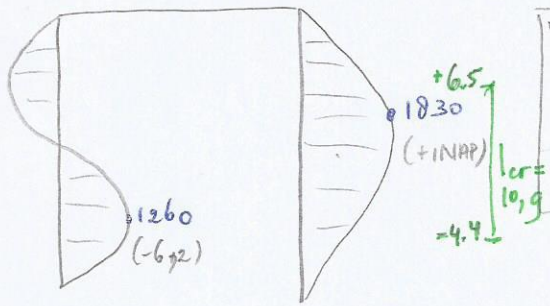


| zone | l(m) | from | to | EI | EA |
|------|------|------|------|--------------------|--------------------|
| 1 | 4 | 10,5 | 6,5 | * | * |
| 2 | 10,9 | 6,5 | -4,4 | $2,11 \times 10^6$ | $1,13 \times 10^7$ |
| 3 | 7,6 | -4,4 | -12 | * | * |

\bullet height cr. zone = $+6,0 \text{ t/m} - 1,9 \text{ m} \Rightarrow l_{cr} = 7,9 \text{ m}$
 $M = 1560$
 \bullet EI cr. zone = $M_{Ed} = 1560 \rightarrow (EI)_{Ed, min} = 2,74 \times 10^6$
 $EA = 1,46 \times 10^7$

Iteration #12:

$M_{res} = 1830$



| zone | l(m) | from | to | EI | EA |
|------|------|-------|------|--------------------|--------------------|
| 1 | 4,5 | +10,5 | +6 | * | * |
| 2 | 7,9 | 6 | -1,9 | $2,74 \times 10^6$ | $1,46 \times 10^7$ |
| 3 | 10,1 | -1,9 | -12 | * | * |

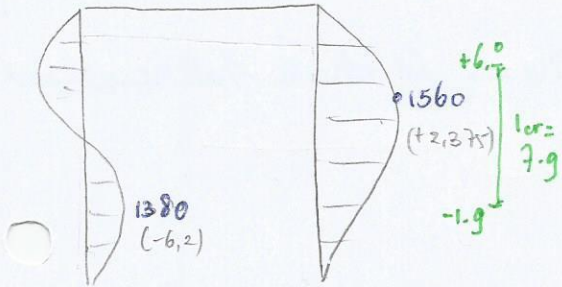
• Height cr. zone = $+6,5 \text{ t/m} - 4,4 \text{ m} \Rightarrow l_{cr} = 10,9 \text{ m}$

• EI cr. zone = $M_{Ed} = 1830 \rightarrow (EI)_{Ed, min} = 2,11 \times 10^6$

EA = $1,13 \times 10^7$.

Cond = Iteratie proces loopt vast!

Iteratie #13



| zone | l(m) | from | to | EI | EA |
|------|------|-------|-------|--------------------|--------------------|
| 1 | 4,0 | +10,5 | +6,5 | * | * |
| 2 | 10,9 | +6,5 | -4,4 | $2,11 \times 10^6$ | $1,13 \times 10^7$ |
| 3 | 7,6 | -4,4 | -12,0 | * | * |

• Height cracked zone = $+6,0 \text{ t/m} - 1,9 \text{ m} \Rightarrow l_{cr} = 7,9 \text{ m}$

• EI cr. zone: $M_{Ed} = 1560 \rightarrow (EI)_{Ed, min} = 2,74 \times 10^6$

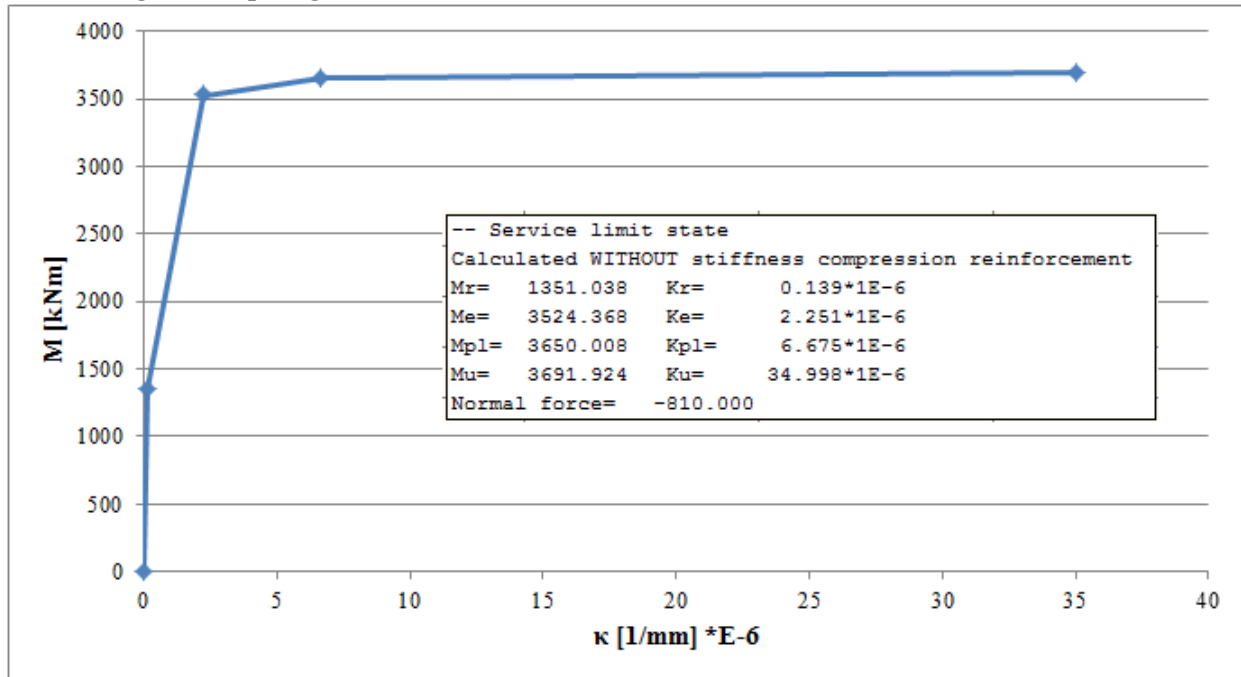
APPENDIX C2

ITERATION PROCESS RIGHT WALL

“WALLS ONLY; HINGED”

Case b: EI (κ , N)

M-N- κ diagram diaphragm walls:



Iteration process EI right wall (N = -810 kN)

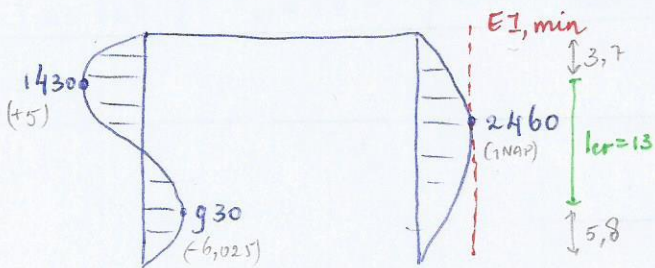
| | | $M_{Ed,max}$ | κ_{Ed} | | $(EI)_{Ed,min}$ | EA | E | | $l_{cracked}$ | |
|-------------|------------------|--------------|---------------|-----------|------------------------|----------|----------------------|-------|---------------|------|
| Iteration # | | [kNm] | [1/mm] | [1/m] | [kNm ² /m'] | [kN/m'] | [kN/m ²] | [MPa] | Note: | [m] |
| Procedure 1 | 1 | 2460 | 1.217E-06 | 1.217E-03 | 2.02E+06 | 1.08E+07 | 7.19E+06 | 7189 | E < 11000 | 13 |
| | 2 | 1540 | 3.226E-07 | 3.226E-04 | 4.77E+06 | 2.55E+07 | 1.70E+07 | 16972 | E > 11000 | 5 |
| | 3 | 2200 | 9.640E-07 | 9.640E-04 | 2.28E+06 | 1.22E+07 | 8.11E+06 | 8114 | E < 11000 | 10.9 |
| | 4 | 1630 | 4.101E-07 | 4.101E-04 | 3.97E+06 | 2.12E+07 | 1.41E+07 | 14132 | E > 11000 | 6.1 |
| | 5 | 2110 | 8.765E-07 | 8.765E-04 | 2.41E+06 | 1.28E+07 | 8.56E+06 | 8559 | E < 11000 | 10.5 |
| | 6 | 1650 | 4.295E-07 | 4.295E-04 | 3.84E+06 | 2.05E+07 | 1.37E+07 | 13658 | E > 11000 | 6.4 |
| | 7 | 2060 | 8.280E-07 | 8.280E-04 | 2.49E+06 | 1.33E+07 | 8.85E+06 | 8846 | E < 11000 | 10.1 |
| | 8 | 1690 | 4.684E-07 | 4.684E-04 | 3.61E+06 | 1.92E+07 | 1.28E+07 | 12829 | E > 11000 | 6.8 |
| | 9 | 2020 | 7.891E-07 | 7.891E-04 | 2.56E+06 | 1.37E+07 | 9.10E+06 | 9102 | E < 11000 | 10 |
| | 10 | 1720 | 4.976E-07 | 4.976E-04 | 3.46E+06 | 1.84E+07 | 1.23E+07 | 12291 | E > 11000 | 7.1 |
| | 11 | 2020 | 7.891E-07 | 7.891E-04 | 2.56E+06 | 1.37E+07 | 9.10E+06 | 9102 | E < 11000 | 9.9 |
| | 12 | 1720 | 4.976E-07 | 4.976E-04 | 3.46E+06 | 1.84E+07 | 1.23E+07 | 12291 | E > 11000 | 7.1 |
| | 13 | 2020 | 7.891E-07 | 7.891E-04 | 2.56E+06 | 1.37E+07 | 9.10E+06 | 9102 | E < 11000 | 9.9 |
| | FINAL | 1870 | 6.433E-07 | 6.433E-04 | 2.91E+06 | 1.55E+07 | 1.03E+07 | 10335 | E < 11000 | 8.5 |
| Procedure 2 | left wall_check | 1455 | 2.400E-07 | 2.400E-04 | 6.06E+06 | 3.23E+07 | 2.16E+07 | 21553 | | |
| | right wall_check | 2105 | 8.717E-07 | 8.717E-04 | 2.41E+06 | 1.29E+07 | 8.59E+06 | 8586 | | |

Note: $M_{Ed,max}$ is the maximum occurring moment in the cracked zone. We consider only one EI (which is the corresponding minimum EI) over this cracked height.

Overview iteration steps right wall (see next pages):

4) Iteration process to find cracked height & EI-distr. right wall.

$M_r = 1351$

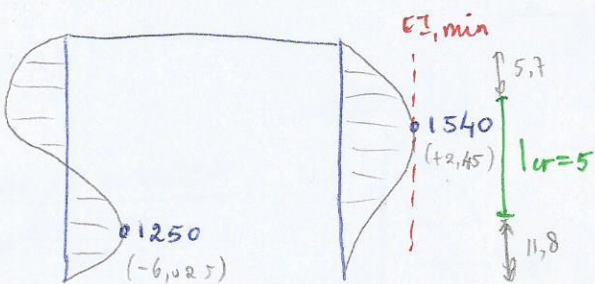


Iteration #0 = 1st assume right wall tot. uncr.

| zone | l(m) | from | to | EI (kNm ² /m) | EA (kN/m) |
|------|------|-------|-----|--------------------------|--------------------|
| 1 | 22,5 | +10,5 | -12 | $9,67 \times 10^6$ | $5,16 \times 10^7$ |

Height cracked zone = +6,8 t/m -6,2 m $\Rightarrow l_{cr} = 13$ m

EI cracked zone = $M_{Ed} = 2460 \rightarrow (EI)_{Ed, min} = 2,02 \cdot 10^6$



Iteration #1

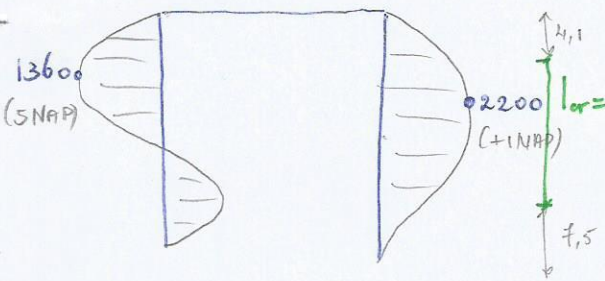
| zone | l(m) | from | to | EI | EA |
|------|------|-------|------|--------------------|--------------------|
| 1 | 3,7 | +10,5 | +6,8 | $9,67 \times 10^6$ | $5,16 \times 10^7$ |
| 2 | 13 | +6,8 | -6,2 | $2,02 \times 10^6$ | $1,08 \times 10^7$ |
| 3 | 5,8 | -6,2 | -12 | $9,67 \times 10^6$ | $5,16 \times 10^7$ |

Height cr. zone = +4,8 t/m -0,2 m $\Rightarrow l_{cr} = 5$ m

EI cr. zone = $M_{Ed} = 1540 \rightarrow (EI)_{Ed, min} = 4,77 \times 10^6$

Iteration # 2

M = 2200

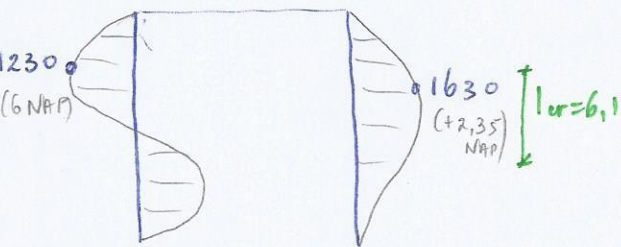


| zone | l(m) | from | to | EI | EA |
|------|------|-------|------|--------------------|--------------------|
| 1 | 5,7 | +10,5 | +4,8 | * | * |
| 2 | 5 | +4,8 | -0,2 | $4,77 \times 10^6$ | $2,55 \times 10^7$ |
| 3 | 11,8 | -0,2 | -12 | * | * |

- Height cr. zone = $+6,4 \text{ m} - 4,5 \text{ m} \Rightarrow l_{cr} = 10,9 \text{ m}$
- EI cr. zone = $M_{Ed} = 2200 \rightarrow (EI)_{Ed, min} = 2,28 \times 10^6$

Iteration # 3:

M = 1630

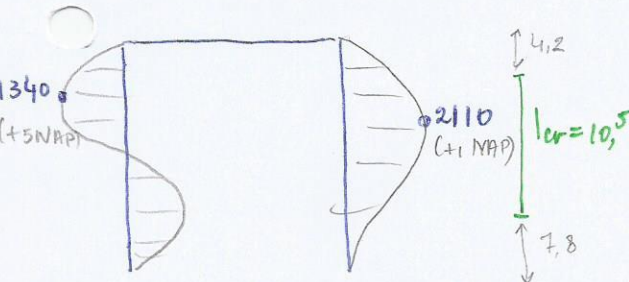


| zone | l(m) | from | to | EI | EA |
|------|------|-------|------|--------------------|--------------------|
| 1 | 4,1 | +10,5 | +6,4 | * | * |
| 2 | 10,9 | +6,4 | -4,5 | $2,28 \times 10^6$ | $1,22 \times 10^7$ |
| 3 | 7,5 | -4,5 | -12 | * | * |

- Height cr. zone = $+5,2 \text{ m} - 0,9 \text{ m} \Rightarrow l_{cr} = 6,1 \text{ m}$
- EI cr. zone = $M_{Ed} = 1630 \rightarrow (EI)_{Ed, min} = 3,97 \times 10^6$

Iteration # 4:

M = 2110

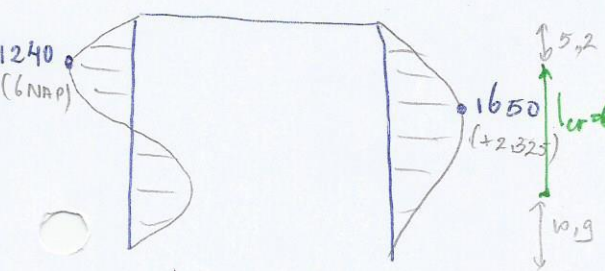


| zone | l(m) | from | to | EI | EA |
|------|------|-------|------|--------------------|--------------------|
| 1 | 5,3 | +10,5 | +5,2 | * | * |
| 2 | 6,1 | +5,2 | -0,9 | $3,97 \times 10^6$ | $2,12 \times 10^7$ |
| 3 | 11,1 | -0,9 | -12 | * | * |

- Height cr. zone = $+6,3 \text{ m} - 4,2 \text{ m} \Rightarrow l_{cr} = 10,5 \text{ m}$
- EI cr. zone = $M_{Ed} = 2110 \rightarrow (EI)_{Ed, min} = 2,41 \times 10^6$

Iteration # 5:

M = 1650

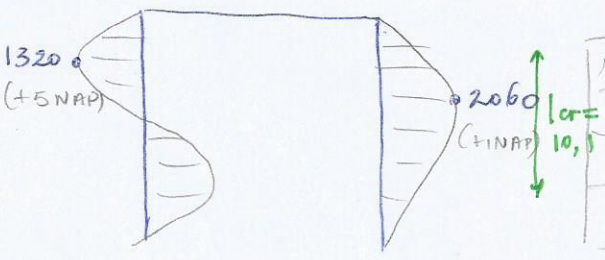


| zone | l(m) | from | to | EI | EA |
|------|------|-------|------|--------------------|--------------------|
| 1 | 4,2 | +10,5 | +6,3 | * | * |
| 2 | 10,5 | +6,3 | -4,2 | $2,41 \times 10^6$ | $1,28 \times 10^7$ |
| 3 | 7,8 | -4,2 | -12 | * | * |

- Height cr. zone = $+5,3 \text{ m} - 1,1 \text{ m} \Rightarrow l_{cr} = 6,4 \text{ m}$
- EI cr. zone = $M_{Ed} = 1650 \rightarrow (EI)_{Ed, min} = 3,84 \times 10^6$

Iteration # 6:

M = 2060

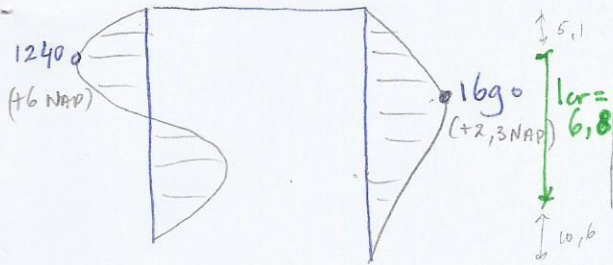


| zone | l(m) | from | to | EI | EA |
|------|------|-------|------|--------------------|--------------------|
| 1 | 5,2 | +10,5 | +5,3 | * | * |
| 2 | 6,4 | +5,3 | -1,1 | $3,84 \times 10^6$ | $2,05 \times 10^7$ |
| 3 | 10,9 | -1,1 | -12 | * | * |

- Height cr. zone = $+6,2 \text{ m} - 3,9 \text{ m} \Rightarrow l_{cr} = 10,1 \text{ m}$
- EI cr. zone = $M_{Ed} = 2060 \rightarrow (EI)_{Ed, min} = 2,49 \times 10^6$

Iteratie # 7

→ M=1690

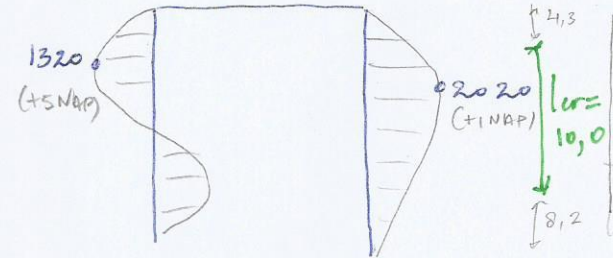


| zone | l(m) | from | to | EI | EA |
|------|------|-------|------|--------------------|--------------------|
| 1 | 4,3 | +10,5 | +6,2 | * | * |
| 2 | 10,1 | +6,2 | -3,9 | $2,49 \times 10^6$ | $1,33 \times 10^7$ |
| 3 | 8,1 | -3,9 | -12 | * | * |

- o) height cr. zone = $+5,4 \text{ t/m} - 1,4 \text{ m} \Rightarrow l_{cr} = 6,8 \text{ m}$.
- o) EI cr. zone = $M_{Ed} = 1690 \rightarrow (EI)_{Ed, \min} = 3,61 \times 10^6$.

Iteratie # 8:

→ M=2020

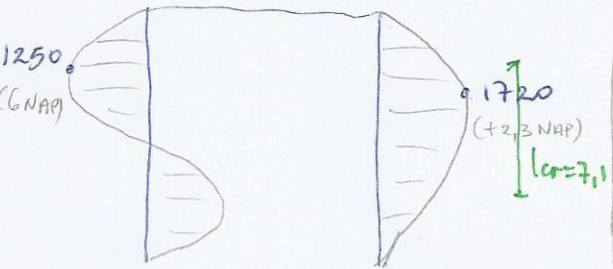


| zone | l(m) | from | to | EI | EA |
|------|------|-------|------|--------------------|--------------------|
| 1 | 5,1 | +10,5 | +5,4 | * | * |
| 2 | 6,8 | +5,4 | -1,4 | $3,61 \times 10^6$ | $1,92 \times 10^7$ |
| 3 | 10,6 | -1,4 | -12 | * | * |

- o) height cr. zone = $+6,2 \text{ t/m} - 3,8 \text{ m} \Rightarrow l_{cr} = 10,0 \text{ m}$.
- o) EI cr. zone = $M_{Ed} = 2020 \rightarrow (EI)_{Ed, \min} = 2,56 \times 10^6$.

Iteratie # 9:

→ M=1720

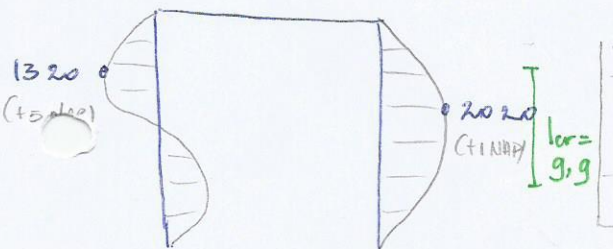


| zone | l(m) | from | to | EI | EA |
|------|------|-------|------|--------------------|--------------------|
| 1 | 4,3 | +10,5 | +6,2 | * | * |
| 2 | 10,0 | +6,2 | -3,8 | $2,56 \times 10^6$ | $1,37 \times 10^7$ |
| 3 | 8,2 | -3,8 | -12 | * | * |

- o) height cr. zone = $+5,5 \text{ t/m} - 1,6 \text{ m} \Rightarrow l_{cr} = 7,1 \text{ m}$.
- o) EI cr. zone = $M_{Ed} = 1720 \rightarrow (EI)_{Ed, \min} = 3,46 \times 10^6$.

Iteratie # 10:

→ M=2020

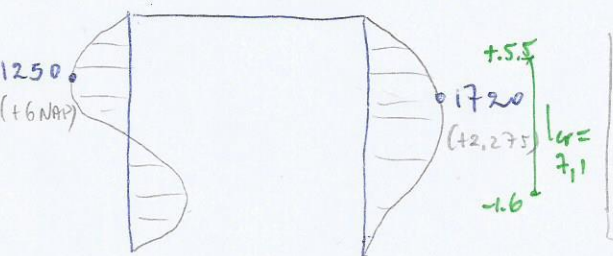


| zone | l(m) | from | to | EI | EA |
|------|------|-------|------|--------------------|--------------------|
| 1 | 5 | +10,5 | +5,5 | * | * |
| 2 | 7,1 | +5,5 | -1,6 | $3,46 \times 10^6$ | $1,84 \times 10^7$ |
| 3 | 10,4 | -1,6 | -12 | * | * |

- o) height cr. zone = $+6,7 \text{ t/m} - 3,8 \text{ m} \Rightarrow l_{cr} = 9,9 \text{ m}$.
- o) EI cr. zone = $M_{Ed} = 2020 \rightarrow (EI)_{Ed, \min} = 2,56 \times 10^6$.

Iteratie # 11:

→ M=1720

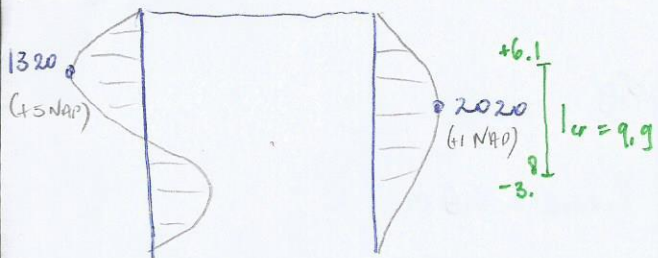


| zone | l(m) | from | to | EI | EA |
|------|------|-------|------|--------------------|--------------------|
| 1 | 4,4 | +10,5 | +6,1 | * | * |
| 2 | 9,9 | +6,1 | -3,8 | $2,56 \times 10^6$ | $1,37 \times 10^7$ |
| 3 | 8,2 | -3,8 | -12 | * | * |

- o) height cr. zone = $+5,5 \text{ t/m} - 1,6 \text{ m} \Rightarrow l_{cr} = 7,1 \text{ m}$.
- o) EI cr. zone = $M_{Ed} = 1720 \rightarrow (EI)_{Ed, \min} = 3,46 \times 10^6$.

Iteratie # 12

→ $M = 2020$



| zone | l(m) | from - to | | EI | EA |
|------|------|-----------|------|--------------------|--------------------|
| 1 | 5 | +10,5 | +5,5 | * | * |
| 2 | 7,1 | +5,5 | -1,6 | $3,46 \times 10^6$ | $1,84 \times 10^7$ |
| 3 | 10,4 | -1,6 | -12 | * | * |

- height CR. zone = +6,1 t/m - 3,8 m → l_{cr} = 9,9 m
- EI CR. zone = $M_{ed} = 2020 \rightarrow (EI)_{ed, min} = 2,56 \cdot 10^6$

Iteratie proces ?

- o) Iteratie # 12 = It. # 10
- o) It. # 11 = It. # 9

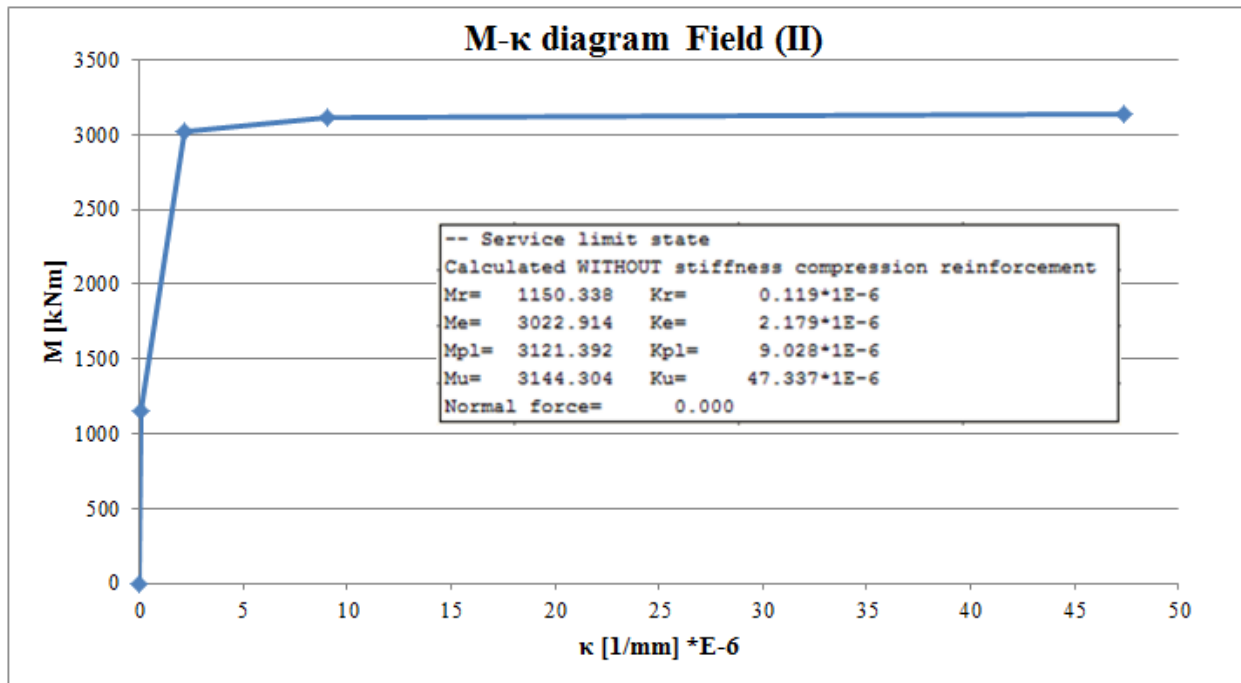
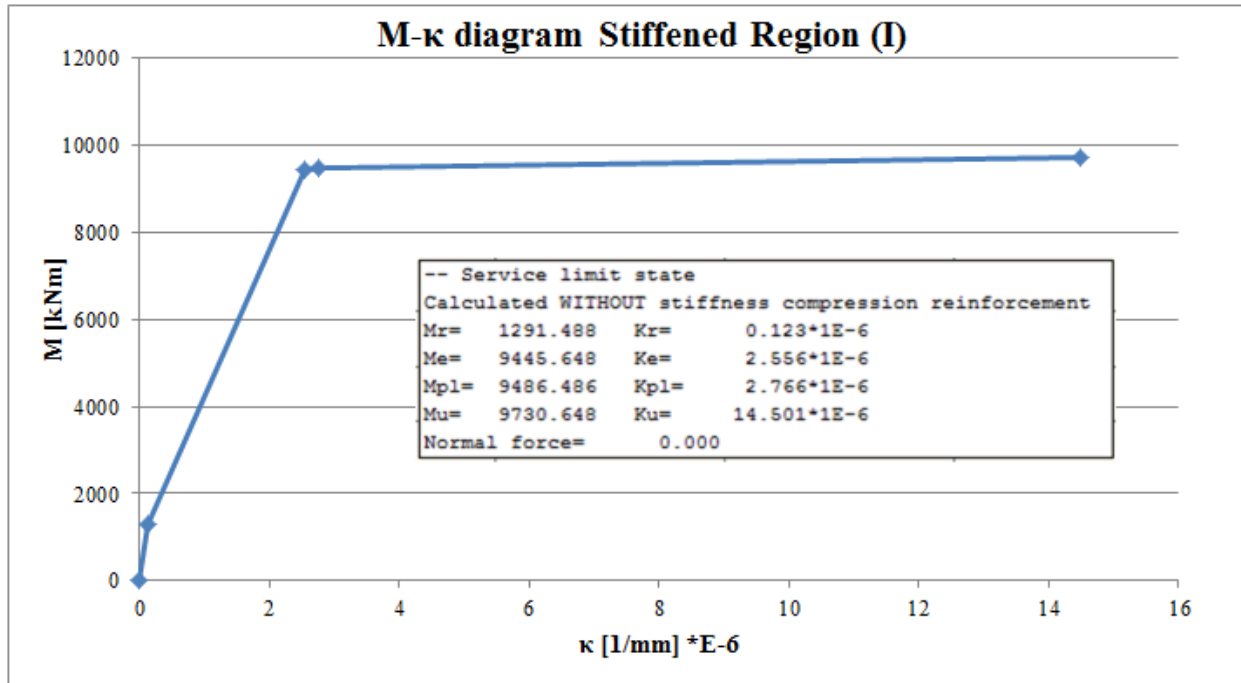
APPENDIX C3

ITERATION PROCESS RIGHT WALL

“WALLS ONLY; CLAMPED”

Case a: EI (κ)

M-κ diagram diaphragm wall for Stiffened Region (I) and Field (II):



Iteration process EI right wall, REGION 1 (N = 0 kN)

| | Iteration # | $M_{Ed,max}$ | κ_{Ed} | | $(EI)_{Ed,min}$ | EA | E | | Note: | $l_{cracked}$ |
|-------------|-------------------|--------------|---------------|-----------|------------------------|----------|----------------------|-----------|-----------|---------------|
| | | [kNm] | [1/mm] | [1/m] | [kNm ² /m'] | [kN/m'] | [kN/m ²] | [MPa] | | |
| Procedure 1 | 1 | 2090 | 3.613E-07 | 3.613E-04 | 5.79E+06 | 3.09E+07 | 2.06E+07 | 20570 | E > 11000 | 1.4 |
| | 2 | 2360 | 4.418E-07 | 4.418E-04 | 5.34E+06 | 2.85E+07 | 1.90E+07 | 18992 | E > 11000 | 1.5 |
| | 3 | 1840 | 2.867E-07 | 2.867E-04 | 6.42E+06 | 3.42E+07 | 2.28E+07 | 22822 | E > 11000 | 1.0 |
| | 4 | 2440 | 4.657E-07 | 4.657E-04 | 5.24E+06 | 2.79E+07 | 1.86E+07 | 18630 | E > 11000 | 1.5 |
| | 5 | 1790 | 2.717E-07 | 2.717E-04 | 6.59E+06 | 3.51E+07 | 2.34E+07 | 23421 | E > 11000 | 0.9 |
| | 6 | 2440 | 4.657E-07 | 4.657E-04 | 5.24E+06 | 2.79E+07 | 1.86E+07 | 18630 | E > 11000 | 1.5 |
| | 7 | 1450 | 1.703E-07 | 1.703E-04 | 8.51E+06 | 4.54E+07 | 3.03E+07 | 30274 | E > 11000 | 0.3 |
| | 8 | 2620 | 5.194E-07 | 5.194E-04 | 5.04E+06 | 2.69E+07 | 1.79E+07 | 17935 | E > 11000 | 1.5 |
| | 9 | 1760 | 2.628E-07 | 2.628E-04 | 6.70E+06 | 3.57E+07 | 2.38E+07 | 23813 | E > 11000 | 0.9 |
| | 10 | 2470 | 4.746E-07 | 4.746E-04 | 5.20E+06 | 2.78E+07 | 1.85E+07 | 18503 | E > 11000 | 1.5 |
| | 11 | 1800 | 2.747E-07 | 2.747E-04 | 6.55E+06 | 3.49E+07 | 2.33E+07 | 23296 | E > 11000 | 0.9 |
| | 12 | 2460 | 4.717E-07 | 4.717E-04 | 5.22E+06 | 2.78E+07 | 1.85E+07 | 18545 | E > 11000 | 1.5 |
| | 13 | 1790 | 2.717E-07 | 2.717E-04 | 6.59E+06 | 3.51E+07 | 2.34E+07 | 23421 | E > 11000 | 0.9 |
| FINAL | 2135 | 3.747E-07 | 3.747E-04 | 5.70E+06 | 3.04E+07 | 2.03E+07 | 20260 | E > 11000 | 1.5 | |
| Procedure 2 | Linkerwand_check | 1970 | 3.255E-07 | 3.255E-04 | 6.05E+06 | 3.23E+07 | 2.15E+07 | 21522 | E > 11000 | 1.3 |
| | Rechterwand_check | 1970 | 3.255E-07 | 3.255E-04 | 6.05E+06 | 3.23E+07 | 2.15E+07 | 21522 | E > 11000 | 1.3 |

TABLE 1 Note: M_{Ed} is the maximum occurring moment in the cracked zone of region 1. We consider only one EI (which is a corresponding minimum EI) over this cracked height.

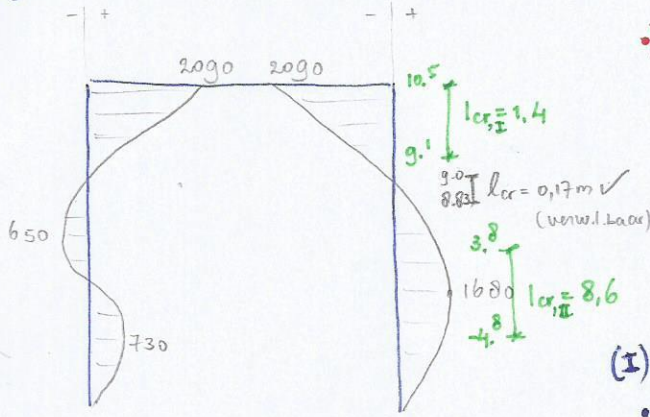
Iteration process EI right wall, REGION 2 (N = 0 kN)

| | Iteration # | $M_{Ed,max}$ | κ_{Ed} | | $(EI)_{Ed,min}$ | EA | E | | Note: | $l_{cracked}$ |
|---------------|---------------------------|--------------|---------------|-----------|------------------------|----------|----------------------|-----------|-----------|---------------|
| | | [kNm] | [1/mm] | [1/m] | [kNm ² /m'] | [kN/m'] | [kN/m ²] | [MPa] | | |
| Procedure 1 | 1 | 1680 | 7.017E-07 | 7.017E-04 | 2.39E+06 | 1.28E+07 | 8.51E+06 | 8513 | E < 11000 | 8.6 |
| | 2 | 1530 | 5.367E-07 | 5.367E-04 | 2.85E+06 | 1.52E+07 | 1.01E+07 | 10137 | E < 11001 | 0.8 |
| | 3 | 1780 | 8.117E-07 | 8.117E-04 | 2.19E+06 | 1.17E+07 | 7.80E+06 | 7797 | E < 11000 | 9.3 |
| | 4 | 1610 | 6.247E-07 | 6.247E-04 | 2.58E+06 | 1.37E+07 | 9.16E+06 | 9164 | E < 11000 | 0.9 |
| | 5 | 1770 | 8.007E-07 | 8.007E-04 | 2.21E+06 | 1.18E+07 | 7.86E+06 | 7860 | E < 11000 | 9.2 |
| | 6 | 1620 | 6.357E-07 | 6.357E-04 | 2.55E+06 | 1.36E+07 | 9.06E+06 | 9061 | E < 11000 | 0.9 |
| | 7 | 2650 | 1.769E-06 | 1.769E-03 | 1.50E+06 | 7.99E+06 | 5.33E+06 | 5327 | E < 11000 | 13.3 |
| | 8 | 1760 | 7.897E-07 | 7.897E-04 | 2.23E+06 | 1.19E+07 | 7.92E+06 | 7924 | E < 11000 | 1.2 |
| | 9 | 1810 | 8.447E-07 | 8.447E-04 | 2.14E+06 | 1.14E+07 | 7.62E+06 | 7619 | E < 11000 | 9.6 |
| | 10 | 1640 | 6.577E-07 | 6.577E-04 | 2.49E+06 | 1.33E+07 | 8.87E+06 | 8866 | E < 11000 | 1.0 |
| | 11 | 1790 | 8.227E-07 | 8.227E-04 | 2.18E+06 | 1.16E+07 | 7.74E+06 | 7736 | E < 11000 | 9.4 |
| | 12 | 1630 | 6.467E-07 | 6.467E-04 | 2.52E+06 | 1.34E+07 | 8.96E+06 | 8962 | E < 11000 | 0.9 |
| | 13 | 1770 | 8.007E-07 | 8.007E-04 | 2.21E+06 | 1.18E+07 | 7.86E+06 | 7860 | E < 11000 | 9.3 |
| Final field 1 | 1310 | 2.946E-07 | 2.946E-04 | 4.45E+06 | 2.37E+07 | 1.58E+07 | 15808 | E > 11000 | 0.5 | |
| Final field 2 | 1330 | 3.166E-07 | 3.166E-04 | 4.20E+06 | 2.24E+07 | 1.49E+07 | 14934 | E > 11000 | 4.8 | |
| Procedure 2 | Rechterwand_check_field 1 | 1175 | 1.461E-07 | 1.461E-04 | 8.04E+06 | 4.29E+07 | 2.86E+07 | 28589 | E > 11000 | 0.1 |
| | Rechterwand_check_field 2 | 1410 | 4.047E-07 | 4.047E-04 | 3.48E+06 | 1.86E+07 | 1.24E+07 | 12389 | E > 11000 | 5.0 |

TABLE 2 Note: M_{Ed} is the maximum occurring moment in the cracked zone of region 2. We consider only one EI (which is a corresponding minimum EI) over this cracked height.

Overview iteration steps right wall (see next pages):

3) Right wall: Iteration process to find cracked height & corresponding EI-distr. (3)



(Plx. file: Clamped-tot-2% A)

Iteration #0: 1st assumption \Rightarrow Right wall totally uncracked!

| zone | cr/uncr. | l(m) | From - To | EI | EA |
|------|----------|------|------------|--------------------|--------------------|
| 1 | uncr. | 1,5 | +10,5 - +g | $1,05 \times 10^7$ | $5,63 \times 10^7$ |
| 2 | uncr. | 21,0 | +g - -12 | $9,67 \times 10^6$ | $5,16 \times 10^7$ |

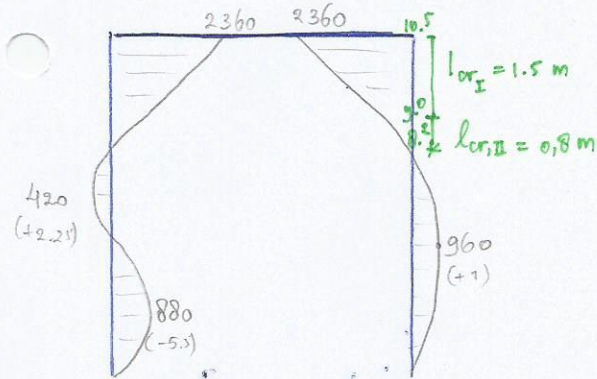
$M_I = 2090$
 $M_{II} = 1680$

(I) Reg. I = +10.5 t/m g.0 m ($M_r = 1291$)

- Cracked height = +9,1 t/m +10,5 m $\Rightarrow l_{cr,I} = 1,4$ m
- $M_{Ed,max} = 2090 \rightarrow (EI)_{Ed,min} = 5,79 \times 10^6$ kNm²/m

(II) Reg. II = +g t/m -12 m ($M_r = 1150$)

- Cracked height = +3,8 t/m -4,8 m $\Rightarrow l_{cr,II} = 8,6$ m
- $M_{Ed,max} = 1680 \rightarrow (EI)_{Ed,min} = 2,39 \times 10^6$ kNm²/m



(Plx. file: Clamped-tot-2% -1B)

Iteration #1.

| zone | cr/uncr. | l(m) | From - To | EI | EA |
|------|----------|------|--------------|--------------------|--------------------|
| 1 | cr | 1,4 | +10,5 - +g.1 | $5,79 \times 10^6$ | $3,09 \times 10^7$ |
| 2 | - | 5,3 | +g.1 - +3,8 | $9,67 \times 10^6$ | $5,16 \times 10^7$ |
| 3 | cr | 8,6 | +3,8 - -4,8 | $2,39 \times 10^6$ | $1,28 \times 10^7$ |
| 4 | - | 7,2 | -4,8 - -12 | $9,67 \times 10^6$ | $5,16 \times 10^7$ |

$M_I = 2360$
 $M_{II} = 960$

(I) Region I

- Cr. height = +10,5 t/m +g.0 $\Rightarrow l_{cr,I} = 1,5$ m.
- $M_{Ed,max} = 2360 \rightarrow (EI)_{Ed,min} = 5,34 \times 10^6$

(II) Region II

- Cr. height = +g.0 t/m +8,2 m $\Rightarrow l_{cr,II} = 0,8$ m.
- $M_{Ed,max}$ (at $y = g$) $\Rightarrow 1530 \Rightarrow (EI)_{Ed,min} = 2,85 \times 10^6$ afschatten

hier M t grootst voor gescheurde zone region II

Iteration #2:

| zone | cr/uncr. | l(m) | From - To | EI | EA |
|------|----------|------|--------------|--------------------|--------------------|
| 1 | CR | 1,5 | +10,5 - +g.0 | $5,34 \times 10^6$ | $2,85 \times 10^7$ |
| 2 | CR | 0,8 | +g.0 - +8,2 | $2,85 \times 10^6$ | $1,52 \times 10^7$ |
| 3 | - | 20,2 | +8,2 - -12 | $9,67 \times 10^6$ | $5,16 \times 10^7$ |

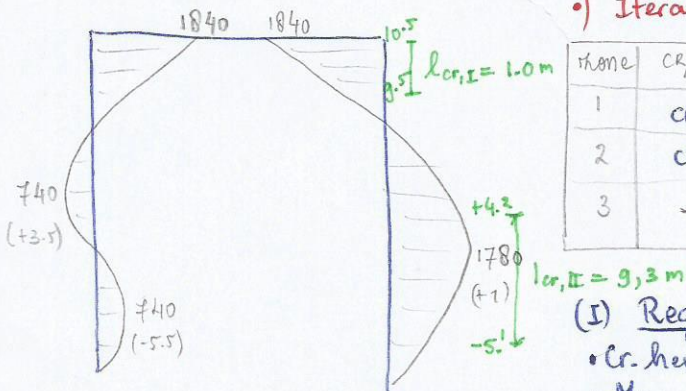
$M_I = 1840$
 $M_{II} = 1780$

(I) Region I

- Cr. height = +10,5 t/m +g.5 $\Rightarrow l_{cr,I} = 1,0$ m.
- $M_{Ed,max} = 1840 \rightarrow (EI)_{Ed,min} = 6,42 \times 10^6$

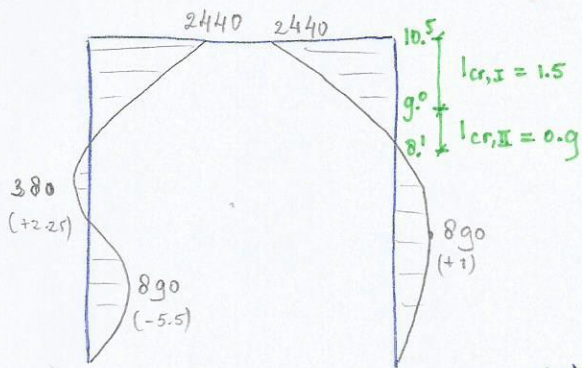
(II) Region II:

- Cr. height = +4,2 t/m -5,1 m $\Rightarrow l_{cr,II} = 9,3$ m.
- $M_{Ed,max} = 1780 \rightarrow (EI)_{Ed,min} = 2,19 \times 10^6$



Iteration #3

$M_I = 2440$
 $M_{II} = 890$ (4)



| none | CR/uncr. | l(m) | From - To | EI | EI |
|------|----------|------|------------|--------------------|--------------------|
| 1 | CR | 1,0 | +10,5 +9,5 | $6,42 \times 10^6$ | $3,42 \times 10^7$ |
| 2 | - | 5,3 | +9,5 4,2 | $9,67 \times 10^6$ | $5,16 \times 10^7$ |
| 3 | CR | 9,3 | +4,2 -5,1 | $2,19 \times 10^6$ | $1,17 \times 10^7$ |
| 4 | - | 6,9 | -5,1 -12 | $9,67 \times 10^6$ | $5,16 \times 10^7$ |

Note: Eigenlijk van +9,5 t/m 9,0 $\rightarrow EI = 1,05 \times 10^7$ & van 9,0 t/m 4,2 $\rightarrow EI = 9,67 \times 10^6$. Houd EI $\frac{1}{2}$ grootste ongesch. zone aan!

Note:
 $M_{II} > 1291$ voor $y \geq 8,4$ m.
 $M_{II} > 1150$ voor $y \geq 8,1$ m.
 Dus 2 zones: $\begin{cases} +10,5 \text{ t/m } 9,0 \\ +9,0 \text{ t/m } 8,1 \end{cases}$

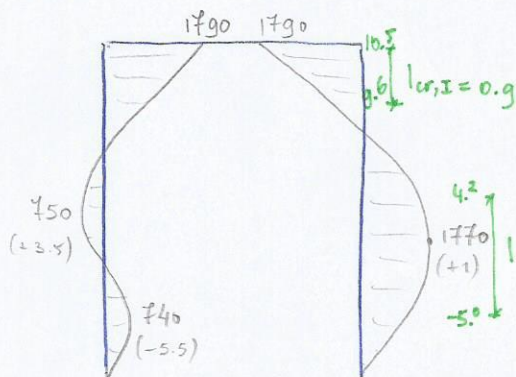
(I) Region I

- Cr. height = +10,5 t/m 9,0 m $\Rightarrow l_{cr,I} = 1,5$ m.
- $M_{Ed,max} = 2440 \rightarrow (EI)_{Ed,min} = 5,24 \times 10^6$ kNm²/m!

(II) Region II:

- Cr. height = +9,0 t/m 8,1 m $\Rightarrow l_{cr,II} = 0,9$ m
- $M_{Ed,max}$ (afschatten @ 9,0 m) = 1610 $\rightarrow (EI)_{Ed,min} = 2,58 \times 10^6$

hier M grootst voor gescheurde zone region II



Iteration #4:

$M_I = 1790$
 $M_{II} = 1770$

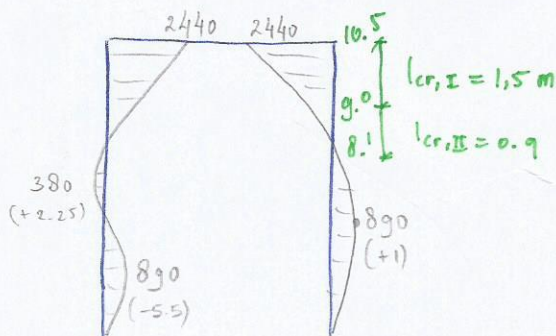
| none | CR/uncr. | l(m) | from - to | EI | EI |
|------|----------|------|------------|--------------------|--------------------|
| 1 | CR | 1,5 | +10,5 +9,0 | $5,24 \times 10^6$ | $2,79 \times 10^7$ |
| 2 | CR | 0,9 | +9,0 +8,1 | $2,58 \times 10^6$ | $1,37 \times 10^7$ |
| 3 | - | 20,1 | +8,1 -12 | $9,67 \times 10^6$ | $5,16 \times 10^7$ |

(I) Region I

- Cr. height = +10,5 t/m +9,0 m $\Rightarrow l_{cr,I} = 0,9$ m.
- $M_{Ed,max} = 1790 \rightarrow (EI)_{Ed,min} = 6,59 \times 10^6$ kNm²/m!

(II) Region II

- Cr. height = +4,2 t/m -5,0 m $\Rightarrow l_{cr,II} = 9,2$ m.
- $M_{Ed,max} = 1770 \rightarrow (EI)_{Ed,min} = 2,21 \times 10^6$ kNm²/m!



Iteration #5:

$M_I = 2440$
 $M_{II} = 890$

| none | CR/uncr. | l(m) | from - to | EI | EI |
|------|----------|------|------------|--------------------|--------------------|
| 1 | CR | 0,9 | +10,5 +9,6 | $6,59 \times 10^6$ | $3,51 \times 10^7$ |
| 2 | - | 5,4 | +9,6 +4,2 | $9,67 \times 10^6$ | $5,16 \times 10^7$ |
| 3 | CR | 9,2 | +4,2 -5,0 | $2,21 \times 10^6$ | $1,18 \times 10^7$ |
| 4 | - | 7 | -5,0 -12 | $9,67 \times 10^6$ | $5,16 \times 10^7$ |

Note:
 $M_I > 1291$ voor $y \geq 8,4$ m
 $M_{II} > 1150$ voor $y \geq 8,1$ m
 Dus 2 zones: $\begin{cases} +10,5 \text{ t/m } 9,0 \text{ m} \\ +9,0 \text{ t/m } 8,1 \end{cases}$

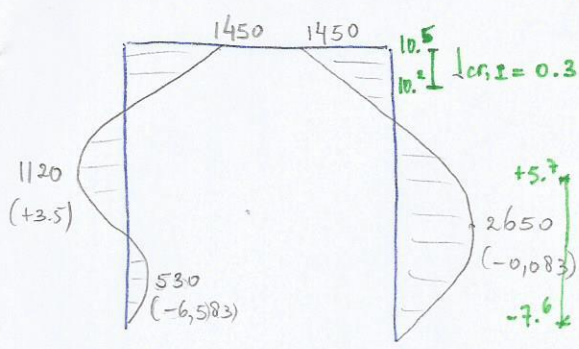
(I) Region I

- Cr. height = +10,5 t/m 9,0 $\Rightarrow l_{cr,I} = 1,5$ m.
- $M_{Ed,max} = 2440 \rightarrow (EI)_{Ed,min} = 5,24 \times 10^6$ kNm²/m!

(II) Region II:

- Cr. height = +9,0 t/m 8,1 m $\Rightarrow l_{cr,II} = 0,9$ m.
- $M_{Ed,max}$ (afschatten @ 9,0 m) = 1620 $\rightarrow (EI)_{Ed,min} = 2,55 \times 10^6$

o) Iteration #6 =



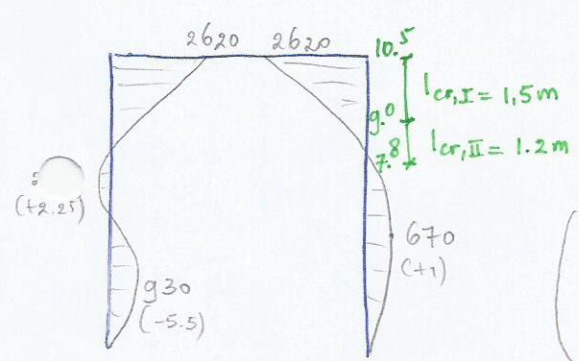
| zone | CR/uncr. | l(m) | from - to | EI | EA |
|------|----------|------|-------------|--------------------|--------------------|
| 1 | CR | 1,5 | +10,5 + 9,0 | $5,24 \times 10^6$ | $2,79 \times 10^7$ |
| 2 | CR | 0,9 | +9,0 + 8,1 | $2,55 \times 10^6$ | $1,36 \times 10^7$ |
| 3 | - | 20,1 | +8,1 -12 | $9,67 \times 10^6$ | $5,16 \times 10^7$ |

(I) Region I

- Cr. height = $+10,5 \text{ t/m} \cdot 10,2 \Rightarrow l_{CR,I} = 0,3 \text{ m}$.
- $M_{Ed,max} = 1450 \rightarrow (EI)_{Ed,min} = 8,51 \times 10^6 \text{ kNm}^2/\text{m}$

(II) Region II

- Cr. height = $+5,7 \text{ t/m} - 7,6 \text{ m} \Rightarrow l_{CR,II} = 13,3 \text{ m}$.
- $M_{Ed,max} = 2650 \rightarrow (EI)_{Ed,min} = 1,50 \times 10^6 \text{ kNm}^2/\text{m}$



o) Iteration #7 =

| zone | CR/uncr. | l(m) | from - to | EI | EA |
|------|----------|------|-------------|----------------------|--------------------|
| 1 | CR | 0,3 | +10,5 +10,2 | $8,51 \times 10^6$ | $4,54 \times 10^7$ |
| 2 | - | 1,2 | +10,2 +9,0 | * $1,05 \times 10^7$ | $5,63 \times 10^7$ |
| 3 | - | 3,3 | +9,0 +5,7 | * $9,67 \times 10^6$ | $5,16 \times 10^7$ |
| 4 | CR | 13,3 | +5,7 -7,6 | $1,50 \times 10^6$ | $7,99 \times 10^6$ |
| 5 | - | 4,4 | -7,6 -12 | $9,67 \times 10^6$ | $5,16 \times 10^7$ |

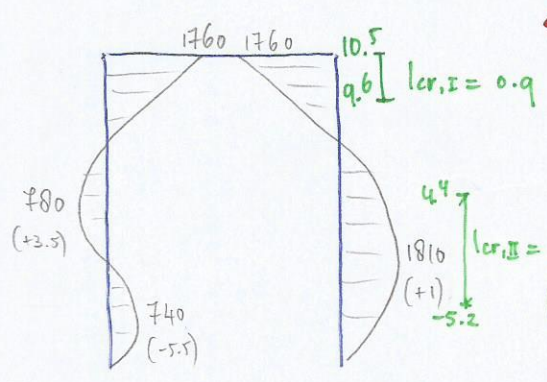
Note = Onderscheid in EI's v/d ongescheurde zones in Reg. I & II!
(De zones zijn op zich te groot, om slechts 1 v/d EI's te laten prevaleren!)

(I) Region I

- Cr. height = $+10,5 \text{ t/m} \cdot 9,0 \text{ m} \Rightarrow l_{CR,I} = 1,5 \text{ m}$.
- $M_{Ed,max} = 2620 \rightarrow (EI)_{Ed,min} = 5,04 \times 10^6$

(II) Region II

- Cr. height = $+9,0 \text{ t/m} \cdot 7,8 \text{ m} \Rightarrow l_{CR,II} = 1,2 \text{ m}$.
- $M_{Ed,max}$ (aflezen @ 9,0 m) = $1760 \rightarrow (EI)_{Ed,min} = 2,23 \times 10^6$



o) Iteration #8 =

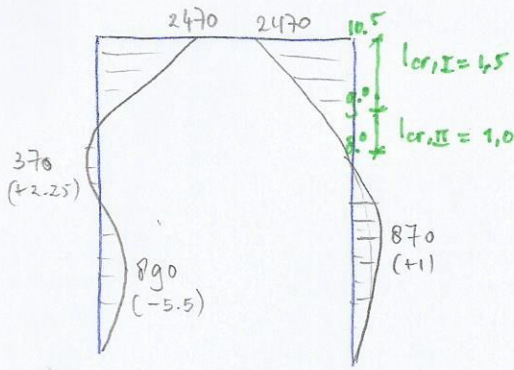
| zone | CR/uncr. | l(m) | from - to | EI | EA |
|------|----------|------|-------------|--------------------|--------------------|
| 1 | CR | 1,5 | +10,5 + 9,0 | $5,04 \times 10^6$ | $2,69 \times 10^7$ |
| 2 | CR | 1,2 | +9,0 + 7,8 | $2,23 \times 10^6$ | $1,19 \times 10^7$ |
| 3 | - | 19,8 | +7,8 -12 | $9,67 \times 10^6$ | $5,16 \times 10^7$ |

(I) Region I =

- Cr. height = $+10,5 \text{ t/m} + 9,6 \text{ m} \Rightarrow l_{CR,I} = 0,9 \text{ m}$.
- $M_{Ed,max} = 1760 \rightarrow (EI)_{Ed,min} = 6,7 \times 10^6 \text{ kNm}^2/\text{m}$

(II) Region II =

- Cr. height = $+4,4 \text{ t/m} - 5,2 \text{ m} \Rightarrow l_{CR,II} = 9,6 \text{ m}$.
- $M_{Ed,max} = 1810 \rightarrow (EI)_{Ed,min} = 2,14 \times 10^6 \text{ kNm}^2/\text{m}$



$M_I = 2470$
 $M_{II} = 870$ (6)

| zone | cr/uncr. | l(m) | from | To | EI | EA |
|------|----------|------|-------|------|--------------------|--------------------|
| 1 | CR | 0,9 | +10,5 | +9,6 | $6,70 \times 10^6$ | $3,57 \times 10^7$ |
| 2 | - | 5,2 | +9,6 | +4,4 | $9,67 \times 10^6$ | $5,16 \times 10^7$ |
| 3 | CR | 9,6 | +4,4 | -5,2 | $2,14 \times 10^6$ | $1,14 \times 10^7$ |
| 4 | - | 6,8 | -5,2 | -12 | $9,67 \times 10^6$ | $5,16 \times 10^7$ |

Note = EI \forall d overstreffende ongeschuilde zone aangehouden!
 2 zones $\left\{ \begin{array}{l} +9,6 \text{ t/m } +9,6 = 0,6 \text{ m} \\ +9,0 \text{ t/m } 4,4 = 4,6 \text{ m} \end{array} \right.$

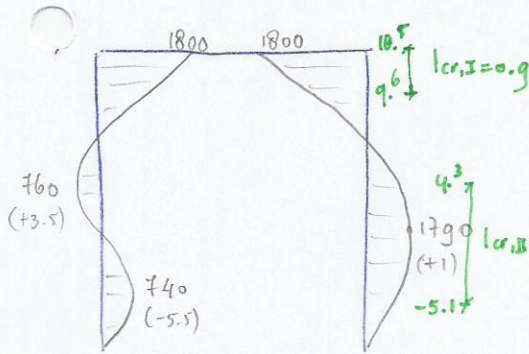
Note:
 $M_I > 1291$ voor: $y \geq 8,3$
 $M_{II} > 1150$ voor: $y \geq 8,0$
 Dus 2 zones: $\left\{ \begin{array}{l} 10,5 \text{ t/m } 9,0 \\ +9 \text{ t/m } 8,0 \end{array} \right.$

(I) Region I:

- Cr. height: $+10,5 \text{ t/m } 9,0 \text{ m} \Rightarrow l_{CR,I} = 1,5 \text{ m}$
- $M_{Ed,max} = 2470 \rightarrow (EI)_{Ed,min} = 5,20 \times 10^6 \text{ kNm}^2/\text{m}$

(II) Region II:

- Cr. height: $+9,0 \text{ t/m } 8,0 \text{ m} \Rightarrow l_{CR,II} = 1,0 \text{ m}$
- $M_{Ed,max}$ (afschatten @ $9,0 \text{ m}$) = $1640 \rightarrow (EI)_{Ed,min} = 2,49 \times 10^6$



o) Iteratie # 10.

$M_I = 1800$
 $M_{II} = 1790$

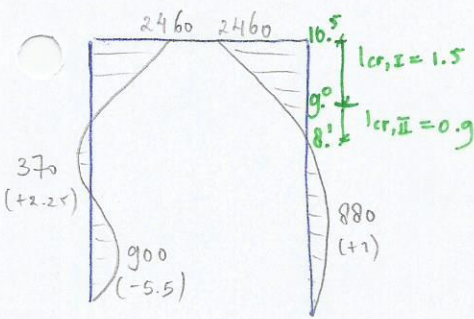
| zone | cr/uncr. | l(m) | from | To | EI | EA |
|------|----------|------|-------|------|--------------------|--------------------|
| 1 | CR | 1,5 | +10,5 | +9,0 | $5,20 \times 10^6$ | $2,78 \times 10^7$ |
| 2 | CR | 1,0 | +9,0 | +8,0 | $2,49 \times 10^6$ | $1,33 \times 10^7$ |
| 3 | - | 2,0 | +8,0 | -12 | $9,67 \times 10^6$ | $5,16 \times 10^7$ |

(I) Region I

- Cr. height: $+10,5 \text{ t/m } 9,6 \text{ m} \Rightarrow l_{CR,I} = 0,9 \text{ m}$
- $M_{Ed,max} = 1800 \rightarrow (EI)_{Ed,min} = 6,55 \times 10^6 \text{ kNm}^2/\text{m}$

(II) Region II:

- Cr. height: $+4,3 \text{ t/m } -5,1 \text{ m} \Rightarrow l_{CR,II} = 9,4 \text{ m}$
- $M_{Ed,max} = 1790 \rightarrow (EI)_{Ed,min} = 2,18 \times 10^6$



o) Iteratie # 11

$M_I = 2460$
 $M_{II} = 880$

| zone | cr/uncr. | l(m) | from | To | EI | EA |
|------|----------|------|-------|------|--------------------|--------------------|
| 1 | CR | 0,9 | +10,5 | +9,6 | $6,55 \times 10^6$ | $3,49 \times 10^7$ |
| 2 | - | 5,3 | +9,6 | +4,3 | $9,67 \times 10^6$ | $5,16 \times 10^7$ |
| 3 | CR | 9,4 | +4,3 | -5,1 | $2,18 \times 10^6$ | $1,16 \times 10^7$ |
| 4 | - | 6,9 | -5,1 | -12 | $9,67 \times 10^6$ | $5,16 \times 10^7$ |

Note: EI overstreffende geschuilde zone aarronden! 2 zones $\left\{ \begin{array}{l} +9,6 \text{ t/m } 9,0 = 0,6 \text{ m} \\ +9 \text{ t/m } 4,3 = 4,7 \text{ m} \end{array} \right.$

(I) Region I

- Cr. height: $+10,5 \text{ t/m } 9,0 \text{ m} \Rightarrow l_{CR,I} = 1,5 \text{ m}$
- $M_{Ed,max} = 2460 \rightarrow (EI)_{Ed,min} = 5,22 \times 10^6$

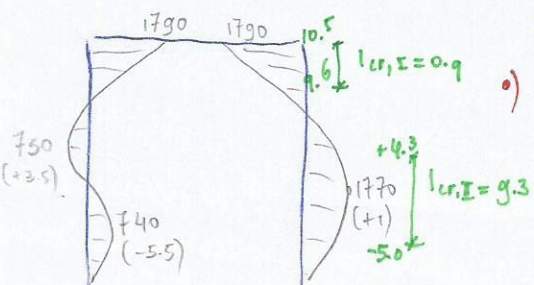
(II) Region II:

- Cr. height: $+9,0 \text{ t/m } 8,1 \text{ m} \Rightarrow l_{CR,II} = 0,9 \text{ m}$
- $M_{Ed,max}$ (afschatten @ $9,0 \text{ m}$) = $1630 \rightarrow (EI)_{Ed,min} = 2,52 \times 10^6$

o) Iteratie # 12

$M_I = 1790$
 $M_{II} = 1790$

| zone | cr/uncr. | l(m) | from | to | EI | EA |
|------|----------|------|-------|------|--------------------|--------------------|
| 1 | CR | 1,0 | +10,5 | +9,0 | $5,22 \times 10^6$ | $2,78 \times 10^7$ |
| 2 | CR | 0,9 | +9,0 | +8,1 | $2,52 \times 10^6$ | $1,34 \times 10^7$ |
| 3 | - | 20,1 | +8,1 | -12 | $9,67 \times 10^6$ | $5,16 \times 10^7$ |



(I) Region I

- Cr. height = +10,5 m - 9,6 m \Rightarrow $l_{cr,I} = 0,9$ m
- $M_{Ed,max} = 1790 \rightarrow (EI)_{Ed,min} = 6,59 \times 10^6$ kNm²/m

(II) Region II:

- Cr. height = +4,3 m - 5,0 m \Rightarrow $l_{cr,II} = 9,3$ m
- $M_{Ed,max} = 1770 \rightarrow (EI)_{Ed,min} = 2,21 \times 10^6$ kNm²/m

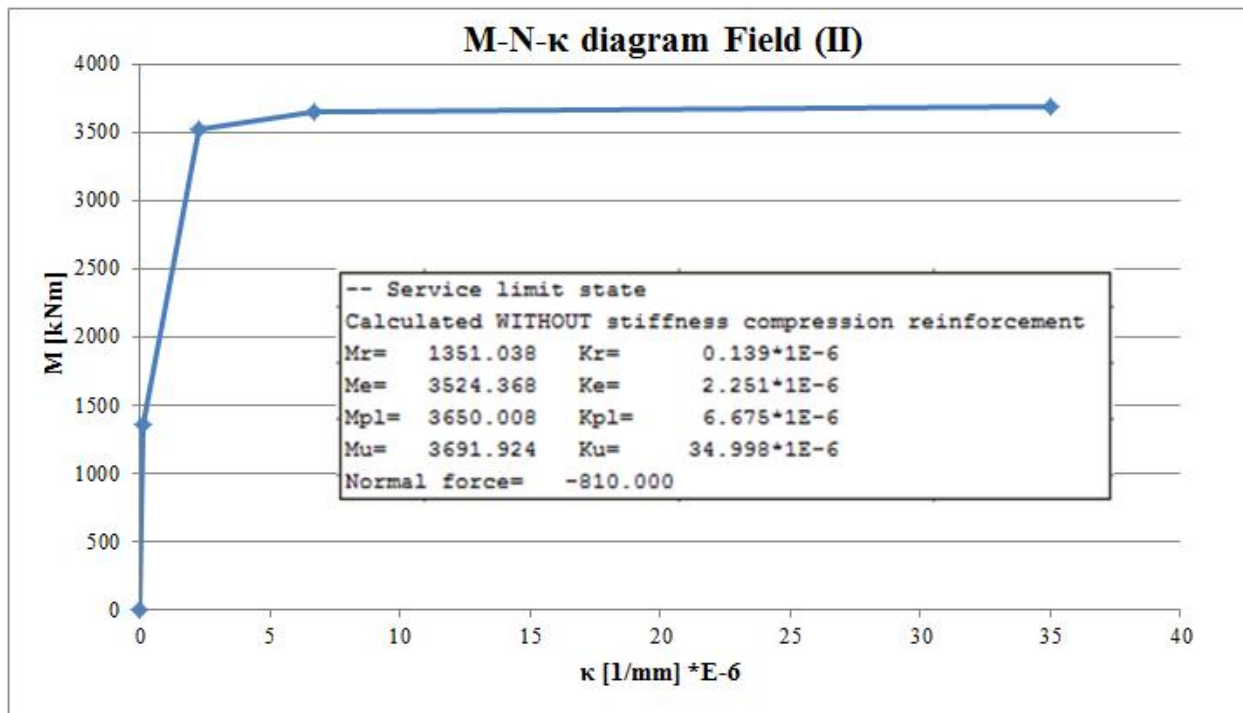
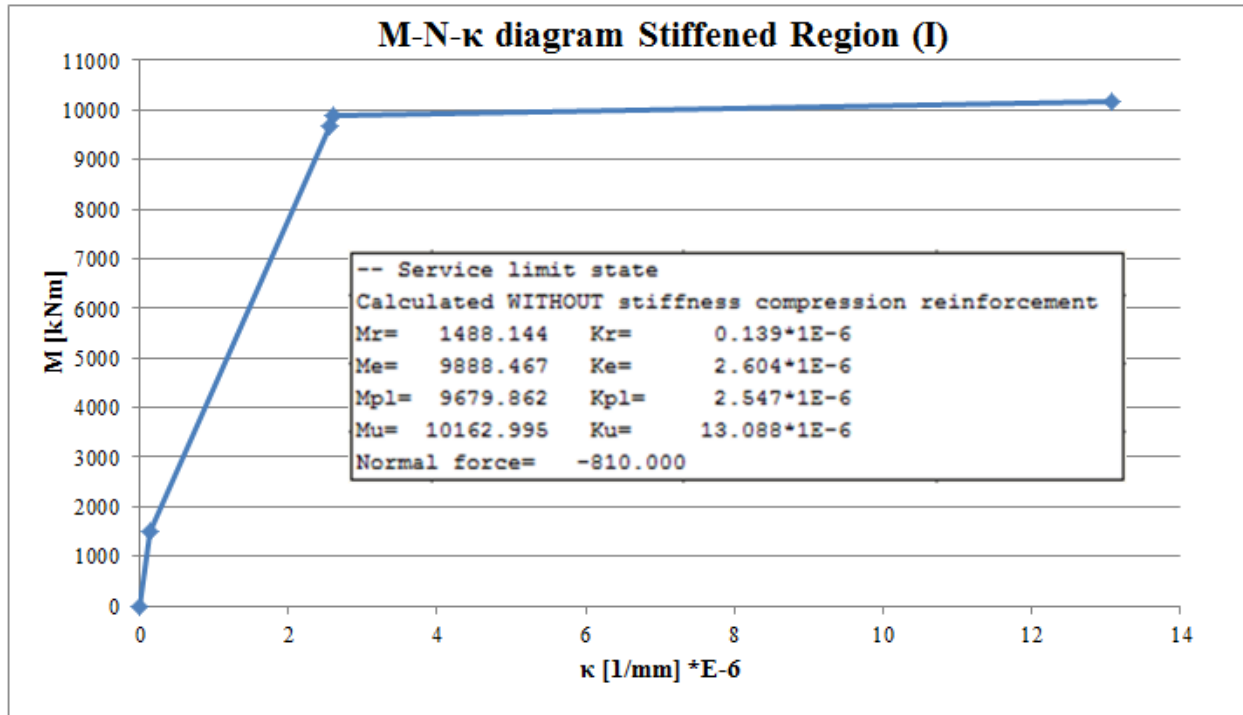
APPENDIX C4

ITERATION PROCESS RIGHT WALL

“WALLS ONLY; CLAMPED”

Case b: EI (κ , N)

M-N- κ diagram diaphragm wall for Stiffened Region (I) and Field (II):



Iteration process EI right wall, REGION 1 (N = -810 kN)

| | Iteration # | $M_{Ed,max}$ | κ_{Ed} | | $(EI)_{Ed,min}$ | EA | E | | Note: | $l_{cracked}$ |
|-------------|-------------------|--------------|---------------|-----------|------------------------|-----------------|----------------------|-------|-----------|---------------|
| | | [kNm] | [1/mm] | [1/m] | [kNm ² /m'] | [kN/m'] | [kN/m ²] | [MPa] | | |
| Procedure 1 | 1 | 2200 | 3.483E-07 | 3.483E-04 | 6.32E+06 | 3.37E+07 | 2.25E+07 | 22461 | E > 11000 | 1.2 |
| | 2 | 2350 | 3.923E-07 | 3.923E-04 | 5.99E+06 | 3.19E+07 | 2.13E+07 | 21296 | E > 11000 | 1.5 |
| | 3 | 2070 | 3.100E-07 | 3.100E-04 | 6.68E+06 | 3.56E+07 | 2.37E+07 | 23739 | E > 11000 | 1.0 |
| | 4 | 2400 | 4.070E-07 | 4.070E-04 | 5.90E+06 | 3.14E+07 | 2.10E+07 | 20964 | E > 11000 | 1.5 |
| | 5 | 2050 | 3.042E-07 | 3.042E-04 | 6.74E+06 | 3.59E+07 | 2.40E+07 | 23964 | E > 11000 | 1.0 |
| | 6 | 2410 | 4.100E-07 | 4.100E-04 | 5.88E+06 | 3.14E+07 | 2.09E+07 | 20901 | E > 11000 | 1.5 |
| | FINAL | 2230 | 3.571E-07 | 3.571E-04 | 6.25E+06 | 3.33E+07 | 2.22E+07 | 22205 | E > 11000 | 1.3 |
| Procedure 2 | Linkerwand_check | 2095 | 3.174E-07 | 3.174E-04 | 6.60E+06 | 3.52E+07 | 2.35E+07 | 23469 | E > 11000 | 1.0 |
| | Rechterwand_check | 2095 | 3.174E-07 | 3.174E-04 | 6.60E+06 | 3.52E+07 | 2.35E+07 | 23469 | E > 11000 | 1.0 |

TABLE 1

Note: M_{Ed} is the maximum occurring moment in the cracked zone of region 1. We consider only one EI (which is a corresponding minimum EI) over this cracked height.

Iteration process EI right wall, REGION 2 (N = -810 kN)

| | Iteration # | $M_{Ed,max}$ | κ_{Ed} | | $(EI)_{Ed,min}$ | EA | E | | Note: | $l_{cracked}$ |
|-------------|-------------------------|--------------|---------------|-----------|------------------------|-----------------|----------------------|-------|-----------|---------------|
| | | [kNm] | [1/mm] | [1/m] | [kNm ² /m'] | [kN/m'] | [kN/m ²] | [MPa] | | |
| Procedure 1 | 1 | 1690 | 4.684E-07 | 4.684E-04 | 3.61E+06 | 1.92E+07 | 1.28E+07 | 12829 | E > 11000 | 6.5 |
| | 2 | uncracked | - | - | - | - | - | - | - | - |
| | 3 | 1730 | 5.073E-07 | 5.073E-04 | 3.41E+06 | 1.82E+07 | 1.21E+07 | 12126 | E > 11000 | 6.8 |
| | 4 | 1530 | 3.129E-07 | 3.129E-04 | 4.89E+06 | 2.61E+07 | 1.74E+07 | 17385 | E > 11000 | 0.3 |
| | 5 | 1750 | 5.267E-07 | 5.267E-04 | 3.32E+06 | 1.77E+07 | 1.18E+07 | 11814 | E > 11000 | 6.9 |
| | 6 | 1550 | 3.323E-07 | 3.323E-04 | 4.66E+06 | 2.49E+07 | 1.66E+07 | 16582 | E > 11000 | 0.4 |
| | Final field 1 | 1370 | 1.574E-07 | 1.574E-04 | 8.70E+06 | 4.64E+07 | 3.09E+07 | 30942 | E > 11000 | 0.2 |
| | Final field 2 | 1470 | 2.546E-07 | 2.546E-04 | 5.77E+06 | 3.08E+07 | 2.05E+07 | 20529 | E > 11000 | 3.5 |
| Procedure 2 | Rechterwand_check_field | 1450 | 2.352E-07 | 2.352E-04 | 6.17E+06 | 3.29E+07 | 2.19E+07 | 21923 | E > 11000 | 3.2 |

TABLE 2

Note: M_{Ed} is the maximum occurring moment in the cracked zone of region 2. We consider only one EI (which is a corresponding minimum EI) over this cracked height.

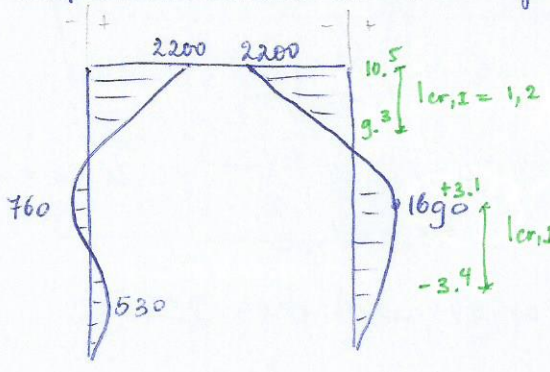
Overview iteration steps right wall (see next pages):

4) Iteration process to find cracked height & corresp. EI-distr. right wall.

Left wall = cracked @ 2 zones \Rightarrow EI-distr. will be sustained during iteration process.

| zone | cr/uncr. | l(m) | from - to | EI (kNm ² /m) | EAL (kN/m) |
|------|----------|------|--------------|--------------------------|--------------------|
| 1 | cracked | 1,3 | +10,5 +9,2 | $7,22 \times 10^6$ | $3,85 \times 10^7$ |
| 2 | uncr. | 0,3 | +9,2 +8,9 | $1,05 \times 10^7$ | $5,63 \times 10^7$ |
| 3 | cracked | 0,2 | +8,9 +8,7 | $8,11 \times 10^6$ | $4,33 \times 10^7$ |
| 4 | uncr. | 20,7 | +8,7 -12 | $9,67 \times 10^6$ | $5,16 \times 10^7$ |

Right wall = The iteration process!



Iteration #0: 1st assumption \Rightarrow Right wall tot. uncr.

| zone | cr/uncr. | l(m) | from - to | EI | EA |
|------|----------|------|------------|--------------------|--------------------|
| 1 | uncr. | 1,5 | +10,5 +9 | $1,05 \times 10^7$ | $5,63 \times 10^7$ |
| 2 | uncr. | 21,0 | +9 -12 | $9,67 \times 10^6$ | $5,16 \times 10^7$ |

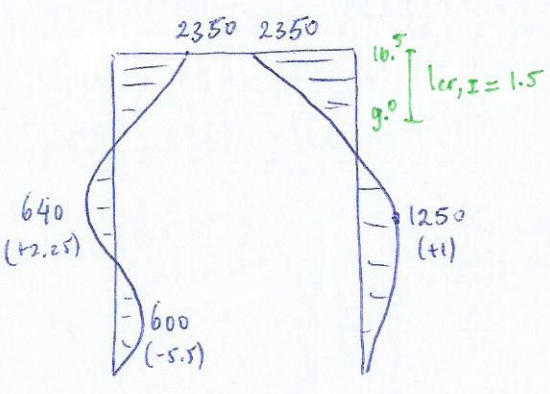
$M_I = 2200$
 $M_{II} = 1690$

I) Region I = +10,5 $\frac{1}{m}$ 9,0 m ($M_R = 1488$)

- Cr. height = +10,5 $\frac{1}{m}$ +9,3 \Rightarrow $l_{cr,I} = 1,2$ m
- $M_{Ed,max} = 2200 \Rightarrow (EI)_{Ed,min} = 6,32 \times 10^6$

II) Region II = +9,0 $\frac{1}{m}$ -12 m ($M_R = 1351$)

- Cr. height = +3,1 $\frac{1}{m}$ -3,4 m \Rightarrow $l_{cr,II} = 6,5$ m.
- $M_{Ed,max} = 1690 \Rightarrow (EI)_{Ed,min} = 3,61 \times 10^6$



Iteration #1 =

| zone | cr/uncr. | l(m) | From - To | EI | EA |
|------|----------|------|-------------|--------------------|--------------------|
| 1 | CR | 1,2 | +10,5 9,3 | $6,32 \times 10^6$ | $3,37 \times 10^7$ |
| 2 | - | 6,2 | +9,3 +3,1 | $9,67 \times 10^7$ | $5,16 \times 10^7$ |
| 3 | CR | 6,5 | +3,1 -3,4 | $3,61 \times 10^6$ | $1,92 \times 10^7$ |
| 4 | - | 8,6 | -3,4 -12 | $9,67 \times 10^7$ | $5,16 \times 10^7$ |

* Note = Eigenlijk van +9,3 $\frac{1}{m}$ 9,0 \Rightarrow EI = $1,05 \times 10^7$ (3m) van +9,0 $\frac{1}{m}$ +3,1 \Rightarrow EI = $9,67 \times 10^7$ (5,9m)

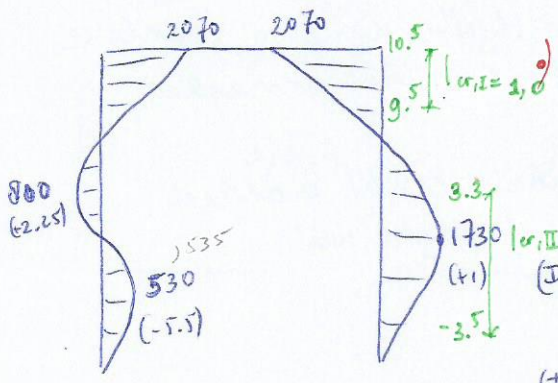
o) houd EI $\frac{1}{m}$ d grootste ongescheurde zone aan!

(I) Region I

- Cr. height = +10,5 $\frac{1}{m}$ 9,0 m \Rightarrow $l_{cr,I} = 1,5$ m.
- $M_{Ed,max} = 2350 \Rightarrow (EI)_{Ed,min} = 5,99 \times 10^6$.

(II) Region II

Cr. height = remains uncracked! (from +9,0 $\frac{1}{m}$ -12,0 m)



Iteration #2 =

| zone | cr/uncr. | l(m) | From - To | EI | EA |
|------|----------|------|--------------|--------------------|--------------------|
| 1 | CR | 1,5 | +10,5 9,0 | $5,99 \times 10^6$ | $3,19 \times 10^7$ |
| 2 | - | 21,0 | +9,0 -12,0 | $9,67 \times 10^6$ | $5,16 \times 10^7$ |

(I) Region I

- Cr. height = +10,5 $\frac{1}{m}$ 9,5 m \Rightarrow $l_{cr,I} = 1,0$ m.
- $M_{Ed,max} = 2070 \Rightarrow (EI)_{Ed,min} = 6,68 \times 10^6$

(II) Region II

- Cr. height = +3,3 $\frac{1}{m}$ -3,5 m \Rightarrow $l_{cr,II} = 6,8$ m.
- $M_{Ed,max} = 1730 \Rightarrow (EI)_{Ed,min} = 2,41 \times 10^6$

Iteration #3:

$M_I = 2400$
 $M_{II} = 1210$ (3)

| zone | cr/uncr. | l(m) | From - To | | EI | EA |
|------|----------|------|-----------|------|--------------------|--------------------|
| 1 | CR | 1,0 | +10,5 | +9,5 | $6,68 \times 10^6$ | $3,56 \times 10^7$ |
| 2 | - | 6,2 | +9,5 | +3,3 | $9,67 \times 10^6$ | $5,16 \times 10^7$ |
| 3 | CR | 6,8 | +3,3 | -3,5 | $3,41 \times 10^6$ | $1,82 \times 10^7$ |
| 4 | - | 8,5 | -3,5 | -12 | $9,67 \times 10^6$ | $5,16 \times 10^7$ |

* Note: Van $+9,5$ t/m $9,0$ m $\Rightarrow EI = 1,05 \times 10^7$ ($l = 0,5$ m)
Van $+9,0$ t/m $+2,3$ m $\Rightarrow EI = 9,67 \times 10^7$ ($l = 5,7$ m)
Houd EI grootste ongecheckte zone aan!

(I) Region I

- Cr. height = $+10,5$ t/m $9,0 \Rightarrow l_{CR,I} = 1,5$ m.
- $M_{Ed,max} = 2400 \rightarrow (EI)_{Ed,min} = 5,90 \times 10^6$

(II) Region II:

- Cr. height: $+9,0$ t/m $8,7 \Rightarrow l_{CR,II} = 0,3$ m.
- $M_{Ed,max}$ (afschatten @ $9,0$ m) = $1530 \rightarrow (EI)_{min} = 4,89 \times 10^6$

Iteration #4:

$M_I = 2050$
 $M_{II} = 1750$

| zone | cr/uncr. | l(m) | From - To | | EI | EA |
|------|----------|------|-----------|------|--------------------|--------------------|
| 1 | CR | 1,5 | +10,5 | +9,0 | $5,90 \times 10^6$ | $3,14 \times 10^7$ |
| 2 | CR | 0,3 | +9,0 | +8,7 | $4,89 \times 10^6$ | $2,61 \times 10^7$ |
| 3 | - | 20,7 | +8,7 | -12 | $9,67 \times 10^6$ | $5,16 \times 10^7$ |

(I) Region I

- Cr. height: $+10,5$ t/m $9,5$ m $\Rightarrow l_{CR,I} = 1,0$ m.
- $M_{Ed,max} = 2050 \rightarrow (EI)_{Ed,min} = 6,74 \times 10^6$

(II) Region II

- Cr. height: $+3,3$ t/m $-3,6$ m $\Rightarrow l_{CR,II} = 6,9$ m.
- $M_{Ed,max} = 1750 \rightarrow (EI)_{Ed,min} = 3,32 \times 10^6$

Iteration #5

$M_I = 2410$
 $M_{II} = 1190$

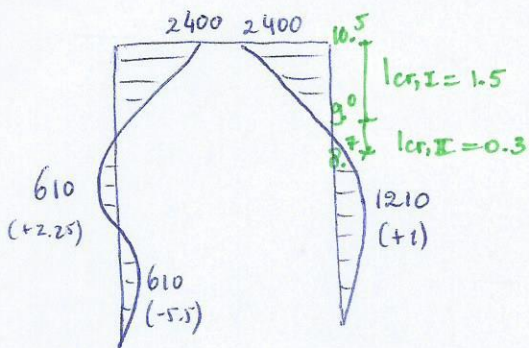
| zone | cr/uncr. | l(m) | from - To | | EI | EA |
|------|----------|------|-----------|------|--------------------|--------------------|
| 1 | CR | 1,0 | +10,5 | +9,5 | $6,74 \times 10^6$ | $3,59 \times 10^7$ |
| 2 | - | 6,2 | +9,5 | +3,3 | $9,67 \times 10^6$ | $5,16 \times 10^7$ |
| 3 | CR | 6,9 | +3,3 | -3,6 | $3,32 \times 10^6$ | $1,77 \times 10^7$ |
| 4 | - | 8,4 | -3,6 | -12 | $9,67 \times 10^6$ | $5,16 \times 10^7$ |

(I) Region I

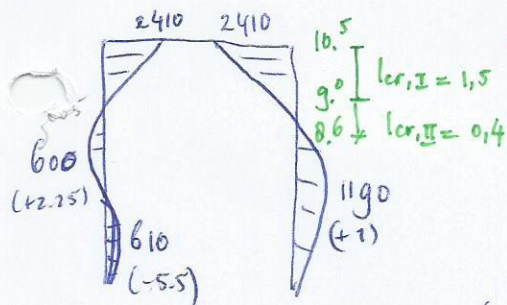
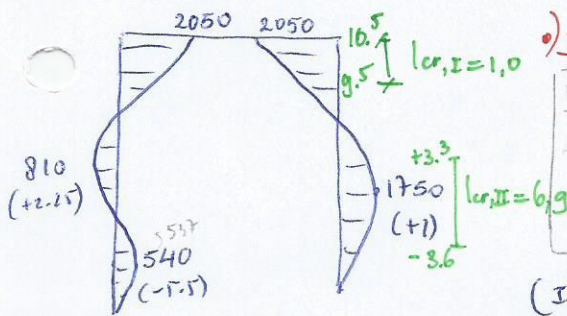
- Cr. height: $+10,5$ t/m $9,0 \Rightarrow l_{CR,I} = 1,5$ m.
- $M_{Ed,max} = 2410 \rightarrow (EI)_{Ed,min} = 5,88 \times 10^6$

(II) Region II:

- Cr. height: $+9,0$ t/m $8,6 \Rightarrow l_{CR,II} = 0,4$ m.
- $M_{Ed,max}$ (afschatten @ $9,0$ m) = $1550 \rightarrow (EI)_{Ed,min} = 4,66 \times 10^6$



$M_{(I)} \geq 1488,1$ voor $y \geq 8,9$ m
 $M_{(II)} \geq 1351$ voor $y \geq 8,7$ m.
Dus 2 zones: $+10,5$ t/m $9,0$ m
 $+9,0$ t/m $8,7$ m.



$M_{(I)} \geq 1488$ voor $y \geq 8,9$ m
 $M_{(II)} \geq 1351$ voor $y \geq 8,6$ m.
Dus 2 zones: $+10,5$ t/m $9,0$ m
 $+9,0$ t/m $8,6$ m

APPENDIX D

PROPERTIES STIFF STRUCTURE

The stiff structure above the diaphragm walls is used to simulate the clamped connection in the Plaxis 2D –Total Model. The stiff structure consists of rigid plates connected by struts. For the Half Model in PCSheetPileWall only the rigid plate was applicable.

❖ **Properties rigid plate in PCSheetPileWall**

In PCSheetPileWall the rigid plate above the real diaphragm wall is realized by choosing a very thick plate with the following properties:

| Input diaphragm wall | | | | | |
|----------------------|-------|-------|--|-------|------------------------|
| Case | b [m] | d [m] | A_{reinf} per side [mm ²] | c [m] | l_{rigid} [m] |
| Rigid plate | 1 | 3.5 | 30000 | 0.1 | 3.5 |

| Output PCSheetPileWall - Rigid plate | | |
|--|-----------|------------------------|
| I | 3.573E+00 | [m ⁴] |
| EI (concrete, inclusive reinforcement) | 1.342E+08 | [kNm ² /m'] |
| EA | 1.315E+08 | [kN/m'] |

❖ **Properties rigid plate & strut in Plaxis 2D**

The EI and EA of the rigid plate following from PCSheetPileWall are used as input in Plaxis 2D:

| Properties rigid plate | | |
|------------------------|-----------|------------------------|
| EI | 1.342E+08 | [kNm ² /m'] |
| EA | 1.315E+08 | [kN/m'] |
| d_{eq} | 3.5 | [m] |
| γ | 24 | [kN/m ³] |
| w (= $\gamma * d$) | 84 | [kN/m/m'] |
| ν | 0.2 | [-] |

Consider the normal stiffness EA of the beam (roof structure) with $EA = 33E+07 \text{ [kN/m}^2\text{]} * 0.9 \text{ [m}^2\text{]} = 29.7 \text{ E}6 \approx 3E+07 \text{ kN/m'}$

| Properties strut (Node-to-node anchor) | | |
|--|----------|---------|
| EA | 3.00E+07 | [kN/m'] |
| $l_{\text{equivalent}}$ | 14.5 | [m] |
| L_{spacing} | 1 | [m] |

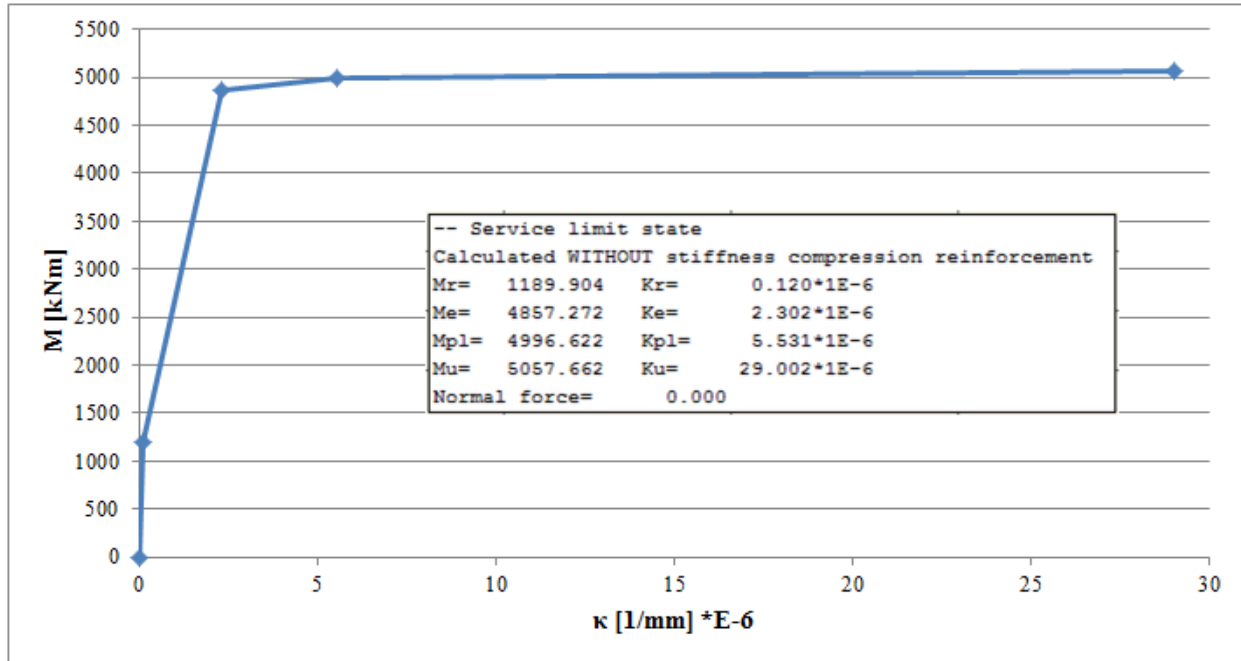
APPENDIX E1

VARIATION HINGED CONNECTION 1

$\rho_{l,tot} = 1\%$
Case a: EI (κ)

| Material properties diaphragm wall | | | | | |
|------------------------------------|-------|---------------------|---------------------|----------------------|---|
| d [m] | b [m] | A [m ²] | I [m ⁴] | A _{s,total} | A _s per side (mm ² /m') |
| 1.5 | 1 | 1.5 | 0.28125 | 1% | 7500 |

M-κ diagram diaphragm walls:



Iteration procedure 2 – Results:

The aimed results (M_{Ed} , δ_v and U_x) are determined based on iteration procedure 2 for EI_{var} . According to iteration procedure 2:

1. Determine the M-line and the (imaginary) cracked zones for EI_0 and EI_{∞} . The cracked zones are defined where $M > M_r$ ($M_r = 1190$ kNm);
2. Determine the ‘average result’, implying that for both walls the average M-line and the average cracked zone are determined based on the results for EI_0 and EI_{∞} ;
3. The average M-line is used to determine the EI-distribution of both walls. Based on the average bending moment, the EI and EA are determined for the average $I_{cracked}$. The EI is determined by means of interpolation in the M-κ diagram;
4. The EI-distribution of both walls is used as input in the Plaxis 2D – Total Model to find the final result for EI_{var} .

❖ **Step 1 & 2: Determining the ‘average result’**

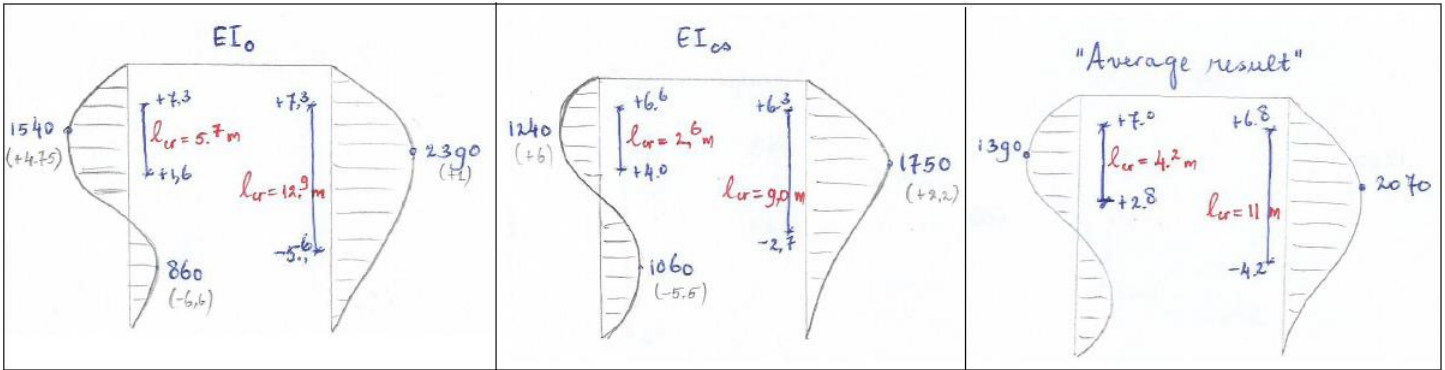


Figure E.1(1): The ‘average result’ based on EI_0 and EI_{∞} .

❖ **Step 3: Input in Plaxis – Total Model**

| | Zone | Cracked/ uncracked | Length | From | To | $M_{Ed,average}$ [kNm/m'] | EI [kNm ² /m'] | EA [kN/m'] |
|------------|------|-----------------------|--------|------|------|------------------------------|------------------------------|---------------|
| | | | [m] | [m] | [m] | | | |
| Left wall | 1 | uncracked | 3.5 | 10.5 | 7 | - | 9.92E+06 | 5.29E+07 |
| | 2 | cracked | 4.2 | 7 | 2.8 | 1390 | 5.81E+06 | 3.10E+07 |
| | 3 | uncracked | 14.8 | 2.8 | -12 | - | 9.92E+06 | 5.29E+07 |
| Right wall | 1 | uncracked | 3.7 | 10.5 | 6.8 | - | 9.92E+06 | 5.29E+07 |
| | 2 | cracked | 11 | 6.8 | -4.2 | 2070 | 1.83E+06 | 9.76E+06 |
| | 3 | uncracked | 7.8 | -4.2 | -12 | - | 9.92E+06 | 5.29E+07 |

Table E.1(1): EI-distribution for both walls used as input in Plaxis 2D – Total Model for iteration procedure 2

❖ **Step 4: Final result EI_{var}**

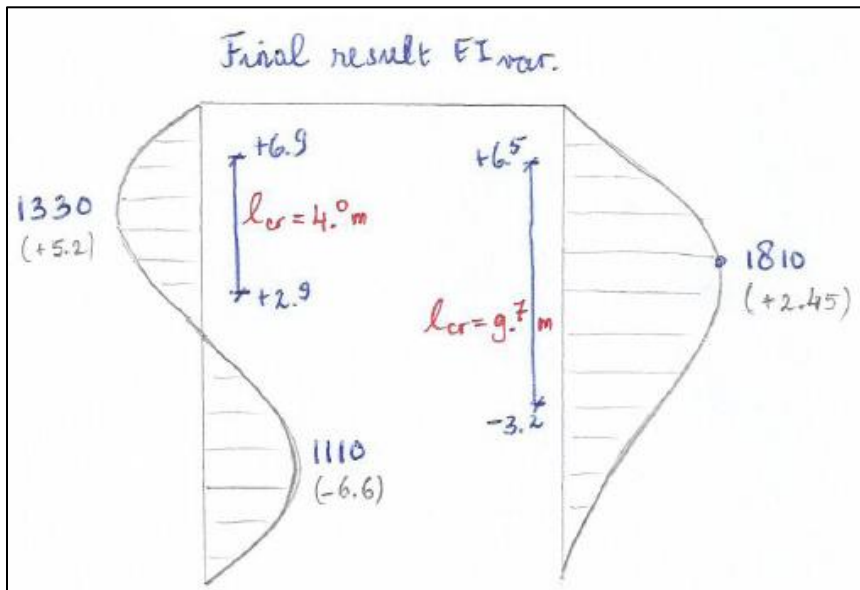


Figure E.1(2): Final result EI_{var} according to iteration procedure 2 in Plaxis 2D – Total Model. (Note: Bending moment values in kNm and levels with regard to NAP are placed between brackets)

| | M_{Ed} [kNm/m'] | δ_v [mm] | U_x [mm] | |
|-------------|----------------------|--------------------|------------|------------|
| | | | Left wall | Right wall |
| EI_0 | 2390 | 91 | -44 | -62 |
| EI_∞ | 1750 | 112 | -64 | -85 |
| EI_{var} | 1810 | 106 | -57 | -78 |

Table E.1(2): Final results for EI_0 , EI_∞ and EI_{var} for $N=0$ kN at $\rho_{l,tot} = 1\%$

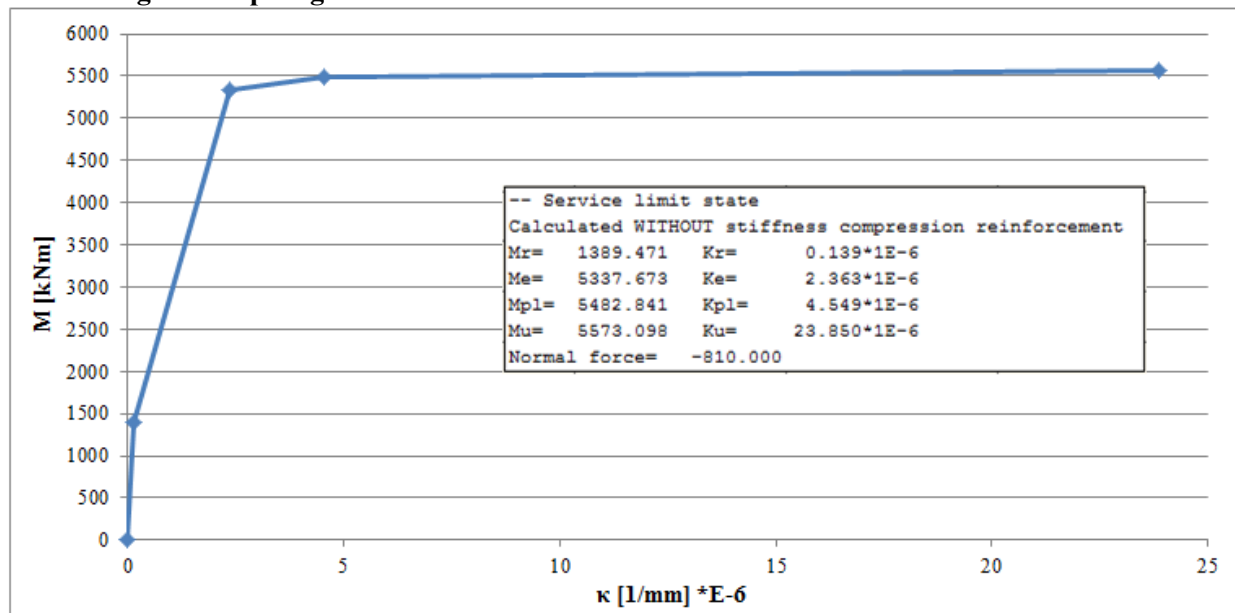
APPENDIX E2

VARIATION HINGED CONNECTION 1

$\rho_{l,tot} = 1\%$
Case b: EI (κ, N)

| Material properties diaphragm wall | | | | | |
|------------------------------------|-------|---------------------|---------------------|----------------------|---|
| d [m] | b [m] | A [m ²] | I [m ⁴] | A _{s,total} | A _s per side (mm ² /m') |
| 1.5 | 1 | 1.5 | 0.28125 | 1% | 7500 |

M-N-κ diagram diaphragm walls:



Iteration procedure 2 – Results:

The aimed results (M_{Ed} , δ_v and U_x) are determined based on iteration procedure 2 for EI_{var} . According to iteration procedure 2:

1. Determine the M-line and the (imaginary) cracked zones for EI_0 and EI_{∞} . The cracked zones are defined where $M > M_r$ ($M_r = 1389$ kNm);
2. Determine the ‘average result’, implying that for both walls the average M-line and the average cracked zone are determined based on the results for EI_0 and EI_{∞} ;
3. The average M-line is used to determine the EI-distribution of both walls. Based on the average bending moment, the EI and EA are determined for the average $I_{cracked}$. The EI is determined by means of interpolation in the M-κ diagram;
4. The EI-distribution of both walls is used as input in the Plaxis 2D – Total Model to find the final result for EI_{var} .

❖ **Step 1 & 2: Determining the ‘average result’**

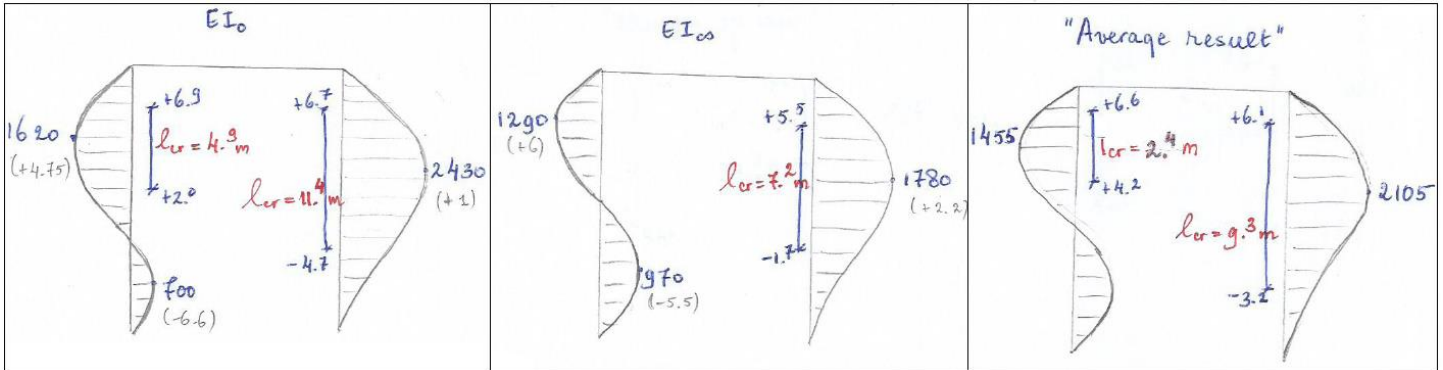


Figure E.2(1): The ‘average result’ based on EI_0 and EI_{cs} .

❖ **Step 3: Input in Plaxis – Total Model**

| | Zone | Cracked/ uncracked | Length | From | To | $M_{Ed,average}$ [kNm/m'] | EI [kNm ² /m'] | EA [kN/m'] |
|------------|------|-----------------------|--------|------|------|------------------------------|------------------------------|---------------|
| | | | [m] | [m] | [m] | | | |
| Left wall | 1 | uncracked | 3.9 | 10.5 | 6.6 | - | 1.00E+07 | 5.33E+07 |
| | 2 | cracked | 2.4 | 6.6 | 4.2 | 1455 | 8.27E+06 | 4.41E+07 |
| | 3 | uncracked | 16.2 | 4.2 | -12 | - | 1.00E+07 | 5.33E+07 |
| Right wall | 1 | uncracked | 4.4 | 10.5 | 6.1 | - | 1.00E+07 | 5.33E+07 |
| | 2 | cracked | 9.3 | 6.1 | -3.2 | 2105 | 3.88E+06 | 2.07E+07 |
| | 3 | uncracked | 8.8 | -3.2 | -12 | - | 1.00E+07 | 5.33E+07 |

Table E.2(1): EI-distribution for both walls used as input in Plaxis 2D – Total Model for iteration procedure 2

❖ **Step 4: Final result EI_{var}**

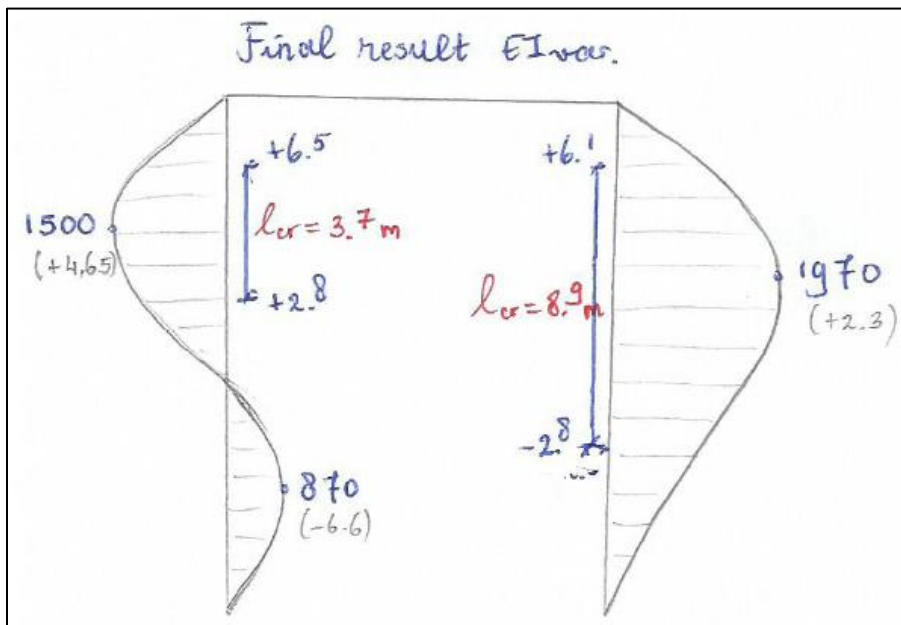


Figure E.2(2): Final result EI_{var} according to iteration procedure 2 in Plaxis 2D – Total Model. (Note: Bending moment values in kNm and levels with regard to NAP are placed between brackets)

| | M_{Ed} [kNm/m'] | δ_v [mm] | U_x [mm] | |
|-------------|----------------------|--------------------|------------|------------|
| | | | Left wall | Right wall |
| EI_0 | 2430 | 101 | -45 | -63 |
| EI_∞ | 1780 | 121 | -65 | -84 |
| EI_{var} | 1970 | 109 | -52 | -73 |

Table E.2(2): Final results for EI_0 , EI_∞ and EI_{var} for $N \neq 0$ kN at $\rho_{l,tot} = 1\%$

APPENDIX F1

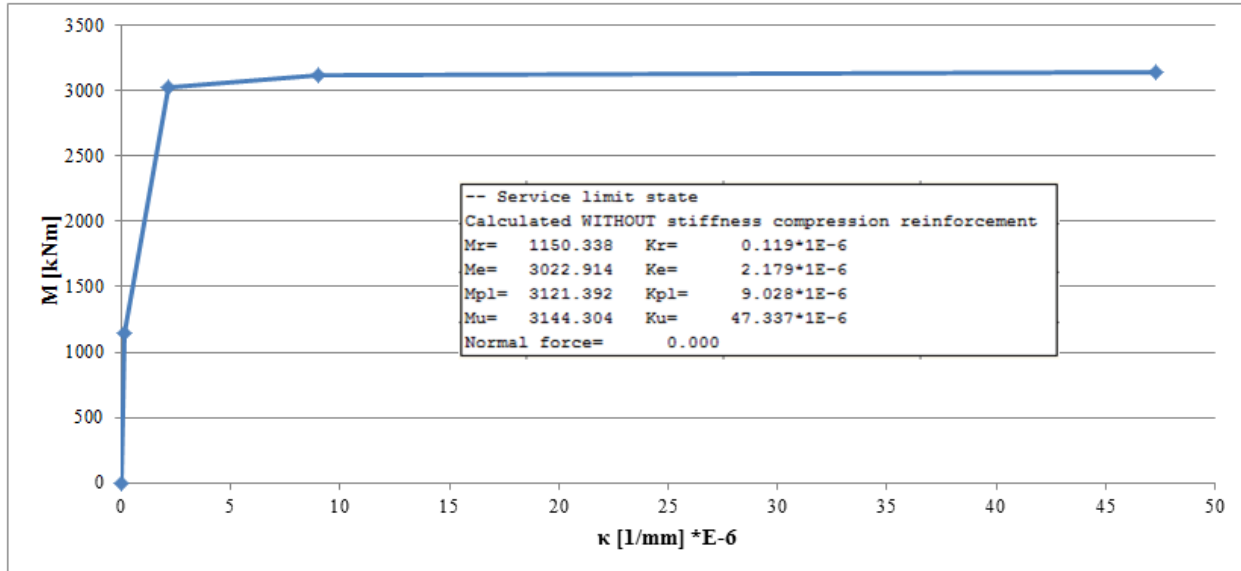
VARIATION HINGED CONNECTION 2

SOIL TYPE 2

Case a: EI (κ)

| Material properties diaphragm wall | | | | | |
|------------------------------------|-------|---------------------|---------------------|----------------------|---|
| d [m] | b [m] | A [m ²] | I [m ⁴] | A _{s,total} | A _s per side (mm ² /m') |
| 1.5 | 1 | 1.5 | 0.28125 | 0.6% | 4595 |

M-κ diagram diaphragm walls:



Iteration procedure 2 – Results:

The aimed results (M_{Ed} , δ_v and U_x) are determined based on iteration procedure 2 for EI_{var} . According to iteration procedure 2:

1. Determine the M-line and the (imaginary) cracked zones for EI_0 and EI_{∞} . The cracked zones are defined where $M > M_r$ ($M_r = 1150$ kNm);
2. Determine the ‘average result’, implying that for both walls the average M-line and the average cracked zone are determined based on the results for EI_0 and EI_{∞} ;
3. The average M-line is used to determine the EI-distribution of both walls. Based on the average bending moment, the EI and EA are determined for the average $l_{cracked}$. The EI is determined by means of interpolation in the M-κ diagram;
4. The EI-distribution of both walls is used as input in the Plaxis 2D – Total Model to find the final result for EI_{var} .

❖ **Step 1 & 2: Determining the ‘average result’**

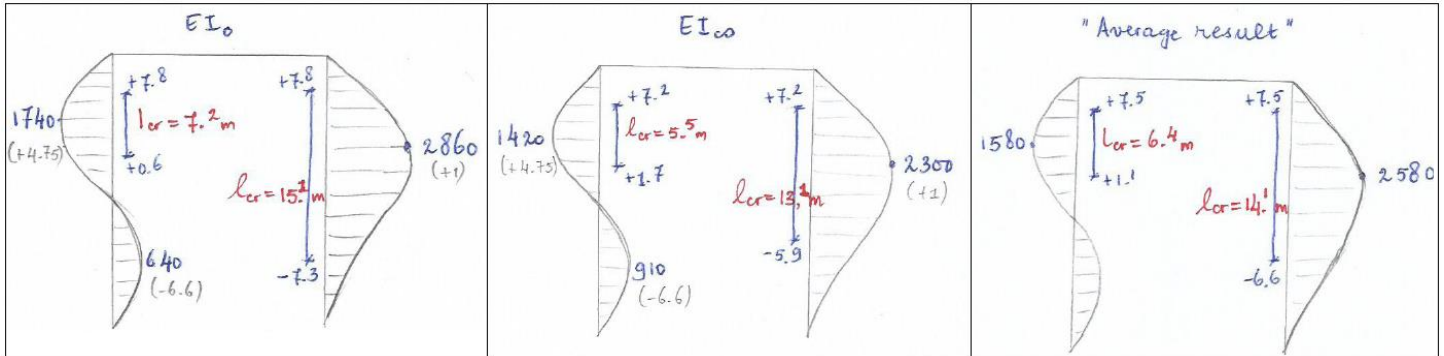


Figure F.1(1): The ‘average result’ based on EI_0 and EI_∞

❖ **Step 3: Input in Plaxis – Total Model**

| | Zone | Cracked/ uncracked | Length | From | To | $M_{Ed,average}$ [kNm/m'] | EI [kNm ² /m'] | EA [kN/m'] |
|------------|------|-----------------------|--------|------|------|------------------------------|------------------------------|---------------|
| | | | [m] | [m] | [m] | | | |
| Left wall | 1 | uncracked | 3 | 10.5 | 7.5 | - | 9.67E+06 | 5.16E+07 |
| | 2 | cracked | 6.4 | 7.5 | 1.1 | 1580 | 2.67E+06 | 1.42E+07 |
| | 3 | uncracked | 13.1 | 1.1 | -12 | - | 9.67E+06 | 5.16E+07 |
| Right wall | 1 | uncracked | 3 | 10.5 | 7.5 | - | 9.67E+06 | 5.16E+07 |
| | 2 | cracked | 14.1 | 7.5 | -6.6 | 2580 | 1.53E+06 | 8.13E+06 |
| | 3 | uncracked | 5.4 | -6.6 | -12 | - | 9.67E+06 | 5.16E+07 |

Table F.1(1): EI-distribution for both walls used as input in Plaxis 2D – Total Model for iteration procedure 2

❖ **Step 4: Final result EI_{var}**

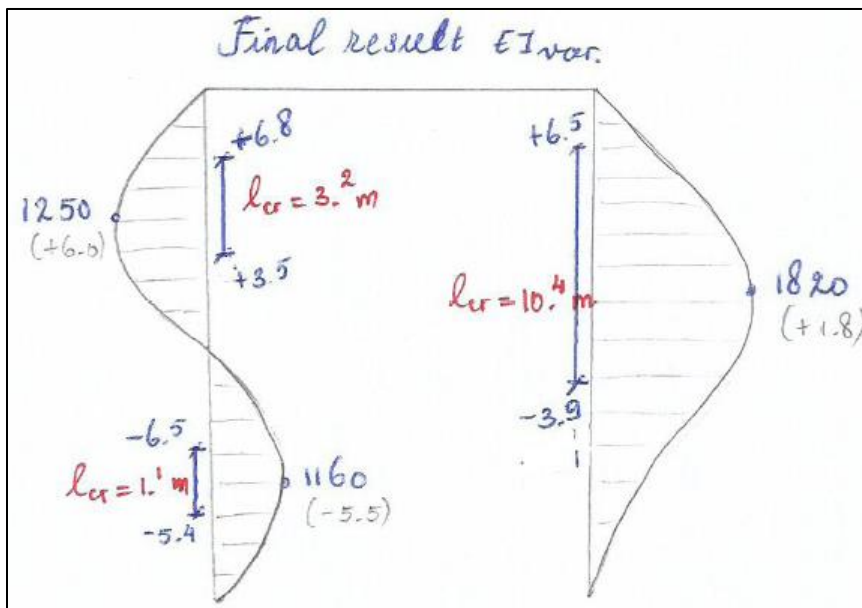


Figure F.1(2): Final result EI_{var} according to iteration procedure 2 in Plaxis 2D – Total Model.
(Note: Bending moment values in kNm and levels with regard to NAP are placed between brackets)

| | M_{Ed} [kNm/m'] | δ_v [mm] | U_x [mm] | |
|-------------|----------------------|--------------------|------------|------------|
| | | | Left wall | Right wall |
| EI_0 | 2860 | 210 | -86 | -131 |
| EI_∞ | 2300 | 245 | -118 | -166 |
| EI_{var} | 1820 | 267 | -137 | -191 |

Table F.1(2): Final results for EI_0 , EI_∞ and EI_{var} for $N=0$ kN at Soil Type 2

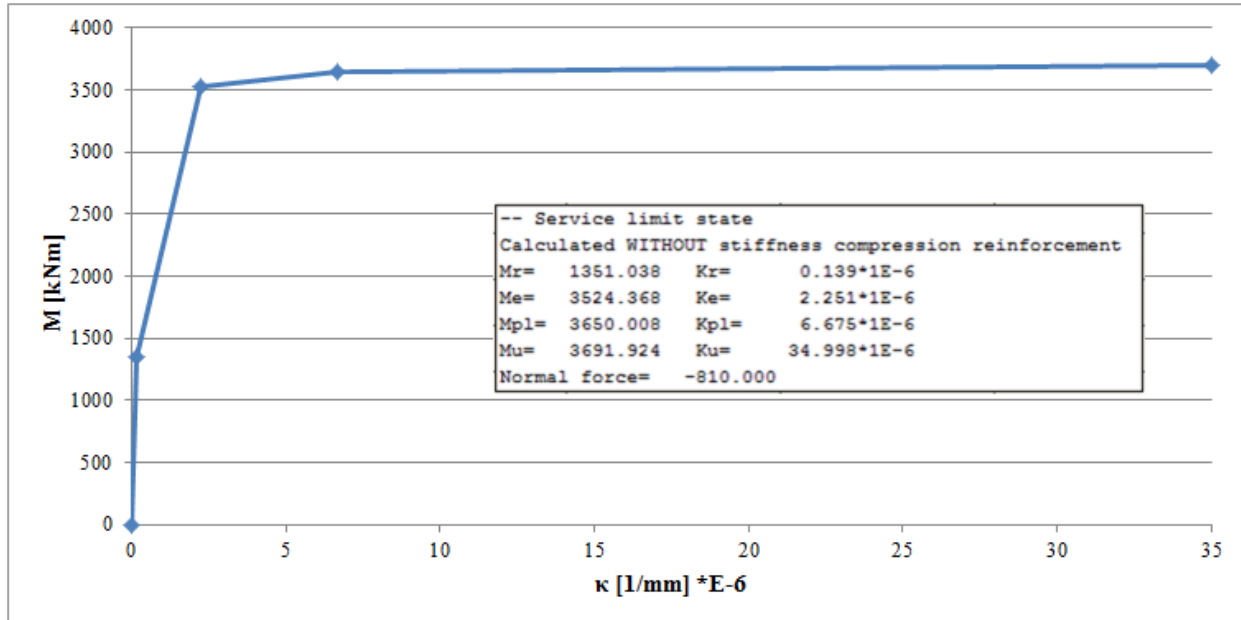
APPENDIX F2

VARIATION HINGED CONNECTION 2

SOIL TYPE 2
Case b: EI (κ , N)

| Material properties diaphragm wall | | | | | |
|------------------------------------|-------|---------------------|---------------------|----------------------|---|
| d [m] | b [m] | A [m ²] | I [m ⁴] | A _{s,total} | A _s per side (mm ² /m') |
| 1.5 | 1 | 1.5 | 0.28125 | 0.6% | 4595 |

M-N-κ diagram diaphragm walls:



Iteration procedure 2 – Results:

The aimed results (M_{Ed} , δ_v and U_x) are determined based on iteration procedure 2 for EI_{var} . According to iteration procedure 2:

1. Determine the M-line and the (imaginary) cracked zones for EI_0 and EI_{∞} . The cracked zones are defined where $M > M_r$ ($M_r = 1351$ kNm);
2. Determine the ‘average result’, implying that for both walls the average M-line and the average cracked zone are determined based on the results for EI_0 and EI_{∞} ;
3. The average M-line is used to determine the EI-distribution of both walls. Based on the average bending moment, the EI and EA are determined for the average $l_{cracked}$. The EI is determined by means of interpolation in the M-κ diagram;
4. The EI-distribution of both walls is used as input in the Plaxis 2D – Total Model to find the final result for EI_{var} .

❖ **Step 1 & 2: Determining the ‘average result’**

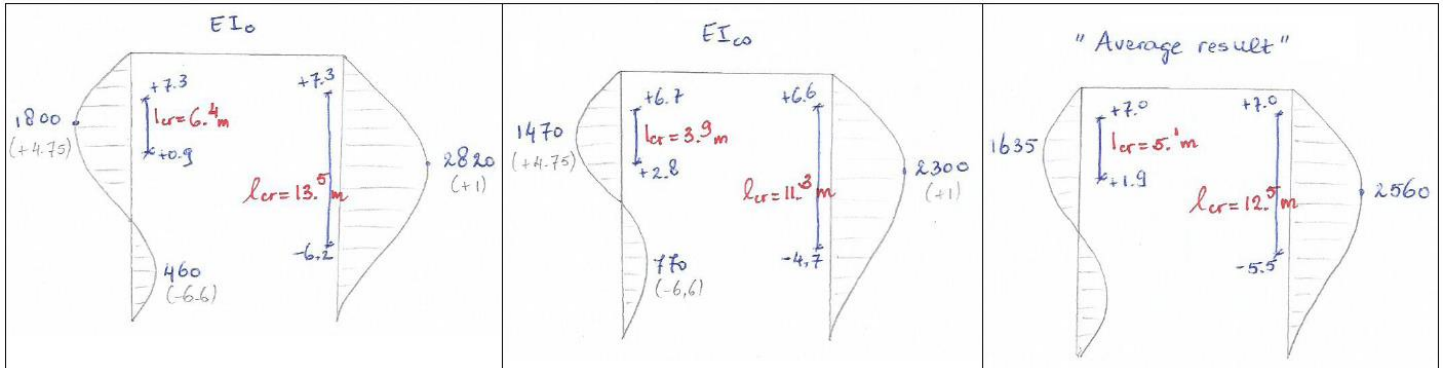


Figure F.2(1): The ‘average result’ based on EI_0 and EI_∞ .

❖ **Step 3: Input in Plaxis – Total Model**

| | Zone | Cracked/ uncracked | Length | From | To | $M_{Ed,average}$ [kNm/m'] | EI [kNm ² /m'] | EA [kN/m'] |
|------------|------|-----------------------|--------|------|------|------------------------------|------------------------------|---------------|
| | | | [m] | [m] | [m] | | | |
| Left wall | 1 | uncracked | 3.5 | 10.5 | 7 | - | 9.72E+06 | 5.18E+07 |
| | 2 | cracked | 5.1 | 7 | 1.9 | 1635 | 3.94E+06 | 2.10E+07 |
| | 3 | uncracked | 13.9 | 1.9 | -12 | - | 9.72E+06 | 5.18E+07 |
| Right wall | 1 | uncracked | 3.5 | 10.5 | 7 | - | 9.72E+06 | 5.18E+07 |
| | 2 | cracked | 12.5 | 7 | -5.5 | 2560 | 1.95E+06 | 1.04E+07 |
| | 3 | uncracked | 6.5 | -5.5 | -12 | - | 9.72E+06 | 5.18E+07 |

Table F.2(1): EI-distribution for both walls used as input in Plaxis 2D – Total Model for iteration procedure 2

❖ **Step 4: Final result EI_{var}**

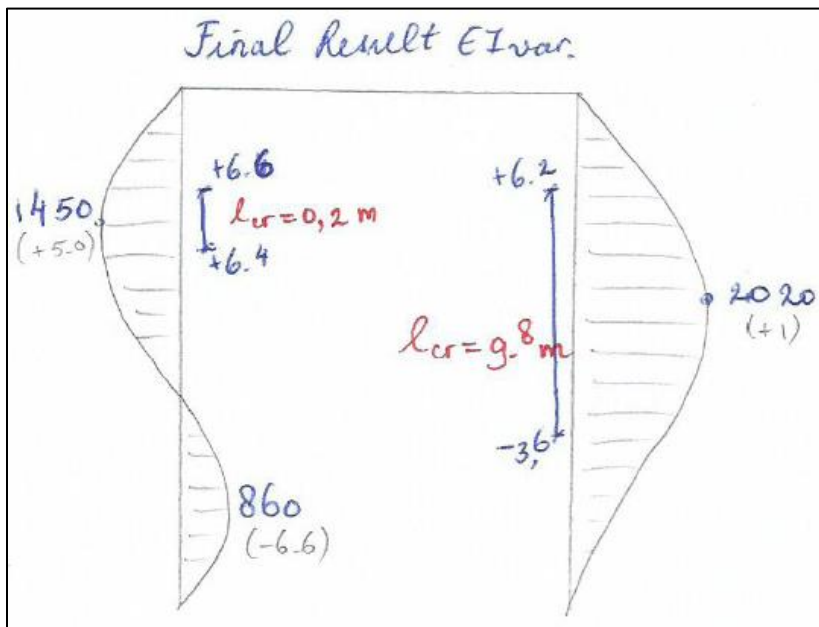


Figure F.2(2): Final result EI_{var} according to iteration procedure 2 in Plaxis 2D – Total Model. (Note: Bending moment values in kNm and levels with regard to NAP are placed between brackets)

| | M_{Ed} [kNm/m'] | δ_v [mm] | U_x [mm] | |
|-------------|----------------------|--------------------|------------|------------|
| | | | Left wall | Right wall |
| EI_0 | 2820 | 232 | -88 | -133 |
| EI_∞ | 2300 | 268 | -119 | -167 |
| EI_{var} | 2020 | 274 | -124 | -177 |

Table F.2(2): Final results for EI_0 , EI_∞ and EI_{var} for $N \neq 0$ kN at Soil Type 2